GEOCHEMICAL MODELING OF NCG INJECTION IN A GEOTHERMAL WELL USING DOUBLET WELL MODEL

A THESIS SUBMITTED TO
THE GRADUATE SCHOOL OF NATURAL AND APPLIED SCIENCES
OF
MIDDLE EAST TECHNICAL UNIVERSITY

BY

BUĞRAHAN İLGİN

IN PARTIAL FULFILLMENT OF THE REQUIREMENTS
FOR
THE DEGREE OF MASTER OF SCIENCE
IN
PETROLEUM AND NATURAL GAS ENGINEERING

JULY 2021

Approval of the thesis:

GEOCHEMICAL MODELING OF NCG INJECTION IN A GEOTHERMAL WELL USING DOUBLET WELL MODEL

submitted by **BUĞRAHAN İLGİN** in partial fulfillment of the requirements for the degree of **Master of Science** i**n Petroleum and Natural Gas Engineering, Middle East Technical University** by,

Prof. Dr. Halil Kalıpçılar
Dean, Graduate School of **Natural and Applied Sciences** _____

Assoc. Prof. Dr. Çağlar Sınayuç
Head of the Department, **Petroleum and Natural Gas Eng.** _____

Prof. Dr. Serhat Akın
Supervisor, **Petroleum and Natural Gas Eng., METU** _____

Dr. Selçuk Erol
Co-Supervisor, **Petroleum and Natural Gas Eng., METU** _____

Examining Committee Members:

Asst. Prof. Dr. İsmail Durgut
Petroleum and Natural Gas Eng, METU _____

Prof. Dr. Serhat Akın
Petroleum and Natural Gas Eng., METU _____

Prof. Dr. Ö. İnanç Türeyen
Petroleum and Natural Gas Eng., ITU _____

Date: 29.07.2021

I hereby declare that all information in this document has been obtained and presented in accordance with academic rules and ethical conduct. I also declare that, as required by these rules and conduct, I have fully cited and referenced all material and results that are not original to this work.

Name Last name: Buğrahan İlgin

Signature:

ABSTRACT

GEOCHEMICAL MODELING OF NCG INJECTION IN A GEOTHERMAL WELL USING DOUBLET WELL MODEL

İlgin, Buğrahan
Master of Science, Petroleum and Natural Gas Engineering
Supervisor : Prof. Dr. Serhat Akın
Co-Supervisor: Dr. Selçuk Erol

July 2021, 118 pages

Geothermal energy is regarded as an environmentally friendly source of energy. However, the amount of non-condensable gases (NCG), which are co-produced with brine, are significantly high in the geothermal fields of Turkey. To overcome the NCG emission produced by power plants, which is mainly CO_2, one of the efficient methods is re-injecting the captured NCG into the reservoir. The ultimate aim of the reinjection is to mineralize CO_2 in the reservoir as carbonate minerals. In this thesis, a reactive transport modeling study is conducted with TOUGHREACT to scrutinize a potential operation of brine-CO_2 injection in a deep fractured metamorphic reservoir formation. A comprehensive geologic model is constructed and utilized in TOUGHREACT with Petrasim interface to simulate reactive transport phenomenon during NCG injection. The developed doublet well model in which a re-injection and a production well are included is calibrated with field measurements. PHREEQC is used to evalaute the reaction-paths between minerals and aqueous species. These evaluations help to determine possible secondary minerals to select in reactive transport model developed with TOUGHREACT. Three rock types with

various mineral compositions are introduced to inspect the interaction between different mineral contents and CO_2 charged brine injection in high temperature geothermal reservoirs. Three different injection scenarios are examined as the brine-CO_2 mixture, supercritical CO_2 injection and brine-CO_2 mixture injection at lower temperature to observe amorphous silica precipitation. The results are compared to those obtained with injection of brine-only. Composition results demonstrate that the reactions of aqueous species and reservoir minerals are highly dependent on the pH and temperature. Results show that Calcite formation is only observed in a scenario where brine and CO_2 is injected as a mixture, whereas in the first two scenario of the study which represent injection of brine-only and injection of CO_2-only, Calcite dissolution is observed. Limited mineralization due to CO_2 occurs and CO_2 is mostly trapped in solution. Moreover, the impact of CO_2 injection is examined on Silica reactions. The results demonstrate that lower injection temperature at 85 °C should be selected for CO_2 injection. For lower injection temperatures at 85 °C, amorpheous silica precipitation around the injection well may be trigerred. This study may guide innovative injection strategies, which will be conducted in Turkish geothermal fields in the near future.

Keywords: Geothermal Energy, Reactive Transport Modeling, CO_2 Injection, Reservoir Modeling, TOUGHREACT

ÖZ

ÇİFT KUYU MODELİ KULLANILARAK JEOTERMAL KUYUDA NCG ENJEKSİYONUNUN JEOKİMYASAL MODELLEMESİ

İlgin, Buğrahan
Yüksek Lisans, Petrol ve Doğal gaz Mühendisliği
Tez Yöneticisi: Prof. Dr. Serhat Akın
Ortak Tez Yöneticisi: Dr. Selçuk Erol

Temmuz 2021, 118 sayfa

Jeotermal enerji çevre dostu bir enerji kaynağı olarak kabul edilmektedir. Ancak jeotermal tuzlu suyu ile üretilen yoğuşmaz gazlar Türkiyenin jeotermal alanlarında önemli ölçüde yüksektir. Jeotermal enerji santralinin çoğunluğunun CO_2 olduğu NCG salınımını aşmak için, etkili yöntemlerden biri, ele geçirilen NCG'nin derin jeolojik formasyonlara yeniden enjekte edilmesidir. Enjeksiyonun temel amacı CO_2'i carbonat minerali olarak mineralize olmasını sağlamaktır. Bu tezde, derin metamorfik formasyona jeotermal tuzlu suyu-CO_2 enjeksiyonunun potansiyel işleyişini incelemek için TOUGHREACT programı ile reaktif taşınım modellemesi yapılmıştır. TOUGHREACT programı kullanılarak kapsayıcı bir jeolojik model oluşturulmuş, NCG enjeksiyonun reaktif taşınımını simüle edebilmek için Petrasim arayüzü kullanılmıştır. Bir enjeksiyon ve bir üretim kuyusu içeren ikili kuyu modeli, saha ölçümleriyle eşleştirilmiştir. Mineraller ve suda çözünmüş türler arasındaki reaksiyon yollarını değerlendirmek için PHREEQC programı kullanılmıştır. Bahsedilen değerlendirmeler, olası ikincil mineral seçimi ve bu minerallerin TOUGHREACT programına tanımlaması konusunda fayda sağlamıştır. Yüksek

sıcaklıktaki jeotermal rezervuarlardaki farklı mineral içerikleri ve CO_2 yüklü jeotermal tuzlu suyu enjeksiyonu arasındaki etkileşimi incelemek için çeşitli mineral bileşimlerine sahip üç kaya türü tanıtılmıştır. CO_2'nin jeotermal tuzlu suyu ile karıştırılıp enjekte edilmesi, CO_2'in süperkritik koşullarda tek başına enjekte edilmesi ve amorf silika çökelmesini gözlemleyebilmek için CO_2'nin daha düşük sıcaklıkta jeotermal tuzlu suyu ile enjekte edilmesi çalışmada incelenen üç farklı enjeksiyon senaryosudur. Senaryolardan elde edilen sonuçlar, tuzlu suyun tek başına enjeksiyonu senaryosu ile kıyaslanmıştır. Sonuçlar minerallerin ve su çözünmüş türlerin reaksiyonlarının sıcaklık ve pH değerlerine fazlasıyla bağlı olduğunu göstermiştir. Elde edilen sonuçlara göre CO_2 enjeksiyonuna bağlı carbonat oluşumu sadece CO_2 ve tuzlu suyun karışım olarak basıldığı senaryoda görülmüştür. Bunun yanında çalışmanın ilk iki senaryosu olan ve tuzlu suyu tek başına enjeksiyonu ve CO_2'in tek başına enjeksiyonu senaryolarında kalsit çözünmesi gözlemlenmiştir. CO_2'ye bağlı mineralizasyon limitli miktardadır ve enjekte edilen CO_2'nin büyük çoğunluğunun çözelti içinde hapsolmaktadır. Bunlara ek olarak, CO_2 enjeksiyonun silika reaksiyonlarına etkisi incelenmiştir. Elde edilen sonuçlara göre 85 C° gibi daha düşük sıcaklıkların CO_2 enjeksiyonu seçilmesi daha uygundur. Ancak amorf silika çökelmesi bu düşük sıcaklıklarda tetiklenebilmektedir. Bu çalışma yakın gelecekte Türkiye jeotermal sahalarında yürütülecek yenilikçi enjeksiyon stratejilerine rehberlik edebilecektir.

Anahtar Kelimeler: Jeotermal Enerji, Reaktif Taşınım Modellemesi, CO_2 Enjeksiyonu, Rezervuar Modellemesi, TOUGHREACT

to my mother and father

ACKNOWLEDGMENTS

I would like to express my gratitude and regards to my supervisors Prof. Dr. Serhat Akın and Dr. Selçuk Erol for their patience, guidance and support during this study.

I would like to thank my colleagues in Petroleum and Natural Gas Engineering department for their technical and morale supports.

I also would like to thank my parents, Şenol İlgin and Ayfer İlgin for their continuous and loving support. I must express my gratitude to Elif Aydemir for the support and encouragement that she provided me for years.

This work is supported by GECO Project, funded by the European Union's Horizon 2020 research and innovation programme under grant agreement No. 818169 .

TABLE OF CONTENTS

LIST OF TABLES

TABLES

LIST OF FIGURES

FIGURES

LIST OF ABBREVIATIONS

ABBREVIATIONS

CGUESS	Provisional concentration of a species
CTOTAL	Total concentration that a species can reach
CWET	Wet heat conductivity
DFN	Discrete fracture network
ECM	Effective continuum method
EOS2	Equation of state module 2 in TOUGHREACT
FIP	Fluid in place
HDR	Hot dry rock
MINC	Multiple interacting continua
NCG	Non-condensable gases
PERM	X-Y permeability
SPHT	Specific heat

LIST OF SYMBOLS

SYMBOLS

A	Cross-sectional area (m^2)
A_r, A_m	Mineral reactive surface area ($m^2\ m^{-3}$), ($m^2_{mineral}\ kg^{-1}_{water}$)
H	Formation thickness
k	Kinetic rate (mol $m^{-2}\ s^{-1}$)
P	Pressure (Pa)
S	Species
T	Temperature (°C)
u	Fluid velocity (cm s^{-1})
ρ	Density (kg m^{-3})
ϕ	Porosity
μ	Fluid viscosity (mPa s)
k	Permeability (m^2) (Darcy)

CHAPTER 1

INTRODUCTION

As the human population in the world increases, demand for the energy considerably increases as well. Increasing energy demand at all levels of society has also increased demand of sustainable and renewable energy sources. Although fossil fuels like coal, petroleum and natural gas have been dominating energy market for decades, it is obvious that sustainable and renewable energy sources will dominate the energy market in the future.

One of the renewable energy sources is geothermal energy, which will be the subject of this thesis. The name geothermal comes from combination of two Greek words geo and thermal, which mean earth and heat, respectively. Geothermal can be described as heat extracted from earth itself. The heat may result from the formation of the earth, which includes magmatic heat sources and radioactive decay of the minerals. There are two techniques to harness geothermal power as a energy source. The first one is the direct use of geothermal energy such as heating of houses or greenhouses. The second one is producing electricity via a power plant[1].

The most important parameter that differs for geothermal energy compared to other renewable resources is sustainability. Geothermal energy does not depend on other environmental factors whereas other renewable resources like solar and wind energies are prone to weather changes. Thus, producing electricity using geothermal energy sounds very attractive due to its availibility.

1.1 Statistics of Geothermal Energy

Electricity production from geothermal energy started in Italy with a 10 kW generator in 1904. Hundred years after it started, geothermal energy has grown to 8904 MW in 25 countries [2]. According to BP's statistics [3], it has grown to more than 13.9 GW in 2020 (Table 1.1). Geothermal energy in Turkey has the largest addition by 232 MW due to attractive incentives such as guaranteed sales at 10.5 ¢/kwh. The US has the largest capacity with 2.6 GW followed by Indonesia with 2.1 GW, Philippines with 1.9 GW and Turkey with 1.5 GW.

												Growth rate per annum		Share
Megawatts	2009	2010	2011	2012	2013	2014	2015	2016	2017	2018	**2019**	2019	2008-18	2019
Mexico	965	965	887	824	823	813	906	926	926	951	**936**	-1.6%	-0.1%	6.7%
US	2382	2405	2409	2592	2607	2514	2542	2517	2483	2541	**2555**	0.6%	1.3%	18.3%
Total North America	3347	3370	3296	3416	3430	3327	3448	3443	3409	3491	**3491**	0.0%	0.9%	25.1%
Chile	–	–	–	–	–	–	–	–	24	48	**40**	-17.3%	–	0.3%
Costa Rica	166	166	218	218	218	218	217	207	207	207	**262**	26.6%	2.2%	1.9%
El Salvador	204	204	151	204	204	204	204	204	204	204	**204**	–	–	1.5%
Guatemala	54	54	54	54	49	49	49	49	49	49	**52**	5.7%	–	0.4%
Honduras	–	–	–	–	–	–	–	–	35	35	**35**	–	–	0.3%
Nicaragua	88	88	88	165	155	155	155	155	155	155	**153**	-0.8%	5.9%	1.1%
Other S. and Cent. America	15	15	15	15	15	12	15	15	15	15	**15**	♦	-0.4%	0.1%
Total S. & Cent. America	527	527	525	656	641	637	640	629	689	713	**761**	6.8%	3.1%	5.5%
Croatia	–	–	–	–	–	–	–	–	–	10	**10**	–	–	0.1%
France	0	0	16	15	16	16	16	16	16	16	**16**	–	–	0.1%
Germany	8	8	8	12	24	29	29	33	32	36	**42**	16.7%	28.2%	0.3%
Iceland	575	575	665	665	665	665	665	663	708	753	**753**	–	2.7%	5.4%
Italy	695	728	728	728	729	768	768	767	767	767	**800**	4.3%	1.3%	5.7%
Portugal	25	25	25	25	25	25	25	25	29	29	**29**	–	1.5%	0.2%
Turkey	77	94	114	162	311	405	624	821	1064	1283	**1515**	18.1%	45.6%	10.9%
Other Europe	1	1	1	1	1	1	1	1	4	4	**4**	♦	16.0%	♦
Total Europe	1381	1431	1557	1608	1771	1909	2128	2325	2620	2898	**3169**	9.4%	8.3%	22.7%
Russian Federation	81	81	81	81	79	78	78	78	74	74	**74**	–	-0.8%	0.5%
Total CIS	81	81	81	81	79	78	78	78	78	78	**74**	-5.1%	-0.3%	0.5%
Ethiopia	7	7	7	7	7	7	7	7	7	7	**7**	–	–	0.1%
Kenya	163	198	198	206	206	366	619	663	673	663	**823**	24.1%	17.9%	5.9%
Total Africa	170	205	205	213	213	373	626	670	680	670	**830**	23.9%	17.4%	6.0%
China	25	24	26	26	26	26	26	26	26	26	**26**	–	0.4%	0.2%
Indonesia	1189	1189	1226	1336	1344	1404	1439	1644	1809	1946	**2131**	9.5%	6.3%	15.3%
Japan	535	537	537	512	512	508	516	526	481	482	**525**	8.9%	-1.0%	3.8%
New Zealand	633	731	731	731	813	924	941	941	941	965	**965**	–	5.0%	6.9%
Philippines	1847	1847	1847	1847	1847	1916	1916	1916	1916	1928	**1928**	–	0.4%	13.8%
Papua New Guinea	56	56	56	56	56	56	56	56	56	56	**56**	–	–	0.4%
Other Asia Pacific	†	†	†	†	†	†	†	†	†	†	**1**	251.5%	-1.9%	♦
Total Asia Pacific	4285	4384	4423	4508	4597	4834	4894	5109	5229	5403	**5632**	3.8%	2.8%	40.2%
Total World	**9791**	**9998**	**10088**	**10482**	**10731**	**11159**	**11814**	**12255**	**12704**	**13253**	**13931**	**5.1%**	**3.6%**	**100%**

Table 1.1 Geothermal Power Capacity of the Countries in 2020 [3]

1.2 Geothermal Energy in Turkey

As discussed in last section, Turkey has a considerable potential for geothermal energy. Due to tectonic activities and geological structure of the western part of Turkey, geothermal potential of Turkey is considerably high.

According to MTA (General Directorate of Mineral Research and Exploration), there are 110 geothermal fields in Turkey, which are mainly located in Western Anatolia (78%), Northern Anatolian (7%) fault zone, Central (9%) and Eastern Anatolian (5%) volcanic regions. A considerable amount (90 %) of the geothermal resources are low to medium enthalpy, which are suitable for direct usage; however, 10 % of them are suitable for electricity generation.[4] Reservoir temperatures of Turkish geothermal fields vary between 22.5 °C and 220 °C. Among these fields, thirteen of them are considered to be suitable for electricity production. Reservoir temperatures and possible electricity generation potentials are shown in the table below.[5]

Table 1.2 Turkey's geothermal sites and their temperatures[5]

Geothermal Region	Temperature (°C)
Kizildere	200-242
Aydın-Germencik	200-232
Alaşehir-Kavaklıdere	213
Salihli Göbekli	182
Canakkale-Tuzla	174
Aydin-Salavatli	171
Kutahya-Simav	162
Izmir-Seferihisar	153
Salihli-Caferbey	150
Aydin-Sultanhisar	145
Aydin-Yilmazkoy	142
Izmir-Balcova	136
Izmir-Dikili	130

From 2002 to 2019, significant investments and developments in geothermal energy have occurred in Turkey. According to MTA's statistics,[4]

- In 2002, 500,000 m^2 of greenhouses were heated but, in 2019, it reached to 4,052,000 m^2.
- Residential heating had been increased to 125,000 houses from 30,000 houses.
- Electricity production increased to 1500 MWe from 15MWe with an increase of 100 folds.

These statistics and data show importance of the geothermal energy in Turkey and her effort for embracing renewable resources.

1.3 NCG Production in Geothermal Power Plants

Non-condensable gases (NCG), such as sulfur oxide, carbon dioxide, methane, ammonia, hydrogen sulfide, hydrogen, are gaseous emissions that are found dissolved in the geothermal water. Since NCG have low boiling point, they do not condense at surface conditions and remain as gas. In geothermal brine, carbon dioxide, sulfur oxide, methane, hydrogen sulfide and hydrogen may be present. Presence of NCG has two main consequences; the first one is environmental and the second one is operational. Exhausting NCG to the atmosphere means that the gases, which create greenhouse effect are released directly. Existence of NCG in the power plant may decrease the power output due to gas accumulation in condenser. [6]

Utilization of geothermal energy for power can cause non-condensable gas emissions, which consist of greenhouse gases. Geothermal fluid naturally may contain NCG, which is dominated by CO_2. [7] Even though NCG production from a geothermal power plant may be lower than a traditional coal power plant, amount of the NCG can reach considerable amounts, which can be considered as a counter argument for counting geothermal as a green energy.

NCG content may vary depending on chemical composition of the reservoir rock. Bertani and Thain [8] stated that average global CO_2 emission factor due to geothermal power production is 122 g/kWh. When different reservoirs in different countries are observed, Iceland has an average emission of 34 g/kWh, whereas California has an average emission of 107 g/kWh. Moreover, there are some countries with an emission significantly larger than the global average. In Italy, the average emission change between 100 and 950 g/kWh. Start-up emissions in Turkey, can reach to 1,300 g/kWh. Italy and Turkey have larger average emissions as the carbonate bearing reservoir rocks contain higher carbonate. The start-up geothermal emission values in Italy and Turkey could be higher than the emission factor of a typical coal power plant. [7] Therefore, reinjection of NCG, which is the major research topic of this thesis is important to overcome high emission factors.

1.4 Capturing Process of NCG in Geothermal Fields

When the brine is utilized at the power plant, it loses its heat and pressure to generate electricity. A considerable amount of NCG is separated from gas-water mixture. Traditionally, the separated NCG is exhausted to the atmosphere and as expected, the emitted NCG contribute to greenhouse effect. The initial step to reinject NCG is capturing it. There are several methods to capture H_2S and CO_2 [9, 10]

- Water absorption
- Amine absorption
- Amine/ low temperature hybrid concept
- The Claus Process
- Liquid redox sulfur recovery
- Burn/scrub process

After suitable and well-designed capturing methodology, the next step is designing operational surface facilities such as compressors and wellhead. A suitable compressor and a pump should be selected to provide adequate mixing of NCG with brine.

After the operational calculations and design, the possible consequences of NCG reinjection in the reservoir should be evaluated with numerical simulation. How the reinjection will affect the reservoir performance and what reactions or interactions it will create in geochemical manners should be studied using simulations.

This study aims to create a generic geothermal NCG injection and production doublet model with well defined conditions operating in a typical geothermal reservoir located in Western Turkey. The developed reservoir simulation model will be used to show how NCG injection affects geothermal reservoirs, which consist of metamorphic rocks with different mineral composition. Sensitivity of several petrophysical and geochemical parameters will be conducted to reveal important parameters and factors that should be accounted while injecting NCG.

CHAPTER 2

LITERATURE REVIEW

To model CO_2 injection in a geothermal reservoir and assess changing geochemistry due to injection, previous studies have been evaluated for understanding injection conditions, rock properties that are suitable for mineralization, reaction rates of the minerals and conditions that are affecting precipitation and dissolution.

The most important element of an analysis to target a geothermal well or assess resource capacity is a geothermal conceptual model developed with the available geological and geophysical information. The conceptual model should be properly implemented in the simulation model, which can be used to plan future operations and understand the consequences of different operations.

There are several parameters and data that should be accounted for while modeling a geothermal reservoir. These parameters are: rock properties, geothermal fluid properties, geological parameters and heat source characteristics. A numerical reservoir model should be calibrated both in static and dynamic stages. Static model gives distribution of temperature, pressure as well as fluid saturations in equilibrium. Dynamic model on the other hand, includes well operations, changing production and injection rates as a function of time. Dynamic model outputs well performance changes and its corresponding effect on the dynamic state created by fluid flow in the reservoir.

2.1 Previous Studies on CO_2 Injection in Geothermal Reservoirs

CarbFix1 is a pioneering project that aims to reduce CO_2 emissions via CO_2 sequestration into basaltic geothermal reservoir and prevent global warming. Both experimental and simulation studies were conducted for CO_2 and basalt interaction

as well as several effects such as pH and temperature effect on CO_2 and rock interaction [11]. CO_2 is injected in aqueous phase so that resulting brine in the geothermal reservoir is acidic. Thus, acidic brine reacts with basaltic reservoir rocks, resulting sequestration of CO_2 in the reservoir by means of mineral deposition. CO_2 forms carbonates in suitable reservoir rock with time and it is found out that within 2 years 95% of the injected CO_2 had been mineralized [11]. In Figure 2.1, it is explained how CarbFix technology works. Carbonated water is acidic, and it reacts with rocks which releases elements like calcium, magnesium and iron. Those elements are the main cations for carbonate minerals. Over time, those cations and dissolved CO_2 form carbonates.

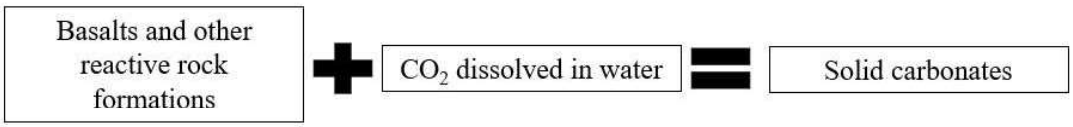

Figure 2.1 How CarbFix technology Works

The critical condition in CarbFix project is the rock. Basaltic rocks are highly reactive and contain elements needed for carbonate mineralization. Comparing metamorphic rocks which are studied in this study with CarbFix results is an objective of the study.

In 2009, Kaieda et al.[12] presented a CO_2 sequestration study in a HDR geothermal site in Japan. In HDR geothermal sites, water is not naturally present in the reservoir, however, magma heats the dry rock. Since the reservoir rock is granite at a temperature of 200°C, the findings are crucial for this study, where CO_2-water mixture will be injected to the reservoir to study possible CO_2 sequestration in metamorphic rocks. Two experimental study were presented in the paper where dissolved CO_2 has a weight fraction 1% and 3%. In both experiments, it was seen that Ca ion amount increased rapidly then decreased. Increase was due to Ca-feldspar

dissolution and decrease was due to calcite precipitation according to stereo microscope.

Carbfix2 project started in 2014 based on the experience gained from CarbFix. Then in 2018 four different geothermal sites in Europe were studied at the framework of Geothermal Emission Control (GECO) project, which aims geothermal power generation with less greenhouse gas emissions. As stated in section 1.3, geothermal power generation usually results in CO_2 emissions, basically due to extracted brine containing dissolved CO_2. The developed technology and methodology facilitate to re-use the emitted CO_2 from the power plant either to enhance the pressure or to store CO_2 in the reservoir. The project includes several partners and contributors from different countries. Four demo-sites from four different countries will be used to inject and monitor CO_2. GECO tries to extend the methodology developed in CarbFix to different reservoir geologies such as sandstones and carbonates. Evaluation of reactions between different reservoir rocks and brine with CO_2 is one of the major targets of the project[13].

Another research about NCG injection in a geothermal reservoir has been conducted in Umurlu geothermal field in Turkey by Yücetaş et al [14] who provided a patented NCG injection system and a well model for NCG injection. The aim of their study was to decrease the CO_2 emission rate by injecting emitted CO_2 back to the reservoir. Yücetaş et al. [14] stated that it is possible to inject CO_2 back to the reservoir at 10 tons/hour. However, the injection rate was determined without making any geochemical calculation or modelling study. Field data and well measurements were considered to calculate NCG injection rate in the pilot field study. Injecting CO_2 provides not only lower rate of emission but also increased reservoir and power plant performance due to increase in reservoir pressure.

2.2 Data Acquisition and Petrophysical and Geological Parameters

There are different parameters that should be introduced as input to a numerical model. These parameters can be described as field-wise or grid-wise. To simplify a model, parameters can be introduced in a larger domain; however, detailed grid-wise introduction of parameters will give more detailed and accurate results, but simulation time would be longer. Introducing these parameters to the numerical model properly plays a key role in reservoir modeling since better description would give better results.

2.2.1 Petrophysical and Geological Properties

Petrophysical properties are the properties of rock. They can be listed as reservoir layer thickness, lithology, porosity, fluid saturation and permeability.

2.2.1.1 Lithology

Lithology or rock type means the composition of rock. It describes the rock's depositional history, mineralogy, and pore structure. [15] During geochemical modeling, lithology of the rock plays an important role since the chemical reactions and mineral activities depend on the composition. For instance, marble is composed of primarily $CaCO_3$ and may contain clay minerals.

2.2.1.2 Porosity

Porosity is defined as the ratio of pore volume to overall (bulk) volume. It can be expressed as fraction or percentage. Porosity is one of the important parameters in reservoir description, since it controls the maximum volume of reservoir fluid. Porosity can be counted as a characteristic feature of a certain rock type. For example, sandstone porosity varies between 5% and 40%. On the other hand,

carbonate porosity is somewhat lower but in the presence of natural fractures, the overall porosity may increase considerably. [16]

$$\phi = \frac{V_{pore}}{V_{bulk}} \qquad \text{(Eq. 2.1)}$$

2.2.1.3 Permeability

Permeability is the measurement of a rock's capacity to flow, measured in Darcies, which is defined by Henry Darcy. Permeability reveals level of communication of interconnected pores, which can change for different rock types. Absolute permeability can be described as single-phase fluid's permeability measurement in a rock; however, effective permeability can be described as a particular fluid's permeability where other immiscible fluid exists. Moreover, relative permeability is the ratio of effective permeability to absolute permeability.[17]

2.2.1.3.1 Cubic Law

Cubic law is one of the permeability models and it is used to define fracture permeability using different porosity values. Cubic law can be expressed using the following equation: [18]

$$k(t) = k_0\left(\frac{\phi(t)}{\phi_0}\right)^n \rightarrow \text{cubic-law } = k(t) = k_0\left(\frac{\phi(t)}{\phi_0}\right)^3 \qquad \text{(Eq. 2.2)}$$

where,

k_0 is the initial permeability

ϕ_0 is initial fracture porosity

n is empirical exponent

Luquot et al. [19] supports the idea that n is constant for a particular rock type whereas Smith et al. support the idea that n can be different for the same rock type. TOUGHREACT's approach, which is used to develop the geochemical model, is

consistent with Luquot and Gouze's model [20]. Another parameter that can affect n is fluid composition that is reacting with rock. According to Noiriel et al. [21], Luhmann et al. [22], and Hao et al. [23], existence of CO_2 alone or CO_2-brine solution can affect permeability and porosity because rock-fluid interaction in sedimentary rocks is variable.[18]

2.3 Mathematics of Geochemical Modeling

Mathematics of numerical modeling includes governing equations and disciplines for geochemical modeling such as flow equations, heat equations and chemical reactions. For geochemical modeling or reservoir modeling of a geothermal reservoir, physical and chemical laws should be stated in a mathematical discipline where equations can be solved with algebraic expressions.

2.3.1 Material Balance (Conservation of mass)

The mass should be conserved in a grid for given time. Munson et al. explains conservation of mass (the continuity equation) using a nondeforming volume and differential equation as shown in (Eq. 2.3). [24]

$$\frac{D}{Dt}\int_{sys}\rho d\forall = \frac{\partial}{\partial t}\int_{cv}\rho d\forall + \int_{cs}\rho \mathrm{V}\cdot \hat{\mathrm{n}} dA \qquad \text{(Eq. 2.3)}$$

where,

$$\int_{sys}\rho d\forall = M_{sys} \qquad \text{(Eq. 2.4)}$$

The formulation gives the general idea of conservation of mass; however, Kleppe explains material balance using porous material considering single fluid with density of ρ flowing at constant rate *u* [25]. Figure 2.2 explains a flux in a porous medium at a given distance. Figure 2.3 explains material balance schematically.

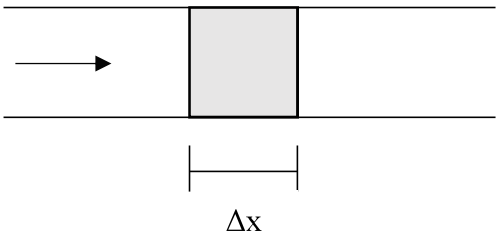

Figure 2.2 Element illustration in a porous medium [25]

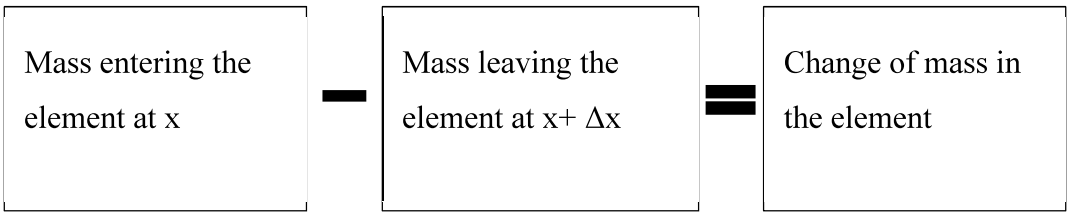

Figure 2.3 Material balance illustration [25]

Considering porosity, Kleppe presents the equation of material balance as shown in (Eq. 2.5). [25]

$$\{u\rho A\}_x - \{u\rho A\}_{x+\Delta x} = \frac{\partial}{\partial t}\{\phi A \Delta x \rho\} \qquad \text{(Eq.2.5)}$$

Where,

u is velocity (m/s)

ρ is density (kg/m^3)

A is area (m^2)

ϕ is porosity

2.3.2 Flow and Transport Equations in Porous Media (Conservation of Momentum)

Darcy is the first one to come up with the explanation of fluid flow in a porous sand volume or porous media. Darcy [26] explained the flow principle in his book which is named originally as "Les fontaines publiques de la ville de Dijon" in French and translated to English as "The Public Fountains of the City of Dijon". Darcy's equation for single phase and horizontal flow is shown in (Eq. 2.13).

$$u = -\frac{k}{\mu}\frac{\partial P}{\partial x} \qquad \text{(Eq.2.6)}$$

Where,

μ is fluid viscosity (cp)

u is the velocity of fluid (cm/s)

k is permeability (darcies)

∂P/∂x pressure difference in given distance

"-" sign is to correct to negativity coming from pressure difference

There have been several theoretical developments for Darcy's equation as seen in Eq. 2.13.

Muskat [25] suggested that "n" in Forchheimer equation should be equal to 2. He also discussed mechanics of fluid flow by combining Brinkman equation both for channel flow and porous media flow. The solution can be expressed in Eq. 2.14.

$$-\frac{\partial P}{\partial x} = u\frac{\mu}{k} - \mu\frac{\partial^2 u}{\partial x^2} \qquad \text{(Eq. 2.7)}$$

The combined equation can be converted to Darcy's porous media equation or Stokes' channel flow equation by neglecting the second term and the first term in right hand side of the equation, respectively.

Numerical modeling of fluid flow equations using finite difference method are explained by Peaceman [27] and Aziz and Settari [28]. They explained how formulation (equations between Eq. 2.1 and Eq. 2.6) can be carried out using backward, central, and forward difference approximations, which were also explained in Artun [29] and Smith [30].

As mentioned before, finite element method can also be used for numerical solution of flow equations. Ewing revealed physical discussions and solutions for numerical simulation of flow equations using finite element method. Moreover, miscible and immiscible displacements of fluids were discussed as well. [31]

2.3.2.1 Fracture Flow Models

Geothermal reservoirs generally consist of fractured rocks. Therefore, fluid flow occurs in high permeable fracture networks. The geothermal fluid exchanges heat with the surrounding rock to enhance the production performance. [32]

Fracture flow can be modeled by combining Darcy's law and Stokes' equation for channel flow. Darcy's law is valid for matrix flow whereas Stokes' equation is valid for fracture flow where matrix blocks are interconnected to fracture networks. However, equations and parameters to be used for fracture flow models should be constructed following physical principles.

2.3.2.1.1 Effective Continuum (Effective Porous Medium) Method

Effective Continuum Method (ECM) can be described as the easiest way to model fractured reservoir fluid flow. According to Pankow et al. [33] and Neumann [34], fracture scale is so large that it can be treated as a homogeneous medium with

effective porosities. Since it is treated as a porous media, Darcy's equation is valid. [35]

Conditions for using effective continuum method are:[36]

- High fracture density
- Randomly distributed fracture orientations
- Fracture apertures with random widths
- Large reservoir domains (regional extension)

The ECM approach is widely used because of its simplicity in defining a regional fractured rock system. It should NOT be compared to small-scale models as, regional scaled models have much more potential to be successful in this method. [37]

2.3.2.1.2 Dual and Multiple Continuum Method

Dual and multiple continuum models are one of the most commonly used methods for modeling fractured media. a special form of double porosity model was introduced by Barenblatt et al. [38]. It has been further developed to include dual permeability and multi porosity models by Warren and Root [39].

An enhanced version of this method is MINC (multiple interacting continua) model [40]. The difference between the classical dual porosity and multiple interacting continua model is porosity and permeability variance in the reservoir model. Dual porosity model includes a main domain, which has lower permeability and high porosity, and a secondary unit which has higher permeability and lower porosity representing a fracture. On the contrary, multi porosity model may include several different porosity and permeability data according to fracture features where fractures with different properties can be defined. [35]

2.3.2.1.3 Discrete Fracture Network (DFN) Method

In essence, DFN method is similar to dual continuum models, but the difference from dual continuum approach is that one of the mediums is impermeable while permeable one is representing fractures. DFN method defines every fracture one by one, which gives a fracture network with impermeable layers in it. Since every fracture is defined individually using properties like fracture density, aperture, and location, a long duration is needed for creation of the DFN model as well as its simulation. However, if fractures are well approximated, DFN models give accurate information and results for the flow characterization of a reservoir. [35]

2.3.3 Heat Balance (Conservation of Energy)

The heat and flow should be considered together in geothermal reservoirs since it directly affects dynamics of the reservoir.

Thermodynamical definition of energy is that it cannot be created or destroyed following the first law of thermodynamics. Moreover, change in energy of a system must be equal to subtraction of energy amount entering to the system and energy amount exiting the system (Eq. 2.8).

$$E_{in} - E_{out} = \Delta E \qquad \text{(Eq.2.8)}$$

In a geothermal system, the internal energy change in a representative volume V must be equal to sum of heat transfer by fluid flow and heat transfer by conduction and gaining energy from sinks and sources. [32]

2.3.4 Boundary Conditions

In numerical modeling there are two main boundary types which are Dirichlet and Neumann boundary. Dirichlet boundary refers to constant pressure or heat at the boundary on the other hand, Neumann boundary refers to constant flux rate or heat flux at boundary conditions. Boundary conditions are the main initiators of fluid flow

calculation in grids. They can be expressed mathematically as seen between (Eq. 2.9) and (Eq. 2.12) [25]

Dirichlet boundary:

$$P(x = 0, t > 0) = P_{bh} \quad \text{(Eq. 2.9)}$$

$$P(x = L, t > 0) = P_R \quad \text{(Eq. 2.10)}$$

Neumann boundary:

$$Q_{bh} = -\frac{kA}{\mu}\left(\frac{\partial \mathrm{P}}{\partial \mathrm{x}}\right)_{x=0} \quad \text{(Eq. 2.11)}$$

$$Q_R = -\frac{kA}{\mu}\left(\frac{\partial \mathrm{P}}{\partial \mathrm{x}}\right)_{x=L} \quad \text{(Eq. 2.12)}$$

2.4 Geochemical Modeling of a Geothermal Reservoir

Geochemical modeling of a geothermal reservoir can be described as modeling using thermodynamics and chemical reactions while considering heat and fluid transport in a system where temperature, pressure, and geology is heterogenous with changing depth and area.

TOUGHREACT is the first non-isothermal reactive transport model based on existing TOUGH2 flow code. [40] Architecture of geochemical modeling using TOUGHREACT and TOUGH2 are shown in Figure 2.4. [41]

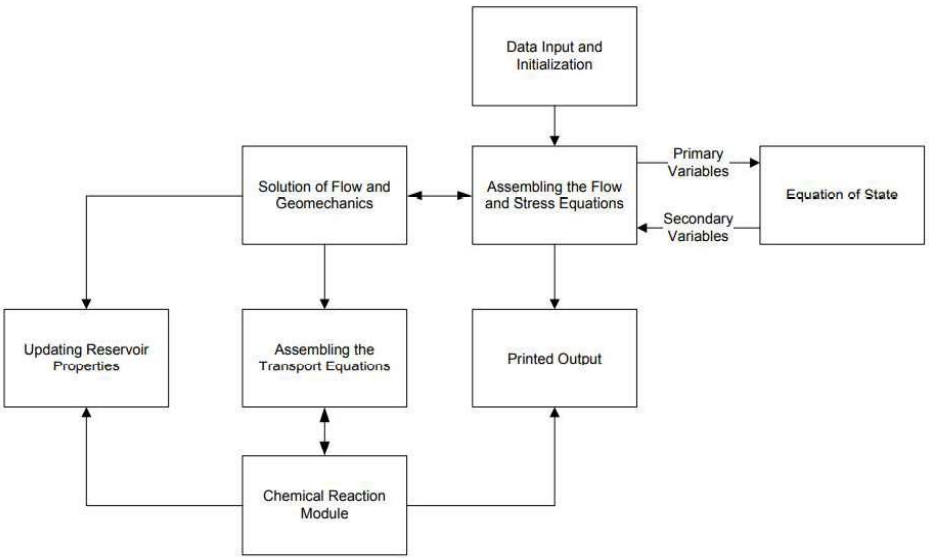

Figure 2.4 Geochemical modeling architecture[41]

Geochemical modeling includes solution of transport and flow equations with chemical reaction module. Therefore, by coupling flow, heat transport and reactive transport, geochemical model is obtained. Stress and geomechanics equations are ignored (i.e. not computed) in this study, since rock expansion and stress factors are not needed in reactive transport models (Figure 2.4). Enabling these can cause excessive run times.

2.4.1 Major Processes and Features

To completely define appropriate chemical system and achieve seamless computation, initial (primary) species should be defined [42]. Thus, model could be calibrated accordingly, and simulation would proceed. The other species defined in the model should be considered as secondary species that include aqueous species, species that will precipitate and dissolve later as a result of the reaction [43] [44].

TOUGHREACT considers reactive transport of minerals and transport of species by advection and diffusion. The software will then proceed either with mineral

dissolution or precipitation defined by local equilibriums. The main features of TOUGHREACT are: [45]

- Gas phase can be introduced in the model with liquid solution both in porous media and fractured rock for heat and mass flow, and chemical reactions.
- The possible effects of heat change are considered since geochemical and thermophysical properties can change.

2.4.2 Governing Equations in Geochemical Modeling

The main principles that geochemical modeling utilizes for multi-phase fluid flow, and reactive transport are shown in Figure 2.5. [45] The other laws that are discussed in numerical model section are also valid in geochemical modeling, since they originate from the same physical foundation. Moreover, geochemical modeling includes all of the aforementioned principles. Steefel [46] explained conservation of mass, conservation of momentum, conservation of solute mass and conservation of energy and their coupling as seen in Figure 2.5.

In Figure 2.5, 5 different couplings of equations are discussed for a single-phase reactive transport system:[46]

1. Coupling of conservation of energy and conservation of momentum describes heat effect on fluid.
2. Coupling of conservation of momentum and conservation of mass describes flow.
3. Coupling of conservation of mass and conservation of solute mass describes dissolution and precipitation with solute concentration.
4. Coupling of conservation of solute mass and conservation of momentum describes mineral dissolution and precipitation with porosity and permeability given by solid matrix and solute concentration.
5. Coupling of conservation of solute mass and conservation of energy describes temperature effect on mineral reaction kinetics.

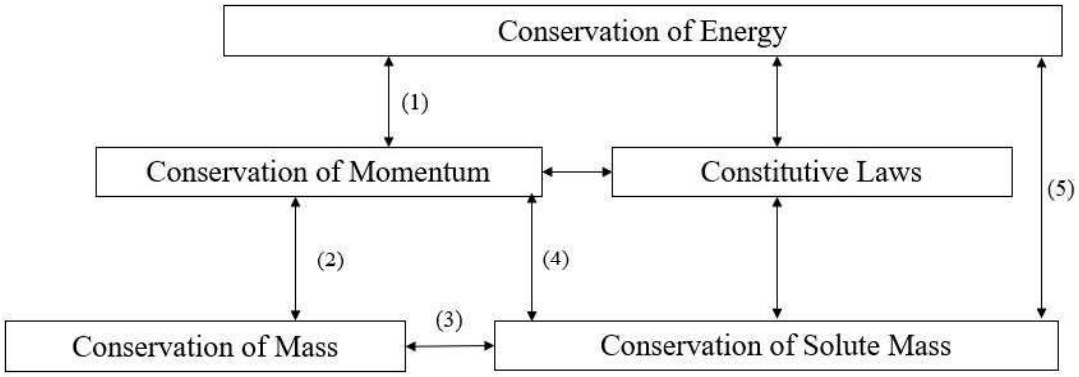

Figure 2.5 Conservation of mass, conservation of momentum, conservation of solute mass and conservation of energy and their couplings [46]

2.4.3 Chemical Reactions

In Steefel's [46] explanation, chemical reaction effect on solute transport is also defined. It basically shows how reacting minerals and aqueous compounds effect the solute transport. Basis species in a geochemical system are named as primary species, other species precipitating due to chemical reactions is considered to be secondary species. [42-44].

Secondary species number that should be accounted in solute transport depends on number of independent reactions as shown below.

$$S_i = \sum_{j=1}^{N_C} v_{ij} S_j \quad i = 1, \dots, N_R \qquad \text{(Eq.2.13)}$$

where S is species, j is the primary species index, i represents secondary species index, N_c is total number of subset of primary species, *v* represents stoichiometric coefficient and N_R is the number of reactions. [45]

2.4.3.1 Chemical Reactions During Carbon Sequestration

Carbonate mineral formation due to CO_2 injection is defined by Eq.2.21. The equation illustrates formation of some carbonate minerals such as calcite, ankerite and magnesite according to changing cation in a solution.

$$(Fe, Ca, Mg)^{2+} + CO_2 + H_2O = \underset{\text{carbonate minerals}}{(Fe, Ca, Mg)CO_3} + 2H^+ \qquad \text{(Eq.2.14)}$$

Other dissolution and precipitation reactions for clay minerals like kaolinite and muscovite are shown below, respectively.

$$Al_2Si_2O_5(OH)_4 + 6H^+ \leftrightarrow 2Al^{3+} + H_2O + 2H_4SiO_4(aq) \qquad \text{(Eq.2.15)}$$

$$KAl_3Si_3O_{10}(OH)_2 + 10H^+ \leftrightarrow 3Al^{3+} + K^+ + 3H_4SiO_4(aq) \qquad \text{(Eq.2.16)}$$

2.4.3.2 Mineral Dissolution/Precipitation Kinetics

Mineral's kinetic rates depend on secondary minerals' kinetic rates. Therefore, all of the kinetic rates should be accounted for. The parameters affecting kinetic rates are pH and temperature. Effect of temperature on kinetic rate can explained by Arrhenius equation.[44] [45]

$$k = k_{25}\exp\left[\frac{-E_a}{R}\left(\frac{1}{T} - \frac{1}{298.15}\right)\right] \qquad \text{(Eq. 2.17)}$$

Where, k_{25} is rate constant at 25 °C, E_a represents activation energy and T is absolute temperature. Moreover, effect of pH can be estimated by (Eq.2.23) (Figure 2.6).

.

$$k_{adj} = k(10^{-pHc}/10^{-pHI})^{\text{slopel}} \quad \text{if } \mathrm{pH_c} < \mathrm{pH_1}$$
$$k_{adj} = k(10^{-pHc}/10^{-pH2})^{-slope2} \quad \text{if } \mathrm{pH_c} > \mathrm{pH_2} \qquad \text{(Eq.2.18)}$$

Figure 2.6 shows calculation of reaction rate for different neutral pH mechanisms. In case of acidic and basic environments, acid and base mechanisms of minerals have to specified. Palandri and Kharaka [47] showed the acid and base mechanism of minerals, which are calculated by using experimental data and formulations for each mechanism and different minerals. One example of the mineral reaction rates is shown for clay group minerals in Table 2.1.

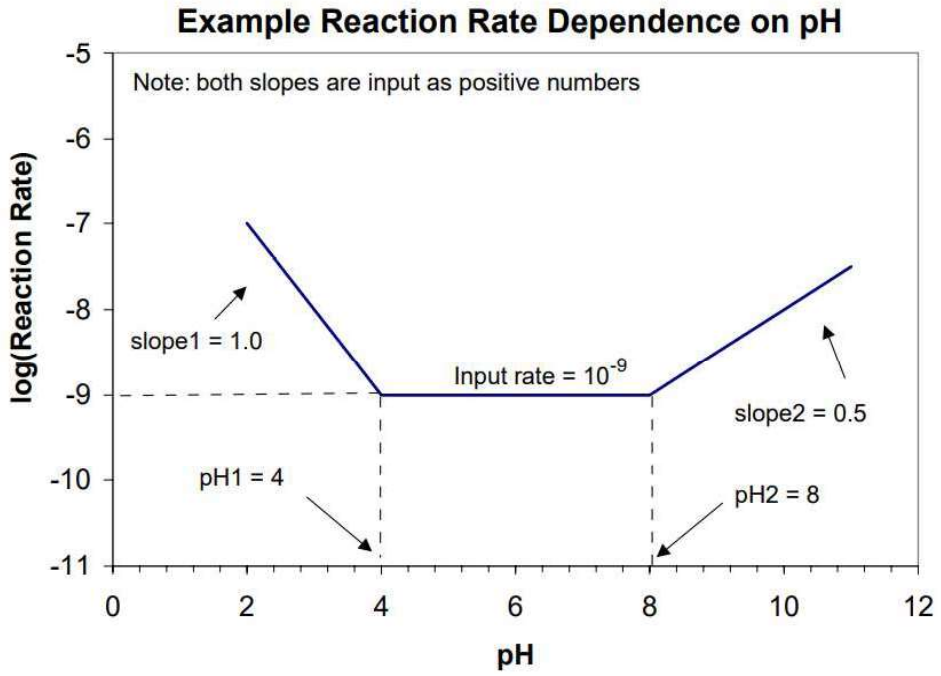

Figure 2.6 Example reaction rate (mol m^{-2} s^{-1}) of silicate minerals with changing pH [48]

Table 2.1 Example for acid and base mechanism [47]

	Acid Mechanism			Neutral		Base Mechanism		
	Log k	E	n	Log k	E	Log k	E	n
Kaolinite	-11.31	65.9	0.777	-13.18	22.2	-17.05	17.9	-0.472
Montmorilloni te	-12.71	48.0	0.220	-14.41	48.0	-14.41	48.0	-0.130
Smectite	-10.98	23.6	0.340	-12.78	35.0	-16.52	58.9	-0.400

2.4.4 Mineral Reactive Surface Area

For calculating reactive surface area in fractures, walls of the fractures are thought as surfaces filled with identical hemisphere shaped grains. Calculation of areas of the walls are related with fracture interface ratio, fracture porosity, which are based on fracture densities and fracture diameter. (Eq. 2.26) explains the reactive surface area calculation approach. [45]

$$A_r = \frac{\pi A_{f-m}}{2\phi_{f-m}} \qquad \text{(Eq. 2.19)}$$

Where, A_r is reactive surface area (m^2/m^3), $A_{f\text{-}m}$ represents fracture matrix interface ratio (m^2/m^3), $\phi_{f\text{-}m}$ represents fracture porosity.

In TOUGHREACT, a reactive surface area is calculated by using a modified form of Eq. 2.19 for each mineral such that the unit of reactive surface becomes $m^2_{mineral}/kg_{water}$.[45]

$$A_m(m^2/kg_{\text{water}}) = \frac{A_r a_{fmr}}{\rho_w \phi_f S_w} \qquad \text{(Eq.2.20)}$$

Where, ρ_w is the density of water, S_w represents saturation of the water, a_{fmr} is the factor representing reduction for water and surface area contact and ϕ_f is the fracture porosity.

For surface area calculation in the rock matrix, cubic packing of truncated sphere structure is used which is showed in Figure 2.7. This method uses grain diameters and approaching surface area of grains with open pore spaces. [49] However, in TOUGHREACT, clay minerals' grains are treated like a plate to be more realistic.[45]

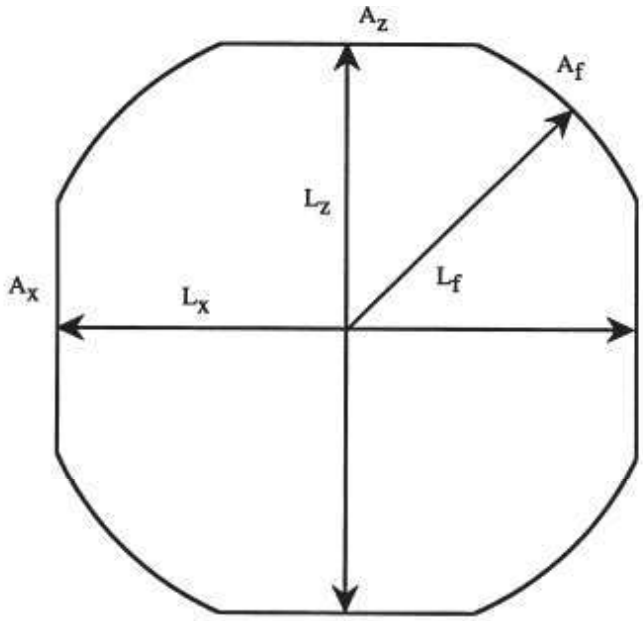

Figure 2.7 Truncated sphere model [50]

2.4.5 Database

PHREEQC is a C++ based computational program to estimate and calculate aqueous chemical reactions [51]. In geochemical modeling of CO_2-water injection, batch reaction module is used to determine secondary products and reaction kinetics. PHREEQC uses its own database; however, CarbFix database can also be implemented. PHREEQC provides observation of mineral precipitation and

dissolution. Moreover, ion exchanges, microbial reactions and other kinetic reactions can be modeled. Note that, PHREEQC is capable of only 1-D reactive transport modeling. [52]

TOUGHREACT requires well defined input data for mineral assembly including secondary minerals. Thanks to third-party databases like PHREEQC, batch reaction and reaction paths can be generated. PHREEQC provides necessary aqueous species and secondary species that are needed to define a well defined model in TOUGHREACT.

CHAPTER 3

STATEMENT OF THE PROBLEM

In Turkey, geothermal reservoirs contain considerable amounts of NCG consisting of CO_2, H_2S, NH_3, H_2, N_2, and CH_4. Among these gases, CO_2 is the most dominant one comprising 98% to 99% of the gas mixture. Re-injecting NCG into the reservoir is a proposed methodology to reduce CO_2 emissions. Re-injectingy CO_2 water mixture into the reservoir provides pressure support to the reservoir and has positive impact in terms of reservoir performance. Re-injecting NCG can lead to precipitation or dissolution of several different minerals in the reservoir rock, which can affect performance of the reservoir. A realistic simulation model should allow the reservoir rock and NCG interaction. Geothermal reservoir rocks in Turkey are predominantly metamorphic rocks with differing mineral compositions. Therefore, different mineral compositions and injection strategies should be examined to understand role and impact of NCG injection. This study aims to create a generic model with well matched conditions that will simulate how NCG injection affects reservoir rocks composed of metamorphic rocks with different mineral compositions and to demonstrate possible mineral and solution trapping of CO_2. It also aims to reveal important parameters and factors that should be accounted while re-injecting NCG.

CHAPTER 4

GEOCHEMICAL AND RESERVOIR MODEL

The reactive transport model is constructed using TOUGHREACT with TOUGH2 EOS2 module, which is developed for CO_2-water mixture. In order to develop a representative model, model construction is divided into three parts, which are static model, reactive natural state model and dynamic model. The gelogical model is based on conceptual model given in Şimşek et al [53]. The developed model is run for 100,000 years to match static pressure and temperature data collected from wells. Reactive natural state model includes a heat source and it uses static model's output as input pressure and temperature. Ractive natural state is run for approximately 100 years depending on the time for the mineral compositions reach to equilibrium. This model is used to populate the dynamic model where mineral compositions are in equilibrium. Finally, dynamic model where injection and production takes place while reactive transport is taken into account is run. Dynamic model uses static model and reactive natural state model's output as input. Three different mineral compositions representing marble, schist and marble with schist sections are used. Keeping it in mind that natural state model would be valid for all of the mineral compositions, one run of static model is necessary, since it does not consider mineral reaction kinetics but pressure and temperature. Three different reactive natural state models are constructed for three different mineral compositions. For each scenario and composition, a unique dynamic model is constructed and run accordingly. For every dynamic model, one producer and injector pair is included . Structural geology is considered to be same for every model.

4.1 Geological Structure of the Model

The simulation model is a sector model developed from a larger simulation model that was used to simulate Kizildere geothermal field. The model dimensions have been selected based on the distance between an injector and a producer. The model has a length of 2900m in X-direction and 2500m in Y-direction. The maximum depth of the model is 3820m in Z-direction. The model is divided into 25 vertical layers whose thicknesses are different. There are 355 grids in each layer, which are constructed using Voronoi gridding method so that total grid number reaches to 8375 (Figure 4.1). To decrease grid number and the simulation run time, grids are created to have larger areas closer to outer boundaries of the model. The grids have smaller areas around injection and production well to accurately capture temperature and pressure transients. This grid selection also enables identifying mineral deposition and dissolution the smallest area of a grid block is 100 m^2, whereas the largest grid block area can reach to 1900 m^2.

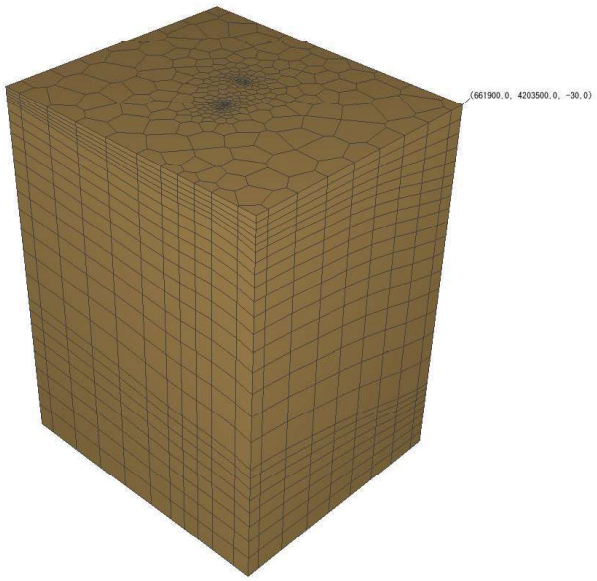

Figure 4.1 Grid structure of the model

Top reservoir boundary condition is defined at the topmost layer, as a cap rock in fixed state, where pressure is constant. A relatively large model is developed in order to guarantee that pressure or temperature transients do not reach the sides of the model. The model includes a cap rock at 700-850 m BSL with alluvial zones reaching to the surface. The top of the metamorphic reservoir rock is at 1000 m, and it reaches 3850 m at the bottom. There is a NW-SE trending highly conductive fault between two wells' drainage zones. Apart from this fault 12 other faults are placed based on Kızıldere geothermal field geology. Fault zone permeabilities are increased compared to rest of the model to get improved at the fault zones. The fault zones have different specific heats and densities. The fault distribution is shown in Figure 4.2 and 4.3.

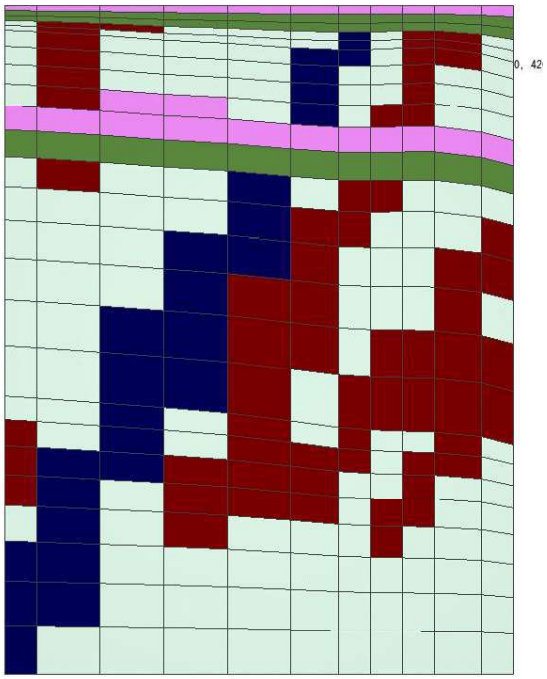

Figure 4.2 Side view of the model (X-Z plane), red represents faults, blue represents the main fault between two wells, pink represents cap rock, green represents alluvial zone and light green represents metamorphic reservoir rock

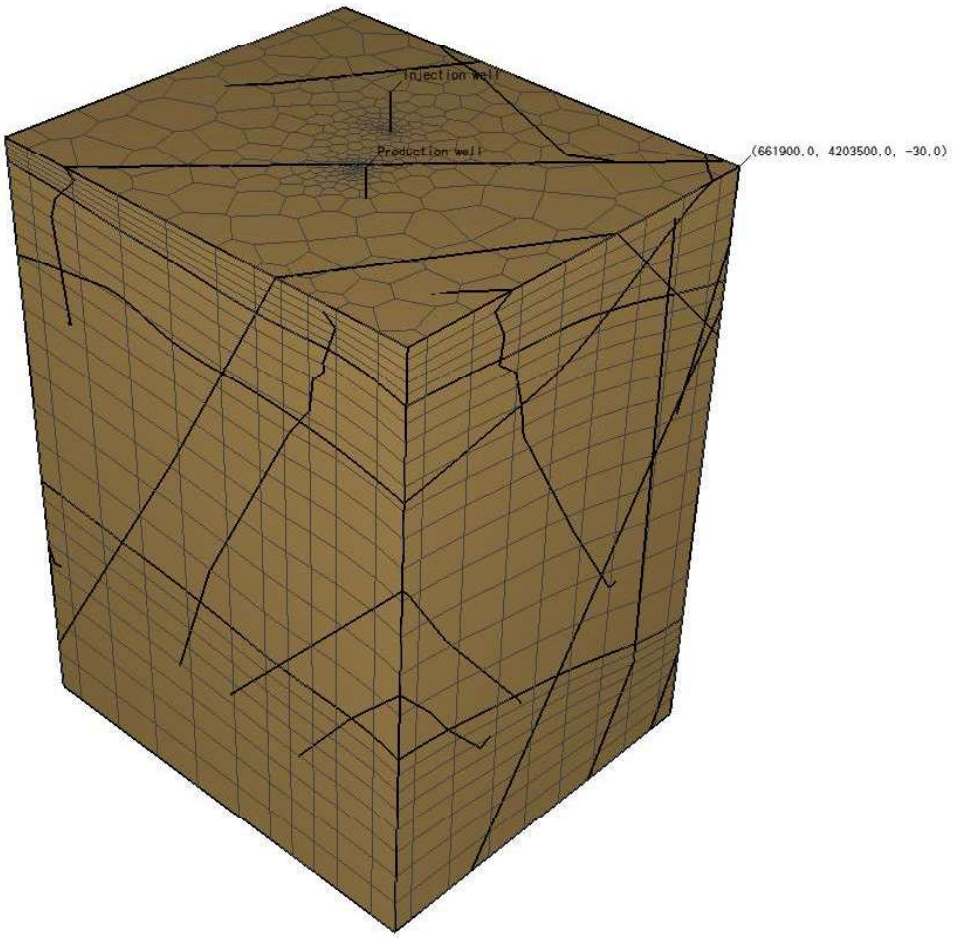

Figure 4.3 Fault distribution of the model

4.2 Rock and Fluid Parameters

Porosity of the model is constant (3%), whereas the permeability is distributed using aforementioned fault zone concept where matrix permeability is 1 mD and fault permeabilities are 2 mD and the highly conductive fault permeability is 70 mD, approximately (Figure 4.4). Other rock properties used in the model are shown in Table 4.1.

Table 4.1 Rock Properties

	Density (kg/m^3)	Porosity	PERM* (m^2)	CWET** (W/(m·K))	SPHT*** (J/(kg·K))
Cap Rock	2600	0.03	$1.0x10^{-17}$	2.0	1000.0
Alluvial	2600	0.03	$1.0x10^{-16}$	2.0	1000.0
Metamorphic	2600	0.03	$1.0x10^{-15}$	2.0	1000.0
Main Fault	2600	0.03	$7.0x10^{-14}$	2.0	1000.0
Other Faults	2600	0.03	$2.0x10^{-15}$	2.0	1000.0

PERM* represents X-Y permeability

CWET** represents wet heat conductivity

SPHT*** represents specific heat

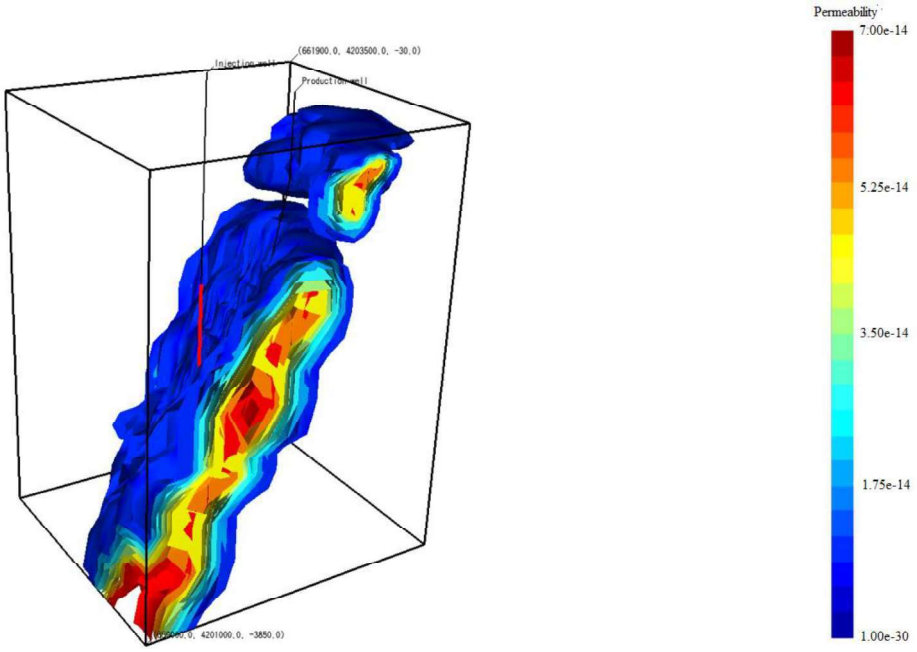

Figure 4.4 Permeability distribution

To get representative temperature data and create conductive heat flux in the model mimicking Kızıldere geothermal reservoir, a heat source is located at the bottom of

the model. A heat sink at the cap rock level is also used so that the model reaches static equilibrium (Figure 4.5).

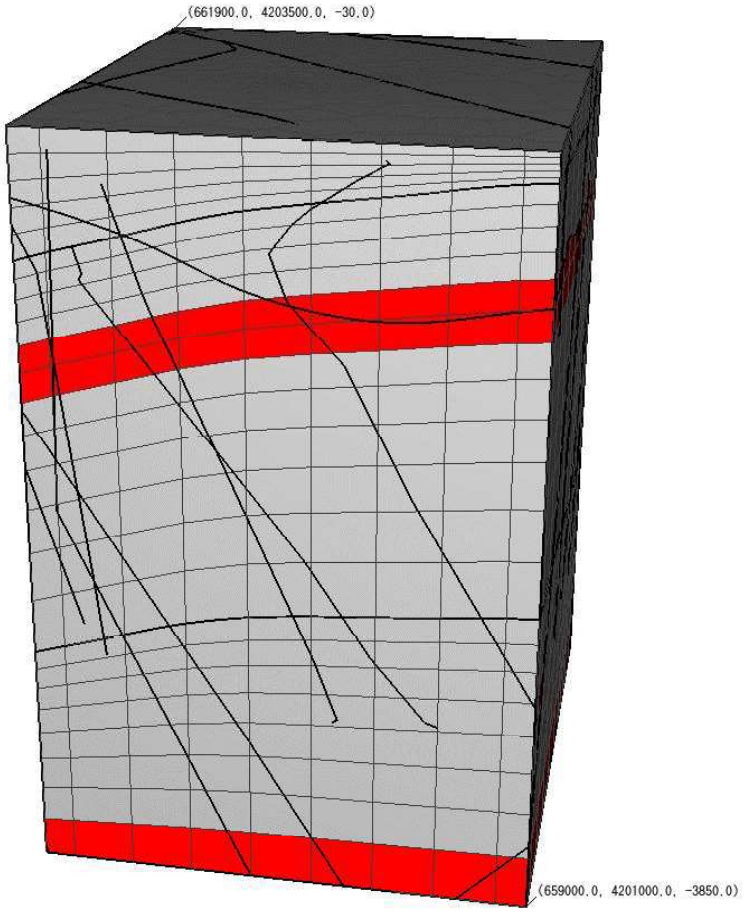

Figure 4.5 Heat sink and source representation (red grids represent the heat source and sink locations)

CO_2 content of geothermal fluid is around 3% at reservoir conditions as stated in Haizlip et al. [54]. Two different sets of water chemistry is used representing reservoir initial water and re-injection (well boundary) water respectively [55]. TOUGHREACT calculates composition of aqueous solution using two parameters, CGUESS and CTOTAL. CGUESS represents the provisional concentration of the species, whereas CTOTAL represents total concentration that can be reached with secondary species. Thus, initial water chemistry used in the model is shown in Table 4.2 and injection water chemistry is shown in Table 4.3.

Table 4.2 Initial water chemistry

Species	CGUESS(mol frac.)	CTOT(mol frac.)
AlO_2^-	1.713×10^{-5}	8.445×10^{-4}
Br^-	5.0×10^{-6}	5.65×10^{-6}
Ca^{+2}	1.166×10^{-5}	1.96×10^{-4}
Cl^-	0.001417	0.002253
F^-	9.715×10^{-4}	9.798×10^{-4}
Fe^{+2}	2.639×10^{-8}	6.639×10^{-7}
H^+	3.918×10^{-7}	1.0965×10^{-6}
HCO_3^-	0.024	0.1981
K^+	1.0×10^{-8}	3.043×10^{-8}
Li^+	3.0×10^{-4}	4.409×10^{-4}
Mg^{+2}	3.94×10^{-6}	2.577×10^{-5}
Mn^{+2}	8.788×10^{-8}	7.132×10^{-7}
Na^+	0.03162	0.0434
$NO3^-$	8.3×10^{-7}	9.67×10^{-7}
$SiO_2(aq)$	1.0×10^{-4}	0.003629

Table 4.3 Injection water chemistry

Species	CGUESS(mol frac.)	CTOT(mol frac.)
AlO_2^-	1.0×10^{-5}	3.28×10^{-5}
Br^-	3.0×10^{-6}	7.97622×10^{-6}
Ca^{+2}	1.0×10^{-4}	2.55003×10^{-4}
Cl^-	0.001	0.003476401
F^-	0.001	0.001445411
Fe^{+2}	4.0×10^{-7}	4.65616×10^{-7}
H^+	1.0×10^{-9}	2.5704×10^{-10}
HCO_3^-	0.004	0.005143033
K^+	0.001	0.004728772
Li^+	3.0×10^{-4}	5.94671×10^{-4}
Mg^{+2}	1.0×10^{-6}	7.30041×10^{-6}
Mn^{+2}	5.415×10^{-8}	7.28×10^{-7}
Na^+	0.05	0.059230265
$NO3^-$	1.0×10^{-6}	1.55161×10^{-6}
SiO_2(aq)	0.005	0.00845

4.3 Static Model

Static model is constructed using aforementioned geological structure by matching static pressure and temperature of the well pair. Moreover, initial temperature, pressure, and CO_2 composition are introduced to the model to establish a starting point for equilibrium state (natural state) (Figure 4.6-4.8). The equations that are used for initial condition are given between (Eq. 3.1) and (Eq. 3.3.), where z is depth and negative.

$$Pressure(Pa) = 2.1E6 + (-8400) \times z \quad \text{(Eq. 3.1)}$$

$$Temperature(C°) = 25.0 + (-0.085) \times z \quad \text{(Eq. 3.2)}$$

$$CO_2\ P_{partial}(Pa) = 2.0E5 + (-2800) \times z \quad \text{(Eq. 3.3)}$$

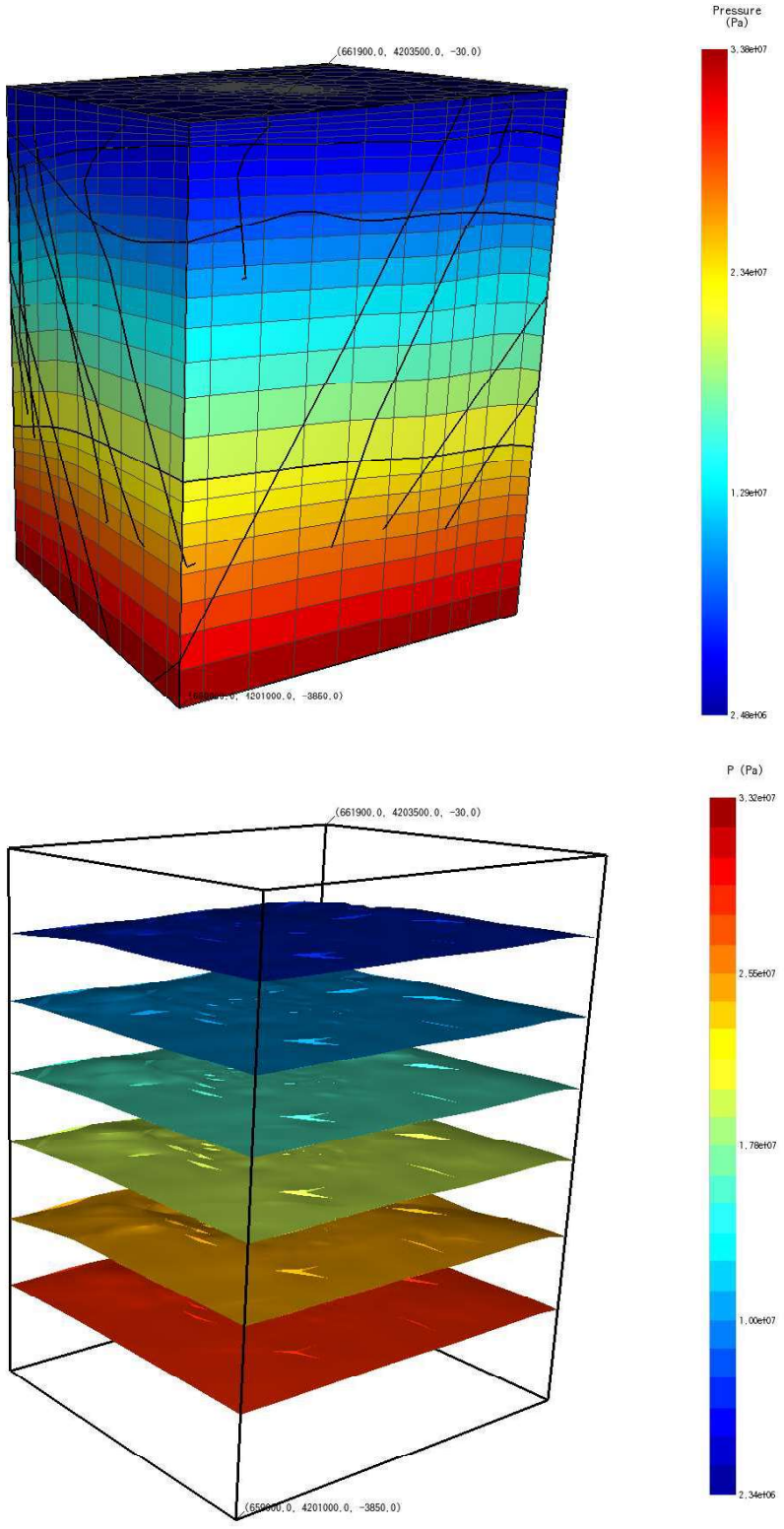

Figure 4.6 Initial pressure input illustration

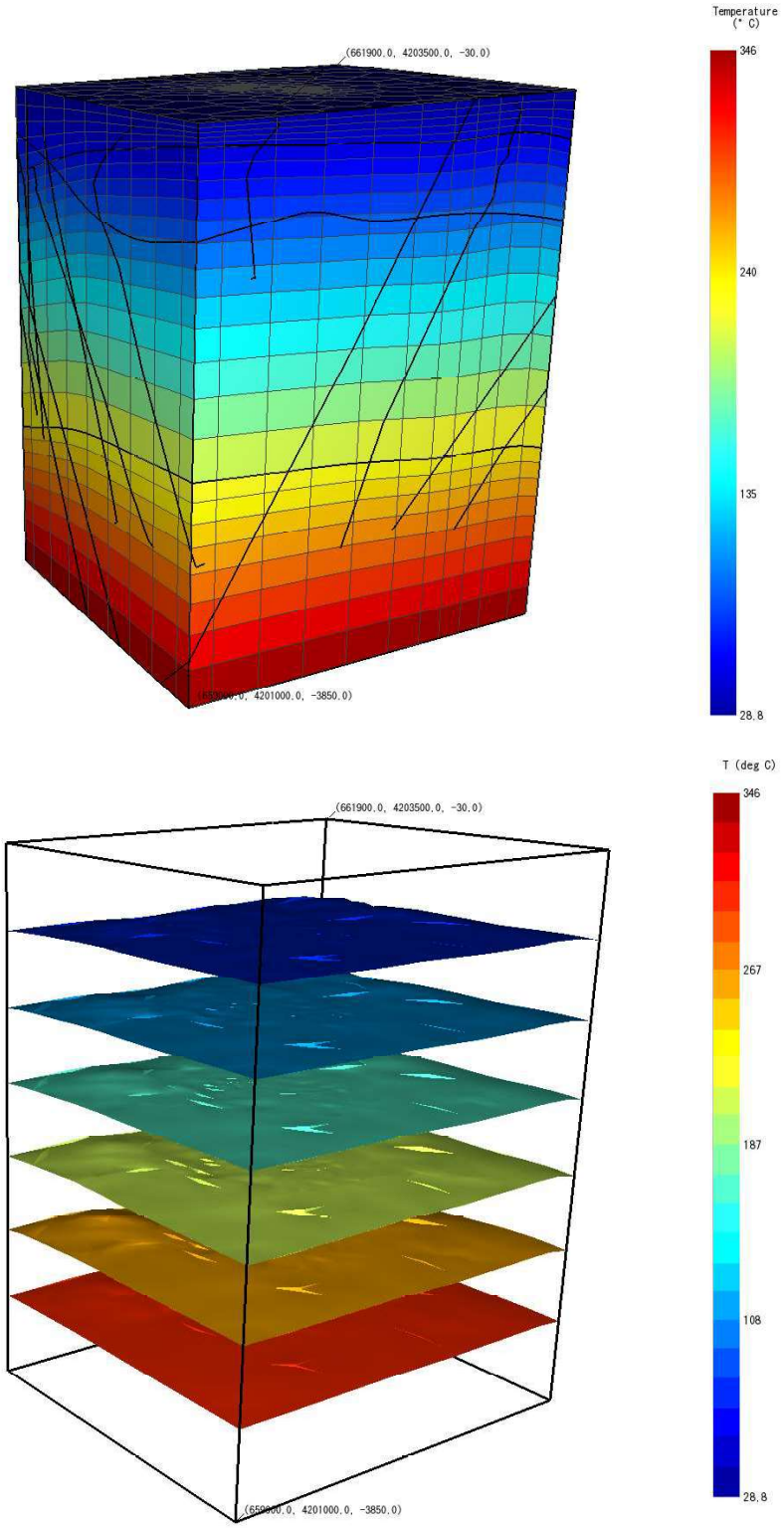

Figure 4.7 Initial temperature input illustration

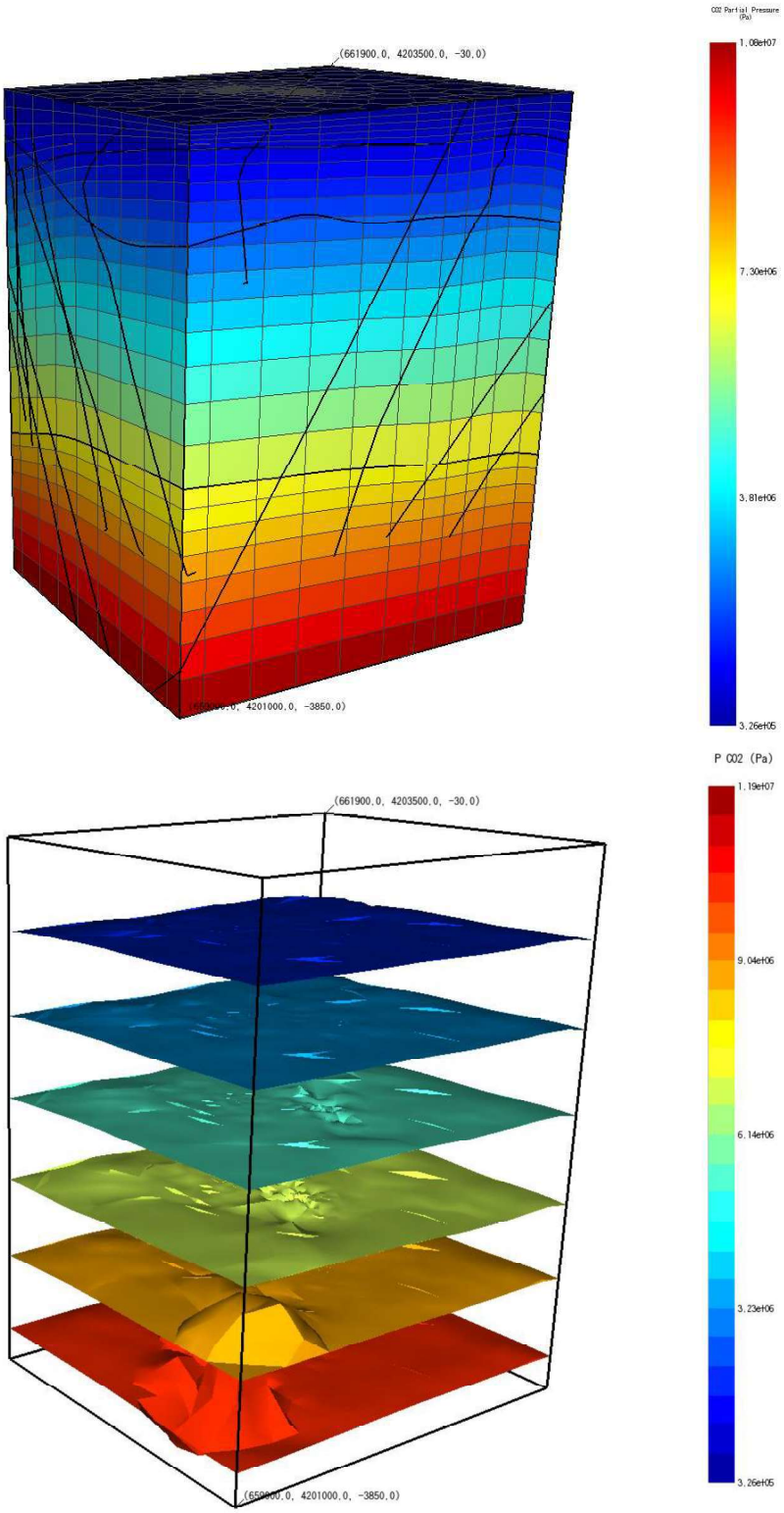

Figure 4.8 Initial CO_2 partial pressure input illustration

With given input data, heat source and boundary conditions, which are explained in section 4.2, the model is run for 100,000 years at which it is expected that the model reaches equilibrium. Model static pressure and temperature data should be matched with measured well data. In order to match measured data with simulated data, several changes such as applying different temperature and pressure gradients and changing cap rock properties have been conducted. Since the model is a doublet-well model and only deals with reservoir and well zone, only the reservoir zones were matched. Thus, as an output of the static model, a static reservoir with matched pressure and temperature is acquired. The matches between measured and simulated data is given between Figures 4.9 through 4.12.

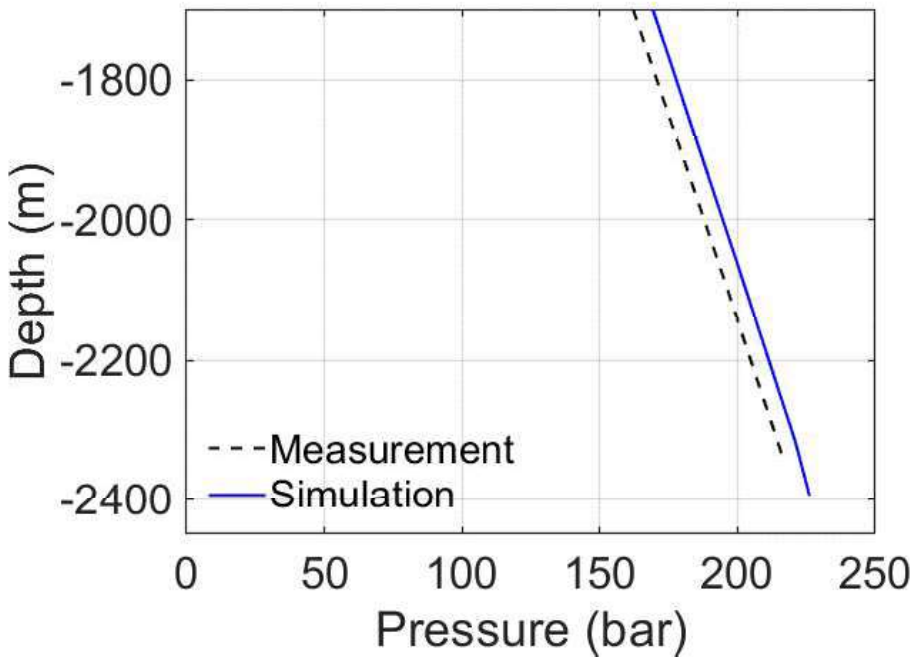

Figure 4.9 Static pressure match of injection well

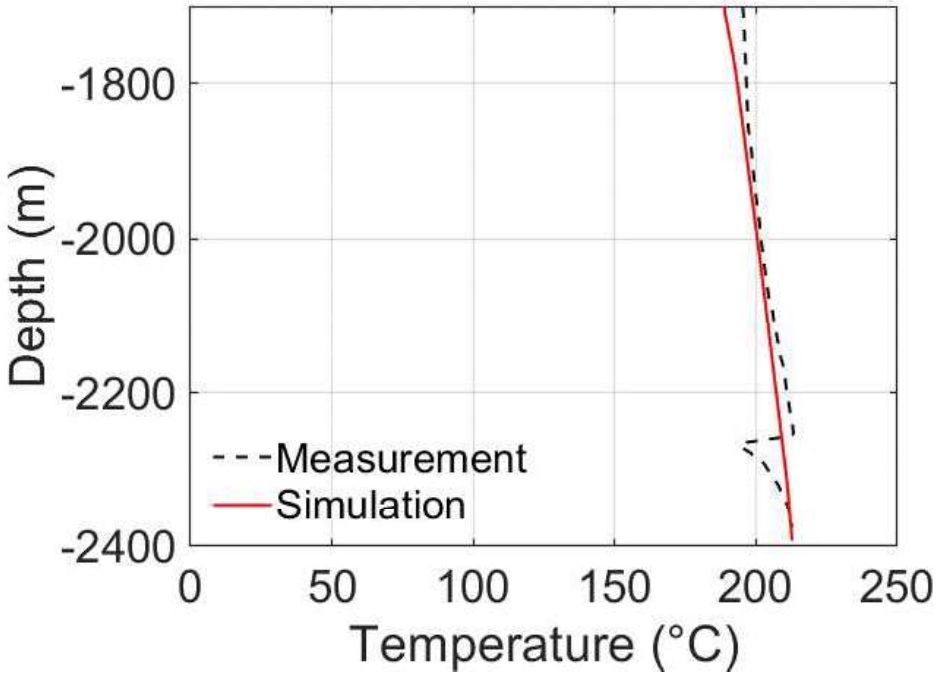

Figure 4.10 Static temperature match of injection well

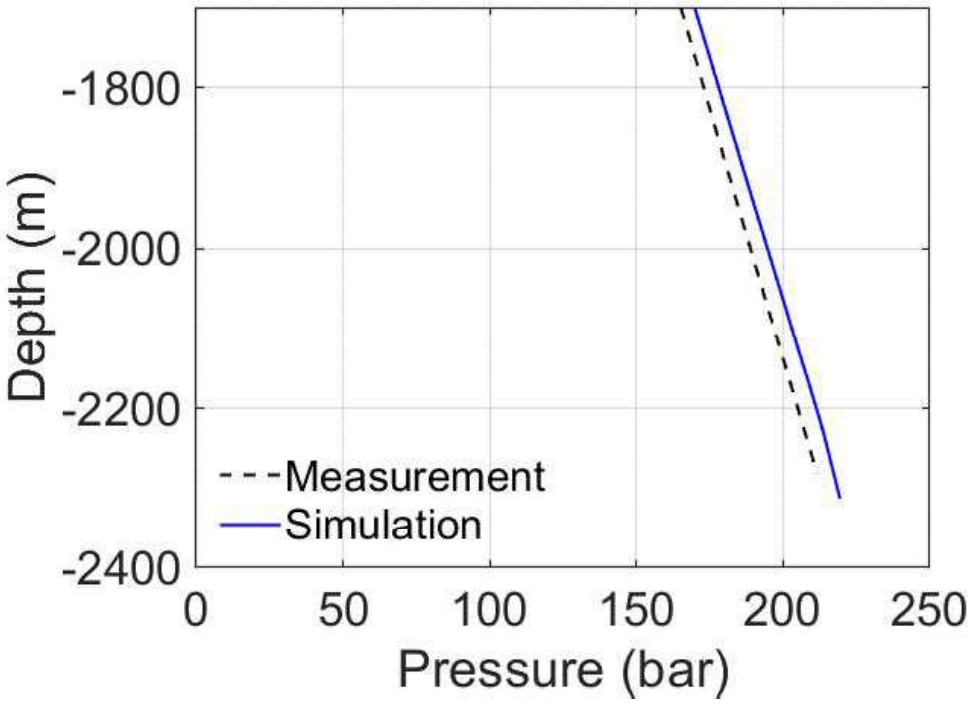

Figure 4.11 Static pressure match of production well

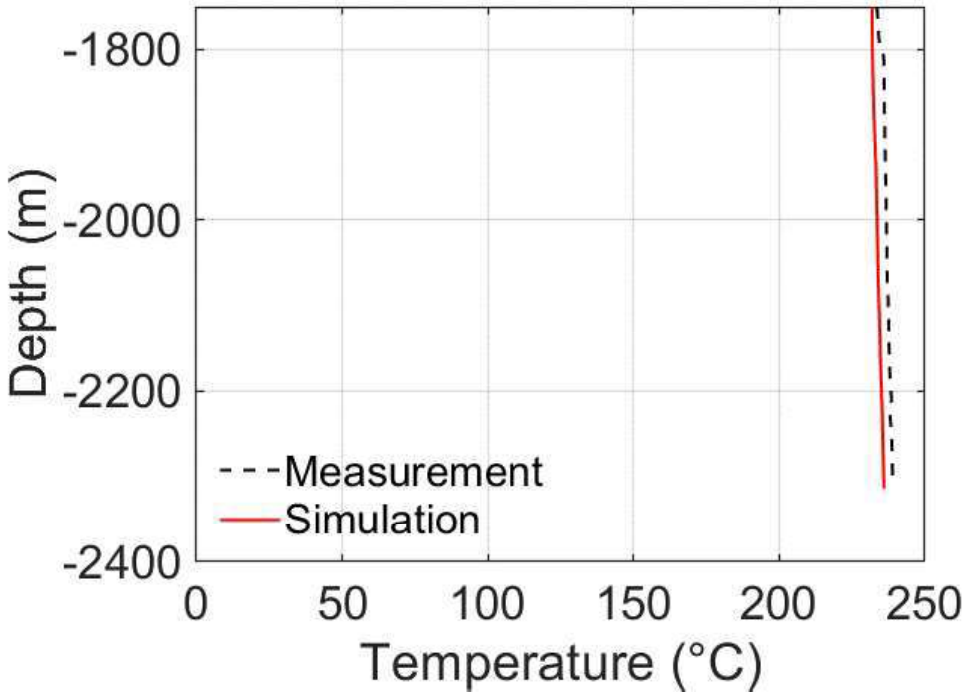

Figure 4.12 Static temperature match of production well

At a depth of 2200 m, (i.e. reservoir zone), difference between measurement data and simulated results are calculated using, Eq. 3.3. Calculated errors are reported in Table 4.4.

$$error(\%) = \frac{|(simulated\ results - measurement)|}{measurement} * 100 \qquad \text{(Eq. 3.4)}$$

Table 4.4 Error in matching pressure and temperature

Name	Error (%)
Pressure of injection well	2.59
Temperature of injection well	1.6
Pressure of production well	2.77
Temperature of production well	1.28

The error values are at desired levels; however, it should be noted that there are some issues with measurement data like unreliable measurements at certain levels, which can be observed in Figure 4.10. There are significantly different consecutive temperature measurements affecting the behavior of temperature change. Moreover, it should be noted that the geological structure of the reservoir and the corresponding grid structure may also cause other sources of uncertainty. At the end of 100,000 years, the model's parameters change because of the heat transport. Since the top layer is at fixed state, temperature, pressure, and CO_2 saturation change accordingly. The reservoir conditions are obtained due to a sealing cap rock. The resulting distributions for temperature, pressure, and CO_2 saturation are shown between Figures 4.13 through 4.15. From the results, it is deduced that pressure slightly changes at the end of natural state modeling; however, temperature and liquid CO_2 saturation change significantly due to the heat source located at the bottom of the model and negative heat flux at cap rock level. Thus, beneath the cap rock, CO_2 is preserved and its saturation distribution is obtained at desired level. Note that, CO_2 stays saturated in the brine remaining in single phase after natural state simulation.

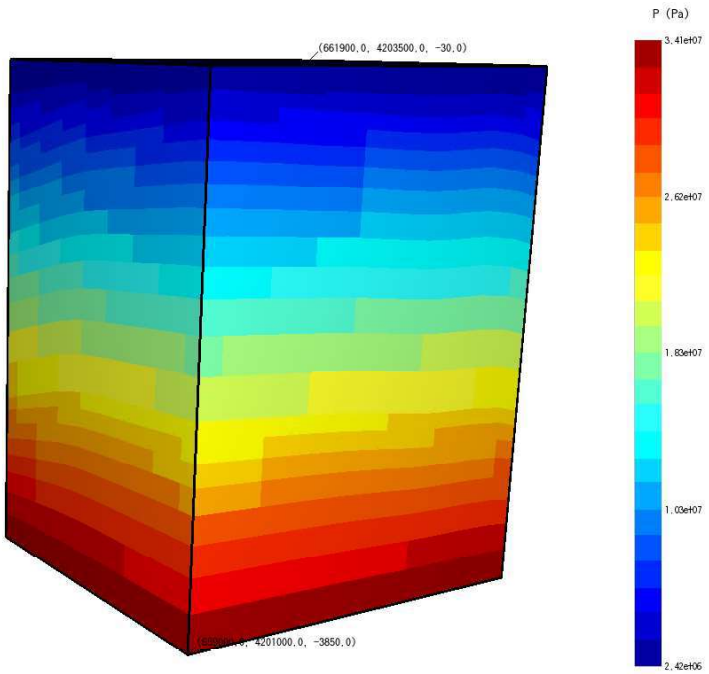

Figure 4.13 Pressure distribution in the model after 100,000 years

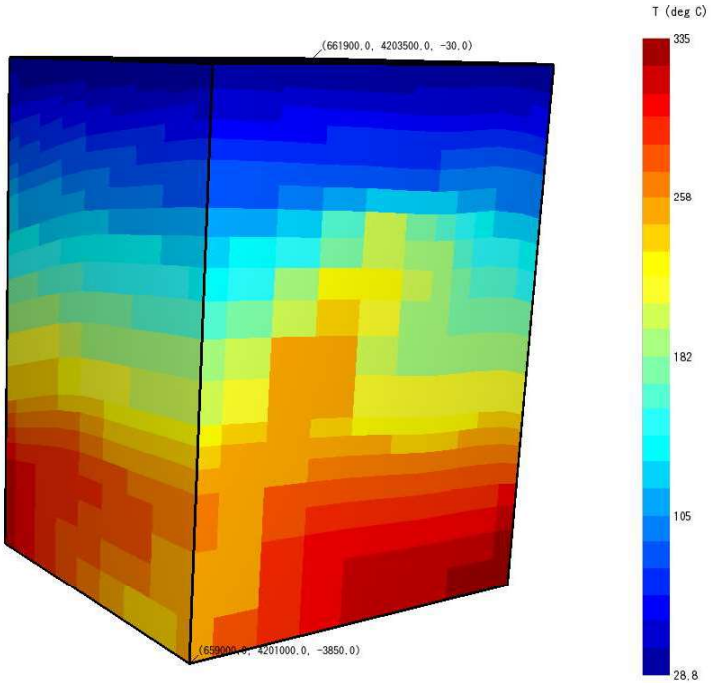

Figure 4.14 Temperature distribution in the model after 100,000 years

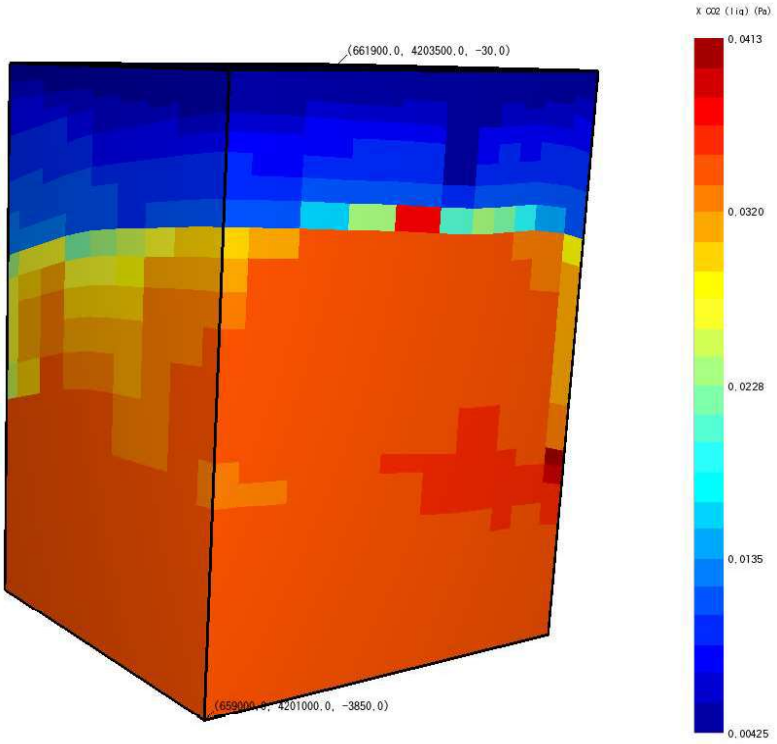

Figure 4.15 CO_2 (liq) distribution in the model after 100,000 years

4.4 Reactive Natural State Model

After matching static pressure and temperature measurements, reactive transport simulation option is enabled in TOUGHREACT. Previously obtained pressure and temperature data is introduced as input to the program. Additionally, three different mineral compositions are constructed for mineral assembly, which are also considered in different scenarios during dynamic modeling. The reason why reactive natural state model is constructed is that to get an output file where minerals reach equilibrium point so that in the dynamic model minerals are ready to react with acidic water with CO_2. Three different reactive natural state models have been constructed for different mineral assemblies. These models are simulated for 100 years guaranteeing the model reach to equilibrium with the input kinetic constraints. The time when minerals reach equilibrium can be different for different mineral compositions, such that for some mineral compositions, it is seen that sometimes 25 years is enough for equilibrium. However, in order to be on the safe side, simulation time of 100 years has been selected.

4.4.1 Mineral Composition

For reactive transport model in TOUGHREACT, secondary minerals that are involved in the reactions of primary minerals must be included in order to avoid any unbalanced chemical reaction (e.g., reactants and productions) Secondary minerals can be a product of a certain reaction and they can either dissolve or precipitate as a result of CO_2 - brine injection. If the secondary minerals are not defined in TOUGHREACT, the model stops prematurely because of chemical reaction error. In this regard, in order to provide stable chemical reactions, secondary minerals should be introduced manually.

In order to find secondary minerals that should be included in the model, PHREEQC software is used. With changing temperature and pH, several secondary minerals could be present regarding to primary mineral contents. PHREEQC computation

identifies secondary aqueous species and possible secondary minerals by evaluating reaction-paths. On the down side, PHREEQC reports every possible secondary mineral. Including all possible secondary minerals that are given by PHREEQC increases run time and can give unrealistic results in TOUGHREACT. In order to find the most probable secondary minerals, Karamanderesi and Ölçenoğlu [56] work for schist and marble zones where X-ray diffraction analysis was used to determine minerals in Kızıldere field has been utilized. According to their findings and the calculations carried out with PHREEQC, possible secondary species are selected and introduced in TOUGHREACT. As it is stated before, three different mineral compositions have been used. The first mineral assembly is mainly composed of schist. The second one includes marble and schist assuming that the reservoir rock is composed of marble with schist layers. The last mineral composition is mainly composed of marble minerals. Mineral compositions are given between Table 4.5 and Table 4.7.

Table 4.5 Mineral composition 1 (Schist)

Mineral Name	Volume Fraction*
Albite	0.0
Ankerite-2	0.0
Calcite	0.03
Chalcedony	0.0
Chlorite	0.2
Dawsonite	0.0
Diaspore	0.01
Dolomite	0.0
Hematite	0.0
Illite	0.0
Kaolinite	0.1
Magnesite	0.0

Muscovite	0.35
Pyrophyllite	0.01
Quartz	0.05
Smectite-Ca	0.05
Smectite-Na	0.05

*The minerals with a volume fraction of 0.0 are secondary minerals.

Table 4.6 Mineral composition 2 (Marble with schist)

Mineral Name	Volume Fraction*
Albite	0.0
Ankerite-2	0.0
Calcite	0.4
Chalcedony	0.0
Chlorite	0.05
Dawsonite	0.0
Diaspore	0.0
Dolomite	0.0
Hematite	0.0
Illite	0.0
Kaolinite	0.05
Magnesite	0.0
Muscovite	0.2
Pyrophyllite	0.01
Quartz	0.05
Smectite-Ca	0.05
Smectite-Na	0.05

*The minerals with a volume fraction of 0.0 are secondary minerals.

Table 4.7 Mineral composition 3 (Marble)

Mineral Name	Volume Fraction*
Albite	0.0
Ankerite-2	0.0
Calcite	0.85
Chlorite	0.02
Dolomite	0.05
Hematite	0.0
Illite	0.0
Kaolinite	0.0
Quartz	0.05
Smectite-Ca	0.0
Smectite-Na	0.0

*The minerals with a volume fraction of 0.0 are the secondary minerals.

The mineral compositions given above are simulated using the aforementioned model. At this stage well flow is not initiated, but reactive transport is enabled, to reach an equilibrium state. The model was run for 100 years until the chemical system nearly reaches to quasi-steady state conditions. The output file obtained from reactive natural state model is then introduced in the dynamic model as geochemical input. An example showing how mineral compositions are changing in the model is shown in Figure 4.16.

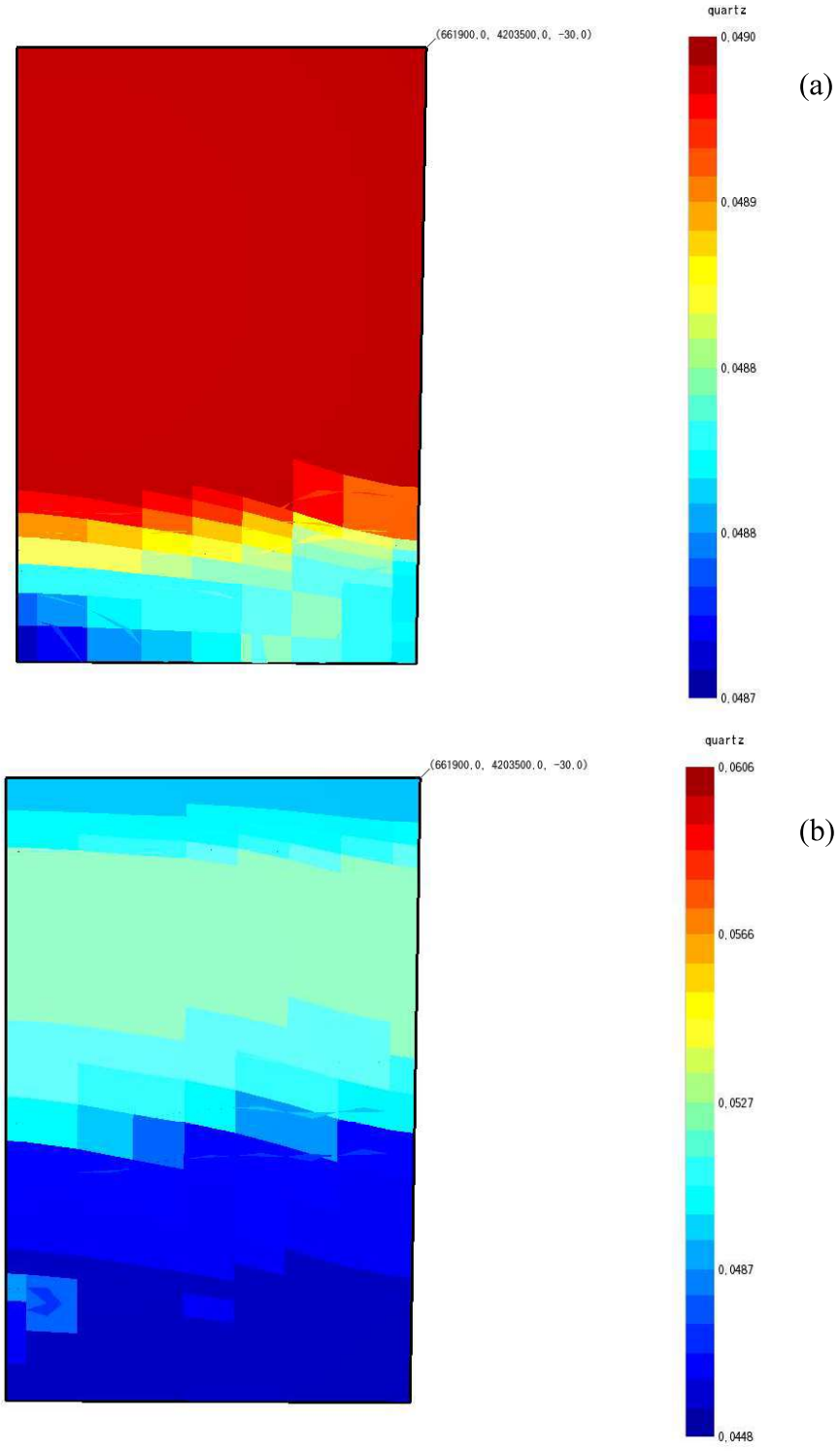

Figure 4.16 Example mineral composition change (a) mineral composition after 1 day (b) mineral composition after 100 years

4.5 Dynamic Model

Dynamic model includes a fixed state boundary condition at top of the model similar to other models. However, in dynamic model, there is no heat source or sink since the input file given by natural state model includes these effects. In the dynamic model, one pair of injection and production wells is included (Figure 4.17). The distance between these wells is approximately 450 m at a depth of 2350m. The well performance and history matching are not available in the dynamic model, since the wells are imaginary, and the purpose is only to observe mineral trapping around injection well.

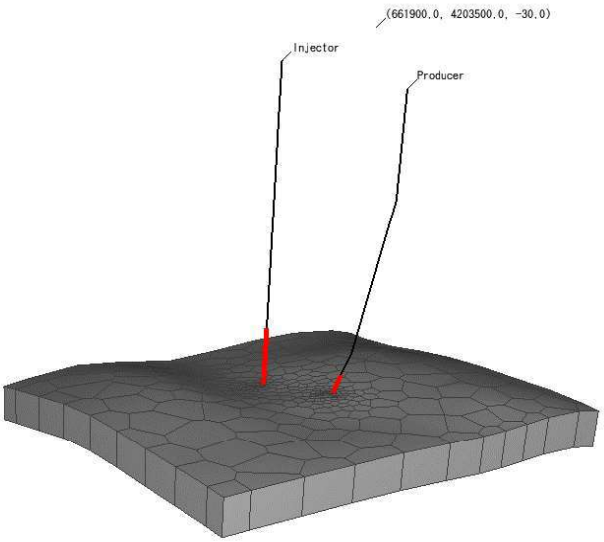

Figure 4.17 Illustration of wells in the model

For the dynamic runs, four different injection strategies are selected with three different mineral composition scenarios. The four injection strategies can be listed as:

- Scenario 1: Re-injection of brine without CO_2

- Scenario 2: Injection of CO_2 without brine
- Scenario 3: Injection of CO_2-brine mixture
- Scenario 4: Injection of CO_2-brine mixture at a lower temperature

The first scenario represents conventional brine injection. The second scenario aims to demonstrate possible effect of injection of CO_2 in supercritical conditions. The third one is the preferred model to demonstrate mineral trapping. The final aims to show possible amorphous silica precipitation at lower temperatures. In each scenario, mineral compositions are kept identical. Hence, a total of twelve different systems are considered in dynamic runs. Each scenario serves a different purpose. The first scenario represents current practice where brine is reinjected without NCG (consisting mainly CO_2) that is released to the atmosphere. The second scenario considers supercritical CO_2 injection, which may radically increase CO_2 around the injection well. The third scenario simulates co-injection of brine and CO_2 close to reservoir conditions. The final scenario is a special case of brine – CO_2 injection aiming to demonstrate the impact of lower injection fluid temperature, which is a subsequent effect of higher electric generation in the power plant. The latter scenario can result in large amount of amorphous silica precipitation in the vicinity of the injection well.

4.5.1 Results

This section represents only Scenario 1 results. The results of other scenarios are given in Appendix A . The similarities between different scenarios are shortly explained in this section.

4.5.1.1 Scenario 1

Scenario 1 includes brine injection without CO_2, but it still affects geochemistry of the reservoir due to lower temperature of the injected brine. Three different mineral assemblies are considered in TOUGHREACT, but only the first mineral scenario is

shown. Other scenarios are given in the Appendix. In all scenarios, injection and production rates are equal to 41.67 kg/s. Production and injection start at the same time.

Table 4.8 Injection and production rates in the model

Well	Brine Rate (kg/s)
Injection well	-41.67
Production well	41.67

4.5.1.1.1 Mineral Assembly 1

This scenario includes schist minerals, which are given in Table 4.5. Mineral volume, aqueous species' volume, porosity, permeability, pH, temperature, and pressure change around the injection well have been illustrated in figures shown below. The injected brine has lower temperature that triggers quartz precipitation around the injection well (Figure 4.18). This is likely due to the thermodynamic behavior of the SiO_2(aq), which is oversaturated in the brine. For muscovite, again due to lower temperature brine, its precipitation is triggered. In addition to that, according to Imasuen et al. [57], smectite may be produced from kaolinite in the temperature range 160-300°C when Mg, Ca and their oxides are present in the brine. It is also observed that ions such as Mg and Ca, which are abundant in brine and their oxides react at suitable temperature with kaolinite to form smectite. This reaction explains why kaolinite volume fraction decreases over time as can be seen in Figure 4.18.

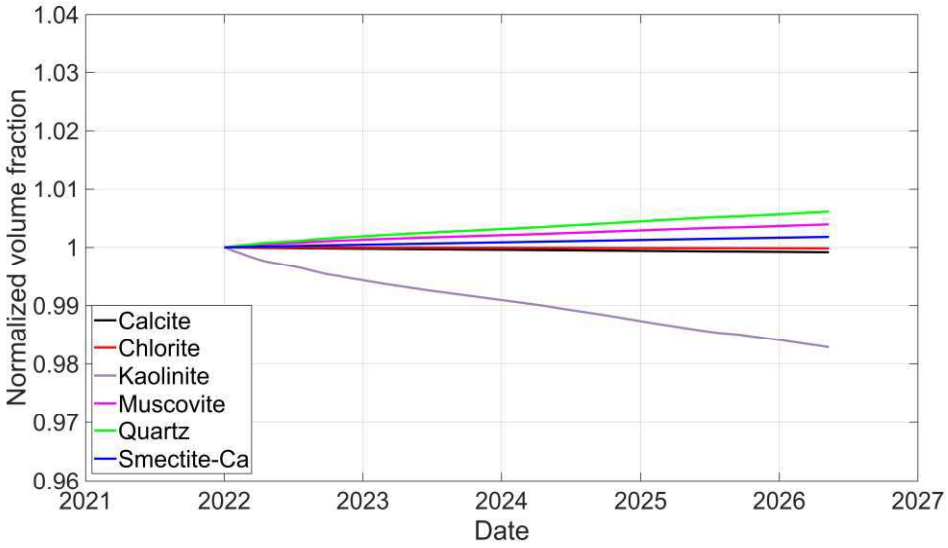

Figure 4.18 Change in mineral volumes around injection well (a grid with an area of 125 m^2 and at a depth of 2450m)

The quantity of aqueous species, shown in Figure 4.19, and pH demonstrated in Figure 4.22 fluctuate over time in the vicinity of the injection well. This indicates that at the injection well grid block, the injected aqueous species thermally equilibrate with the rock minerals in an instant . As precipitation occurs, pH decreases or as dissolution occurs, pH increases. The model shows that precipitation and dissolution occur continuously. Because of precipitation due to chemistry and temperature of the brine, porosity and permeability decreases. During injection of brine, minerals like quartz precipitate and at low porosity zones (i.e. around 5%), permeability decrease is observed with porosity decrease (Zhang et al). [58].

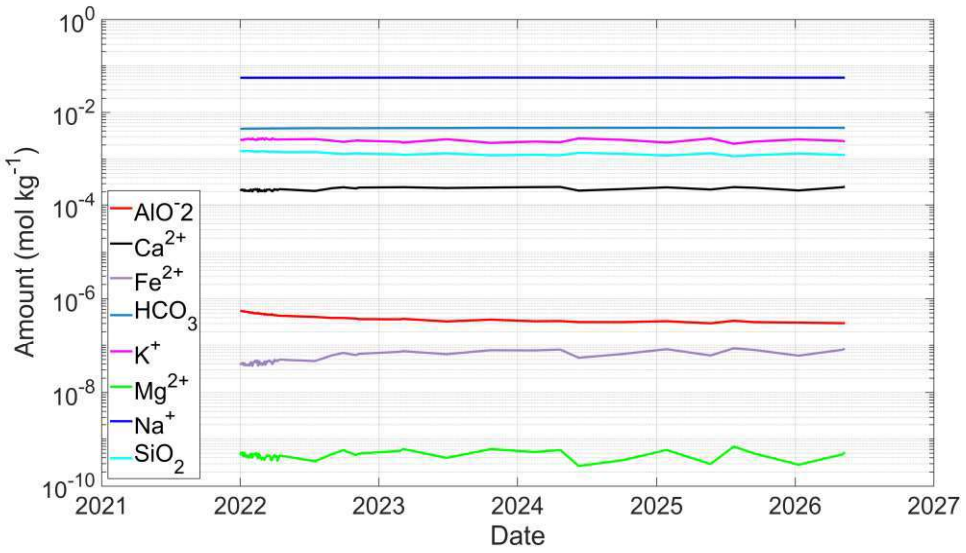

Figure 4.19 Change in volume of aqueous species around injection well (a grid with an area of 125 m^2 and at a depth of 2450m)

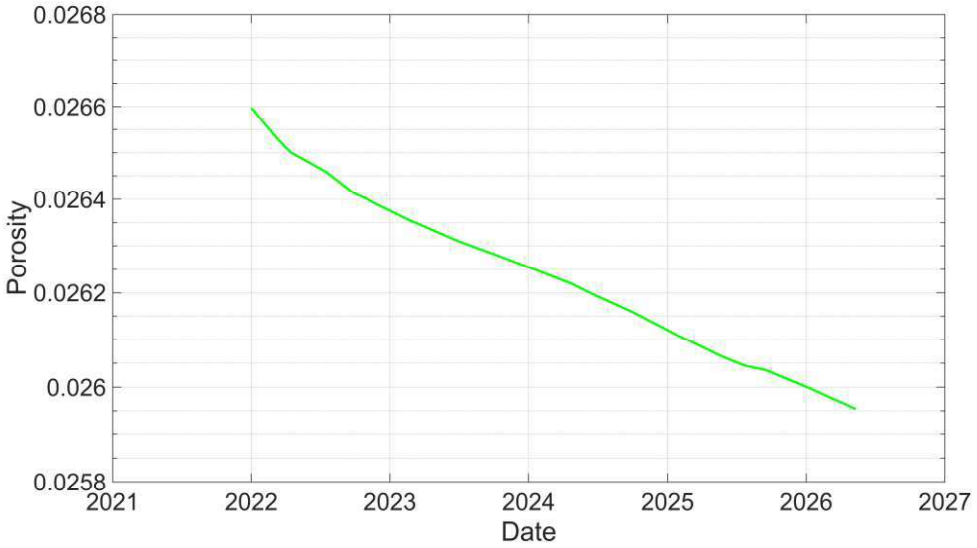

Figure 4.20 Change in porosity around injection well (a grid with an area of 125 m^2 and at a depth of 2450m)

Even though pressure increases, porosity decreases in the model due to mineral precipitations. Porosity increase that may be resulted from pressure increase is not seen in the model due to mineral precipitations.

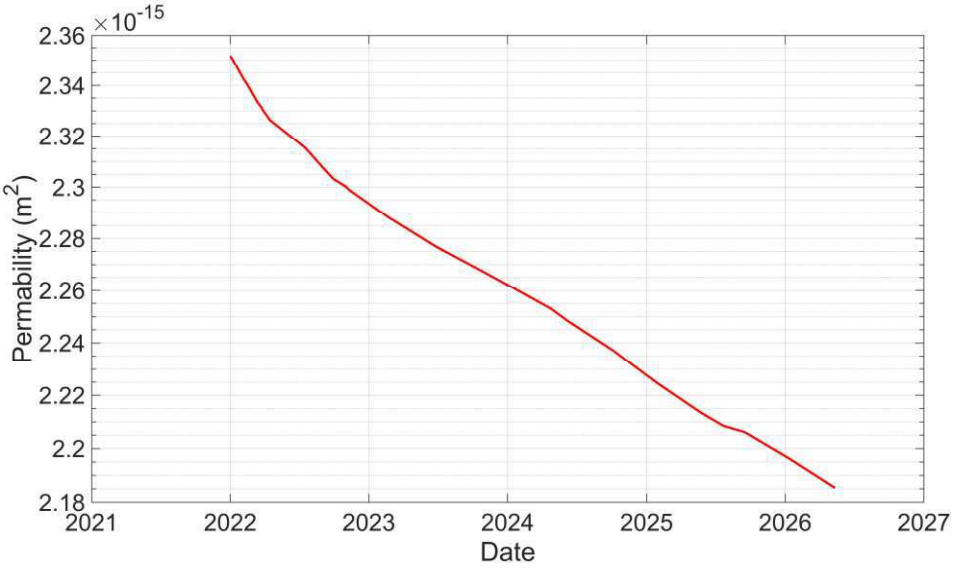

Figure 4.21 Change in permeability around injection well (a grid with an area of 125 m^2 and at a depth of 2450m)

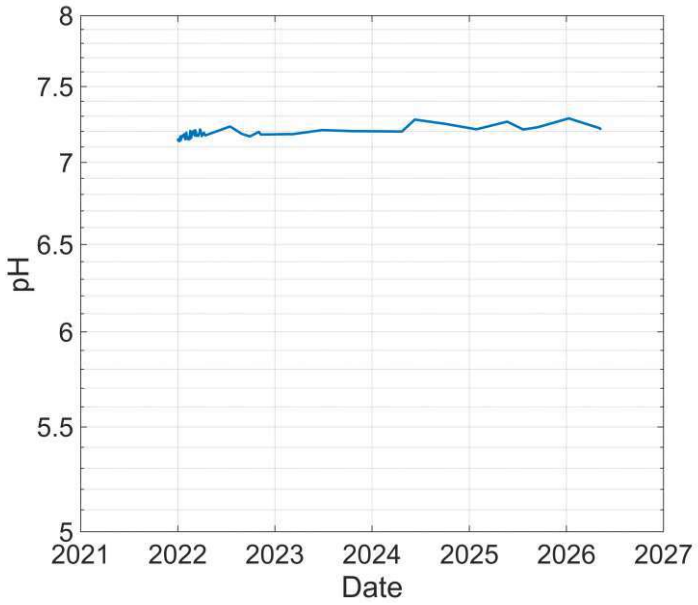

Figure 4.22 Change in pH around injection well (a grid with an area of 125 m^2 and at a depth of 2450m)

Figure 4.23 reveals temperature and pressure change at injection zone, which control the reactions for the minerals to precipitate or dissolve. Temperature quickly decreases from 200 °C to around 110 °C within a short time as the injection commences. Afterwards, the temperature gradually decreases from 110 °C to 98 °C. This small temperature change is crucial for quartz precipitation that may clog the pores and hence effect the permeability. The overpressure due to injection is around 4 bars (Figure 4.23b). According to Evans et al. [59], the fluid injection within overpressure range lower than 100 bars, particularly in sedimentary rocks, do not induce seismicity greater than a magnitude of Ml = 2. Therefore, a mechanical compaction is not expected due to reactions.

It is seen that pressure increase occurs continuously rather than getting constant at a certain point as seen in Figure 4.23. The reason for continuous pressure increase is permeability decrease. With decreasing permeability and constant injection, pressure keep increasing.

a)

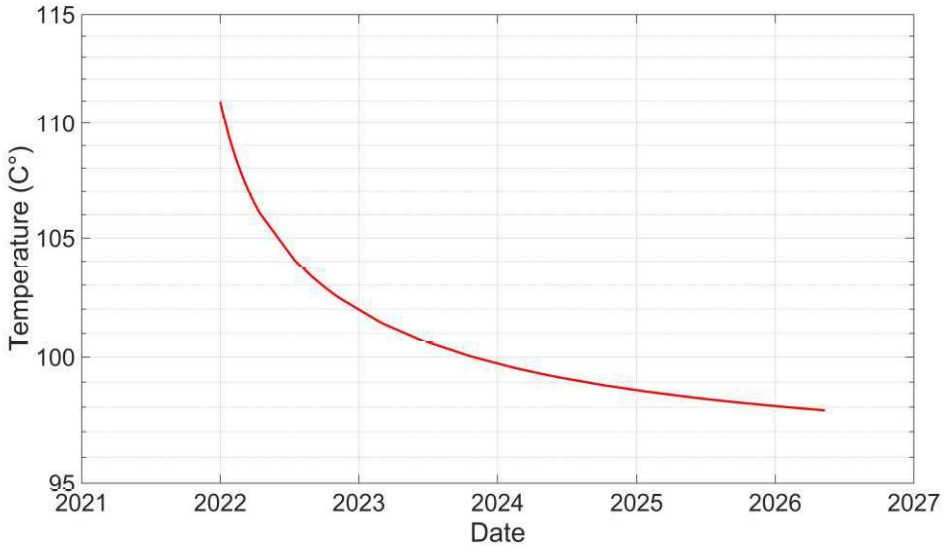

b)

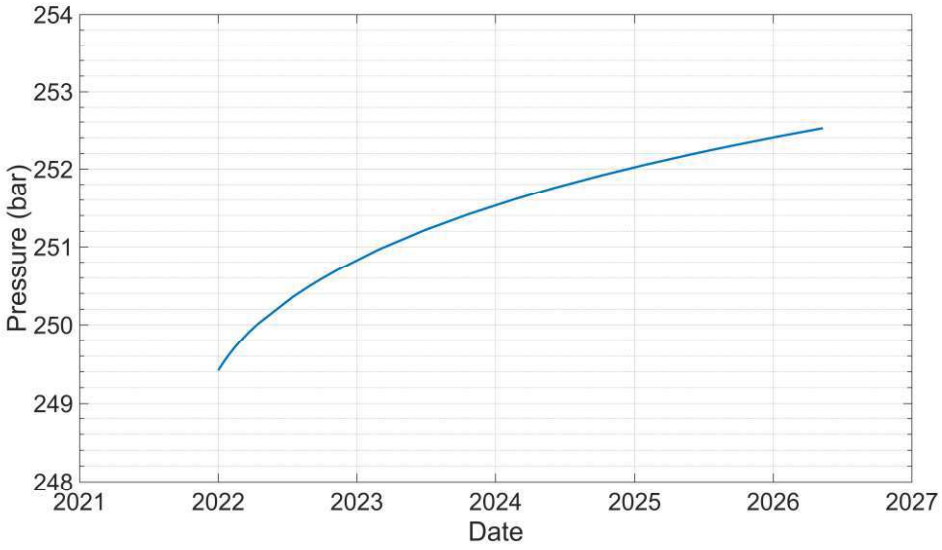

Figure 4.23 a) Temperature b) Pressure results in the vicinity of the injection well (a grid with an area of 125 m^2 and at a depth of 2450m)

Similar results are obtained for Mineral Assembly 2 and 3 (see Appendix A). Discussions provided in this section are also valid for Mineral Assembly 2 and 3. Different from Mineral Assembly 1 and 2, in Mineral Assembly 3 the most dominant mineral is calcite, which has 85% volume fraction, quartz is the only mineral which precipitates in marble.

4.5.1.2 Scenario 2

In Scenario 2, the CO_2 is injected in supercritical state (the enthalpy of the CO_2 is adjusted to supercritical state). Since the reservoir temperature and pressure is not sufficient to keep the injected CO_2 in liquid phase, the injected CO_2 quickly turns into gaseous state and a large gas bubble is observed around injection well as can be seen in Figure 4.24.

Table 4.9 Injection and production rates in the model

Well	Rate (kg/s)
Injection well CO_2	-1.6
Production well	41.67

4.5.1.2.1 Mineral Assembly 1

Mineral Assembly 1 includes schist minerals reported in Table 4.5. CO_2 plum and pH after 5 years have been illustrated in Figure 4.24 and Figure 4.25, respectively. Figure 4.24 demonstrates that the injected supercritical CO_2 turns to gaseous phase and create a gas plume, which is observed instantaneously and expands during injection, in the vicinity of the injection well. Moreover, it can be seen in Figure 4.25, that the CO_2 in gas form significantly decreases the pH in the reservoir from 6.8 to around 5.9. Single phase CO_2 injection is not feasible for a power plant in operation as it will create problems difficult to solve afterwards. Since temperature is high and the pressure is not sufficient CO_2 does not stay in liquid phase at reservoir conditions. In all different mineral compositions, the injected CO_2 decreases the pH and shows similar behavior. Since temperature increases over 200°C and pH decreases around 5, TOUGHREACT simulations have convergence problem and after a certain time reactive transport is stopped. It is for sure that the injected CO_2 without mixing with effluent fluid have an adverse effect in the reservoir. Firstly, the injected CO_2 in supercritical state instantaneously changes its phase to gas and triggers buoyant migration. Secondly, the production performance and the flow conditions in the reservoir may be impaired due to gas build up around the injection well. Injection of CO_2 in supercritical state is more appropriate at lower temperature reservoirs in which CO_2 mineralization process can be more successful.

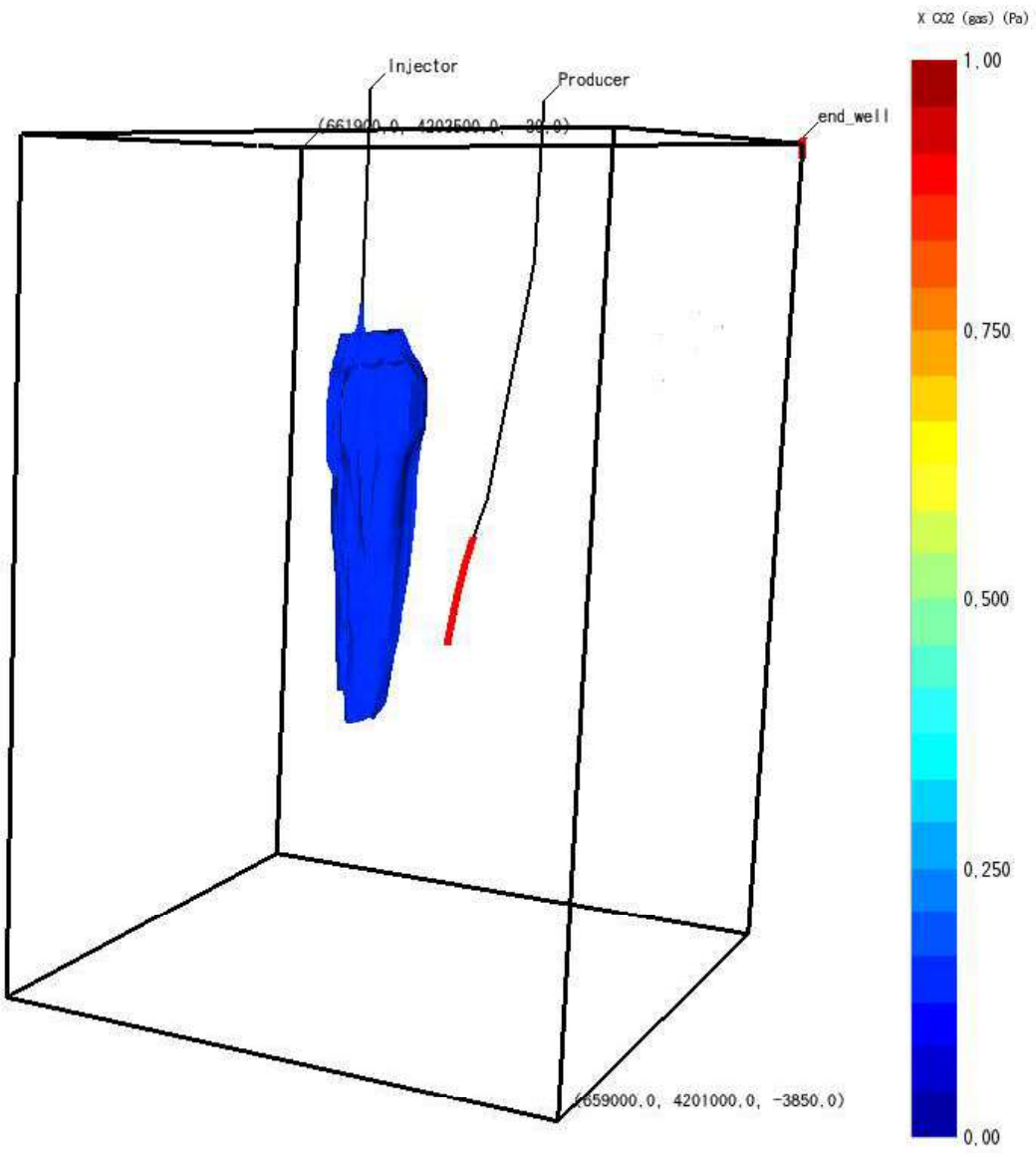

Figure 4.24 CO_2 bubble around injection well

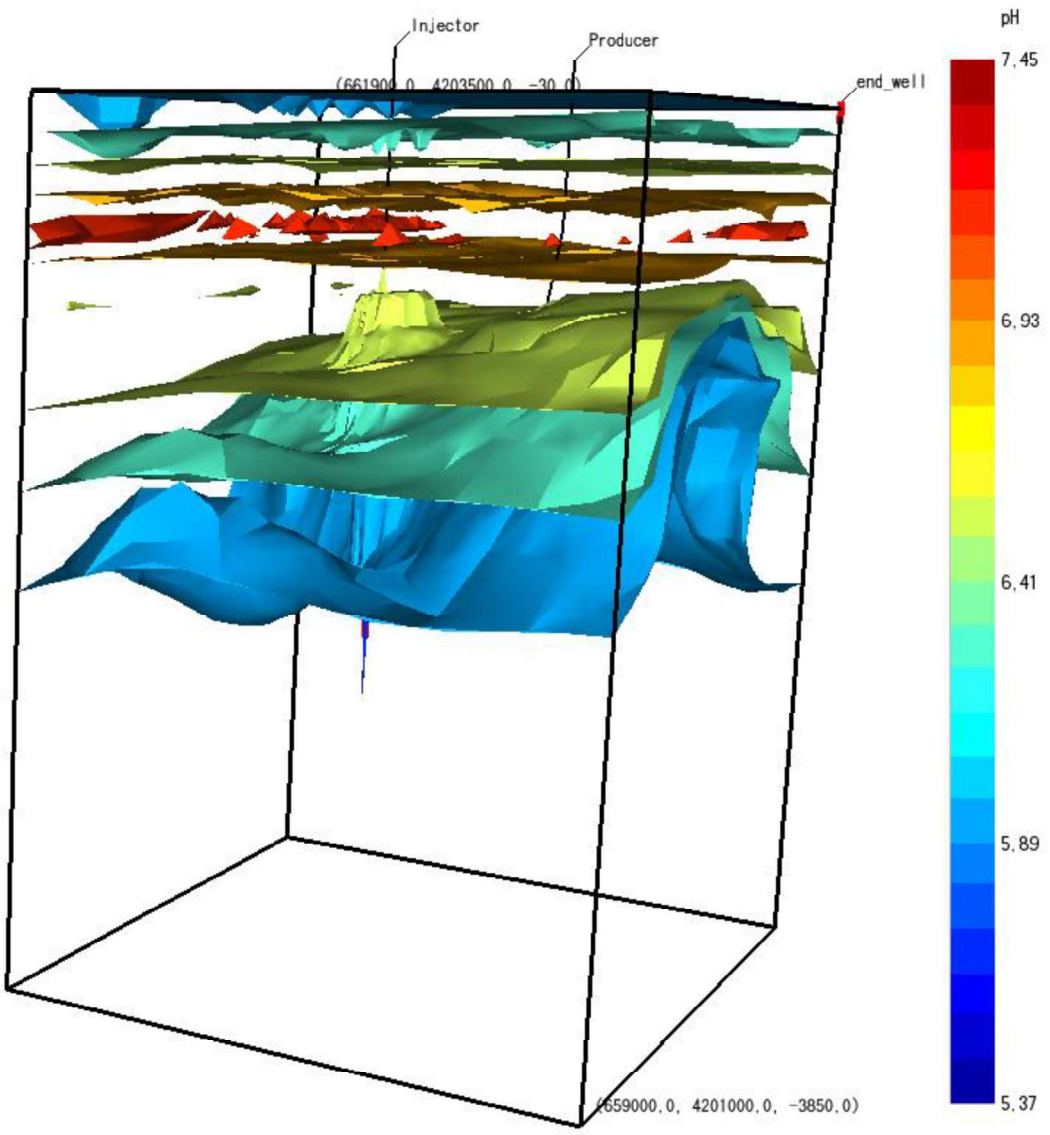

Figure 4.25 pH of the model after CO_2 injection in supercritical state

4.5.1.3 Scenario 3

In Scenario 3, CO_2 and brine are injected together. It is assumed that CO_2 has a weight fraction of 3.8% in the mixture. All of the CO_2 is dissolved at injection pressure and temperature and there is no gaseous CO_2 in the reservoir. This injection scenario is considered to be the most likely scenario for best possible mineral

trapping. It should be noted that the reservoir model already includes CO_2, however, it is in equilibrium where temperature is about 200 °C. On the other hand, the injection mixture temperature is at 100 °C, approximately. The model aims to examine and inspect the possible reactions take place where the injected fluid and the reservoir brine is mixed.

Table 4.10 Injection and production rates in the model

Well	Rate (kg/s)
Injection well (brine)	-41.67
Injection well CO_2(aq)	-1.6
Production well	41.67

4.5.1.3.1 Mineral Assembly 1

Mineral Assembly 1 includes schist minerals, which are given in Table 4.5. Mineral volume, aqueous species' volume, porosity, permeability, pH, temperature, and pressure change around the bottom of injection well have been illustrated in Figures 4.26 through 4.32. Carbonate minerals precipitation cannot be seen in Figure 4.26 as secondary mineral. The reasons are twofold: i) the temperature, which controls the solubility of calcite prevents secondary carbonate precipitation, ii) As Ratouis et al.[60] stated, clay minerals, and Chlorite dominate the reactions and interact with major cations such as Fe^{2+}, Mg^{2+}, and Ca^{2+}, which are used during carbonation as CO_2 is injected. Therefore, conditions are not favorable for Calcite formation. Moreover, Calcite dissolution occurs in the injection zone even though the injected amount of CO_2 is very low. This can be a result of retrograde dissolution of calcite. Figure 4.27 shows that Ca^{2+} ion volume increases, which proves that calcite has been dissolved providing Calcium ion to the solution. Yet another carbonate mineral Ankerite does not precipitate in the model. On the contrary, it is observed that Fe^{2+}

ion decreases compared to that observed in Scenario 1 (Figure 4.19 and Figure 4.27). This can be explained by hematite precipitation, which is another iron bearing mineral. According to Druckenmiller and Maroto-Valer [61], during carbon sequestration in brine iron oxide may precipitate, which explains hematite precipitation in the model. On the other hand, both Smectite-Ca ,which is a clay mineral, and Chlorite precipitate around the injection zone. Gislason et al.[62], stated that carbonate precipitation's biggest limitation is presence of secondary groups like oxides, clays, and chlorites, which compete for divalent cations.

Precipitation of quartz occurs due to temperature decrease and the chemistry of the brine. The solution becomes oversaturated with $SiO_2(aq)$, and Quartz precipitation occurs. In addition to that, other cations like Na^+ and Al^{3+} precipitate into Albite and Muscovite. In addition to that, Smectite may be produced from Kaolinite between 160 and 300°C when Mg, Ca and their oxides are present in the brine (Imasuen et al.[57]). Formation of Smectite from Kaolinite is a chain reaction, which also includes other clay minerals like Illite and Montmorillonite. This explains Smectite precipitation and decrease in Kaolinite volume fraction. Due to the aforementioned precipitations porosity decreases in the injection zone.

Similar results have been obtained for Mineral Assembly 2, which can be seen in the Appendix. On the contrary, in Mineral Assembly 3, since Calcite is the most dominant mineral with 85% weight, Calcite precipitation occurs as seen in Figure A.36. Injected CO_2 interacts with Ca^{2+} ion. CO_2 gives better pressure support mostly in Mineral Assembly 3 (Figure A.37) among all scenarios since CO_2 remains dissolved in brine contributing to solution trapping. In addition to Smectite, Hematite and Albite, Illite precipitation is observed in Scenario 3. This can be explained with chain reaction for formation of Smectite from Kaolinite. Illite is one of the products in the chain reaction and it is seen that some of the Illite does not react to form Smectite. Because of the precipitation due to chemistry and temperature of the brine, porosity and permeability decreases in all scenarios (Figure 4.28 and Figure 4.29).

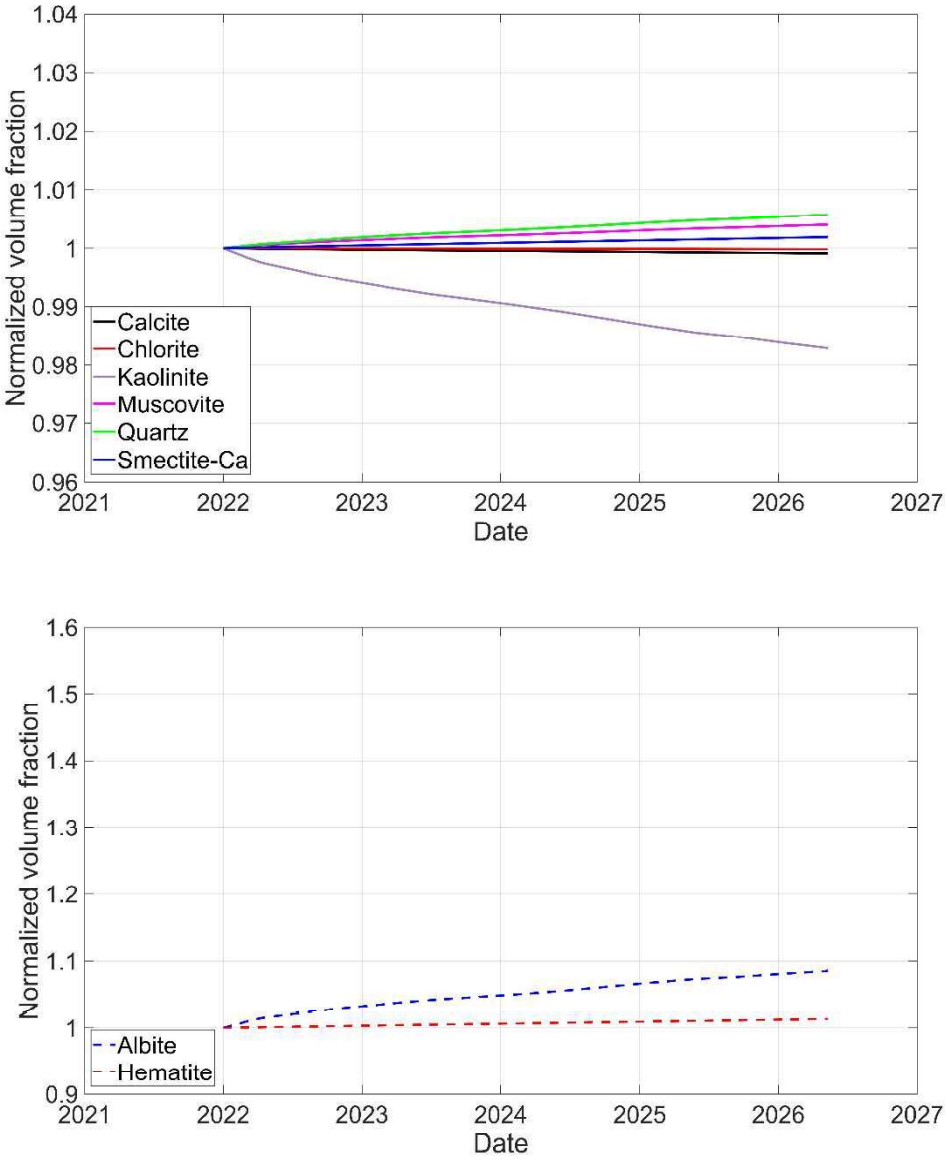

Figure 4.26 Change in mineral volumes around injection well (a grid with an area of 125 m^2 and at a depth of 2450m)

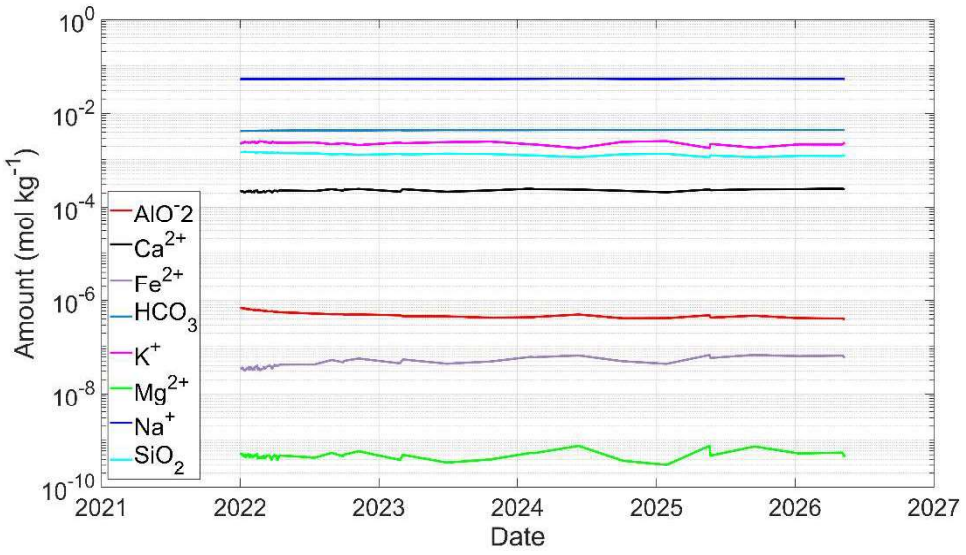

Figure 4.27 Change in aqueous species volume around injection well (a grid with an area of 125 m^2 and at a depth of 2450m)

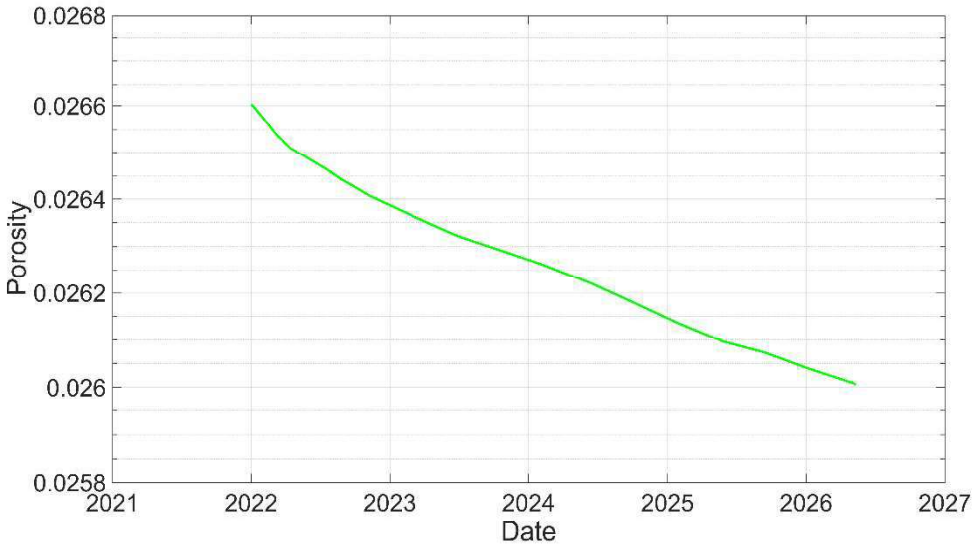

Figure 4.28 Change in porosity around injection well (a grid with an area of 125 m^2 and at a depth of 2450m)

Even though pressure increases, porosity decreases in the model due to mineral precipitations. Porosity increase that may be resulted from pressure increase is not seen in the model due to mineral precipitations.

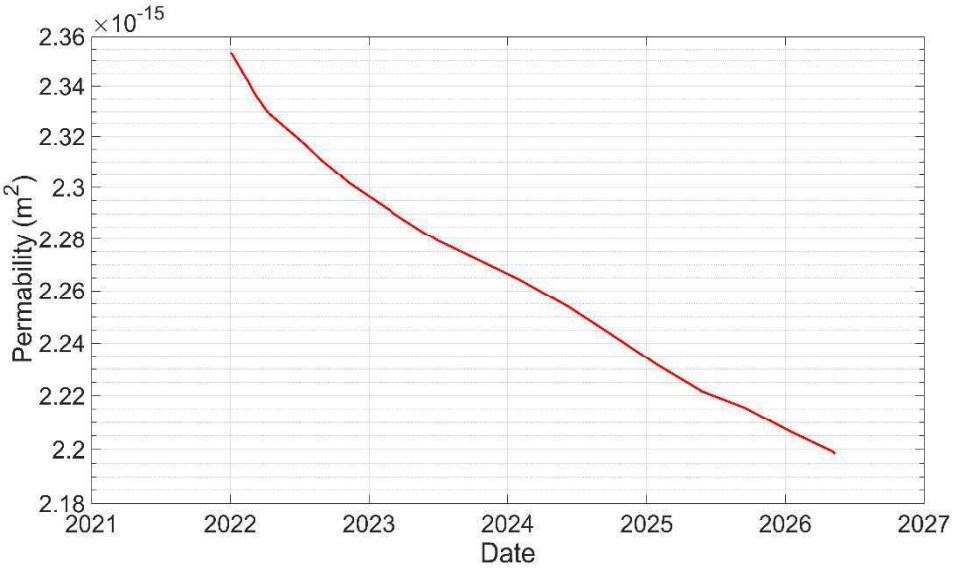

Figure 4.29 Change in permeability around injection well (a grid with an area of 125 m^2 and at a depth of 2450m)

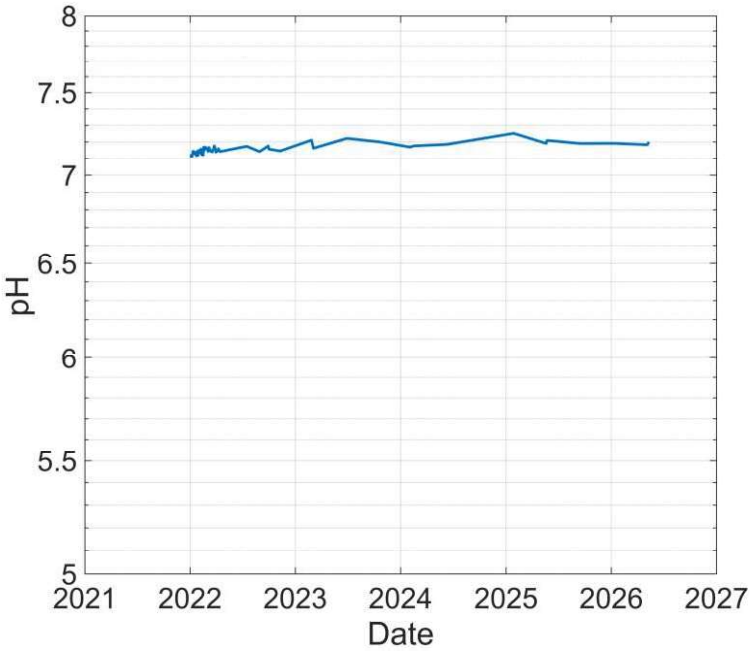

Figure 4.30 Change in pH around injection well (a grid with an area of 125 m^2 and at a depth of 2450m)

It is seen that pressure increase occurs continuously rather than getting constant at a certain point. The reason for continuous pressure increase is permeability decrease. With decreasing permeability and constant injection, pressure keep increasing.

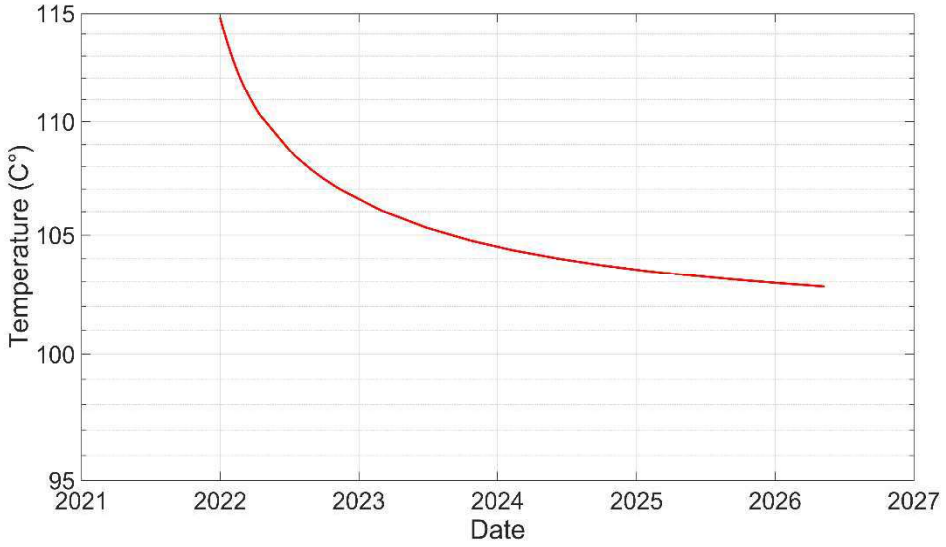

Figure 4.31 Change in temperature around injection well (a grid with an area of 125 m^2 and at a depth of 2450m)

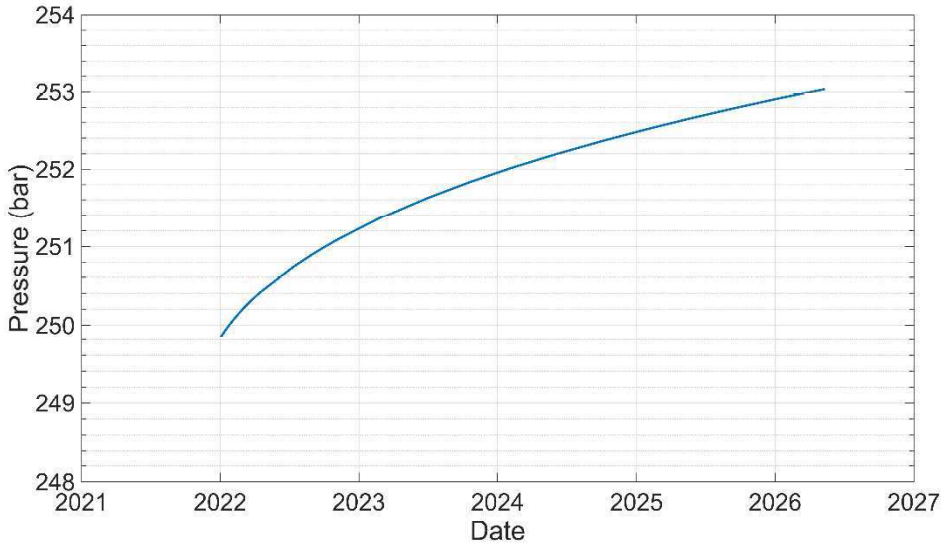

Figure 4.32 Change in pressure around injection well (a grid with an area of 125 m^2 and at a depth of 2450m)

After injection, it is observed that porosity and permeability decrease due to precipitation of minerals like Albite, Illite and Hematite similar to those in Scenario 1. Temperature and pressure data are provided to show injection conditions remain at desired level after 5 years (Figure 4.33). A distance-based comparison between Scenario 1 and 3 between injection and production wells is presented in Figure 4.34 and 4.35. In these graphs injection well is located at 0, whereas production well is located at 446m at a reservoir depth of approximately -2350m. In contrast with CarbFix reactive transport simulation results [60], there is no indication of calcite precipitation. In CarbFix2, injected brine is capable of leaching cations from the basaltic rock; however, in this study, calcite precipitation is not favorable in simulated reservoir conditions. In CarbFix2, brine gets super-saturated with respect to carbonates and precipitation occurs where CO_2 is sequestrated. Since injected CO_2 is dissolved in brine (solubility trapping), injected CO_2 provides extra pressure to the reservoir. From Figure 4.35 and 4.36, it is understood that injected brine mixes with the brine at reservoir conditions as distance from injection point increases. Thus, pH and temperature of the mixture is between these conditions. There is very little amount of calcite dissolution, which can be explained with weak acidity of the brine (Figure 4.33). The main purpose of demonstrating calcite volume change is to show that there is no calcite formation due to CO_2 injection.

The graph shown in Figure 4.33 can be a result of retrograde dissolution of calcite, which leads increase in calcite solubility due to decrease in temperature of the brine, which is explained there in before.

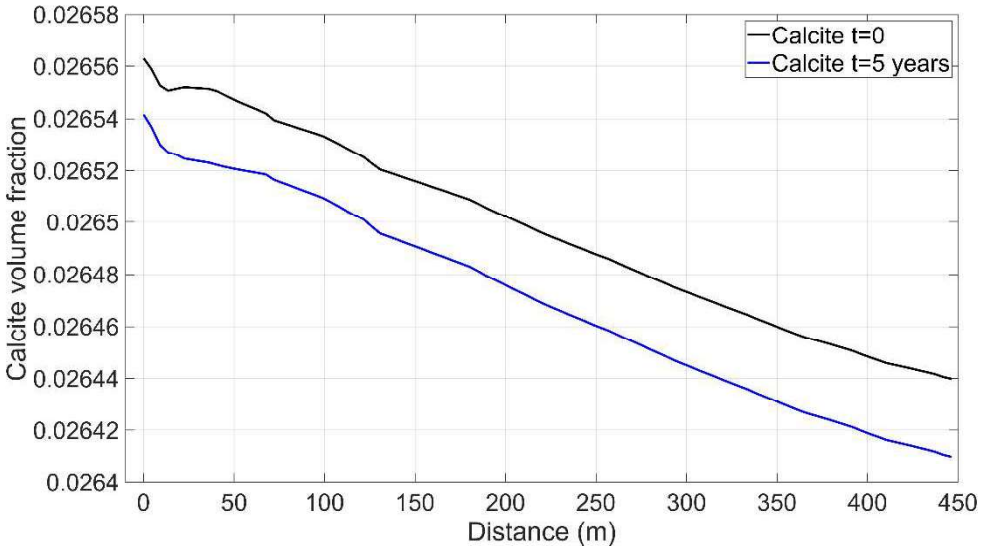

Figure 4.33 Calcite volume fraction comparison between two wells

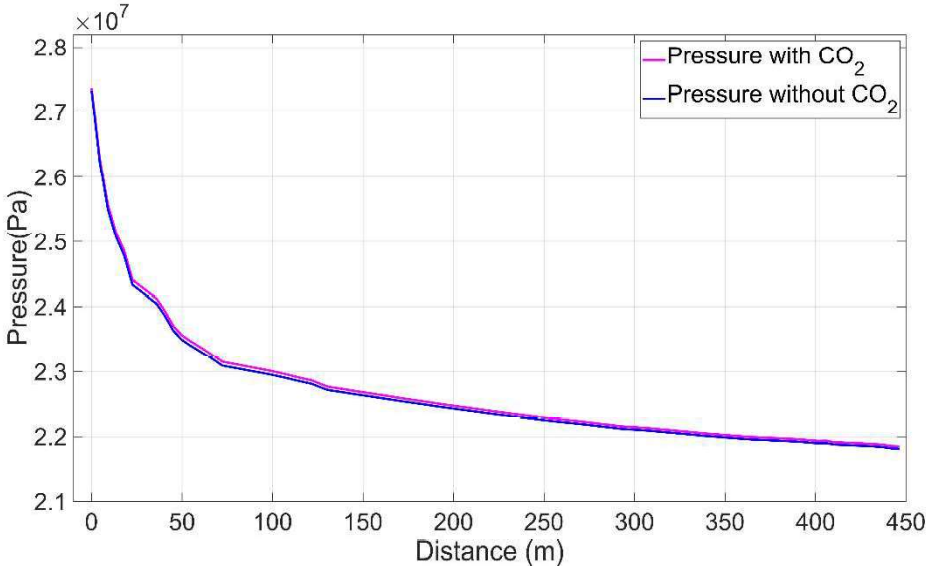

Figure 4.34 Pressure comparison between Scenario 1 and 3 between two wells after 5 years

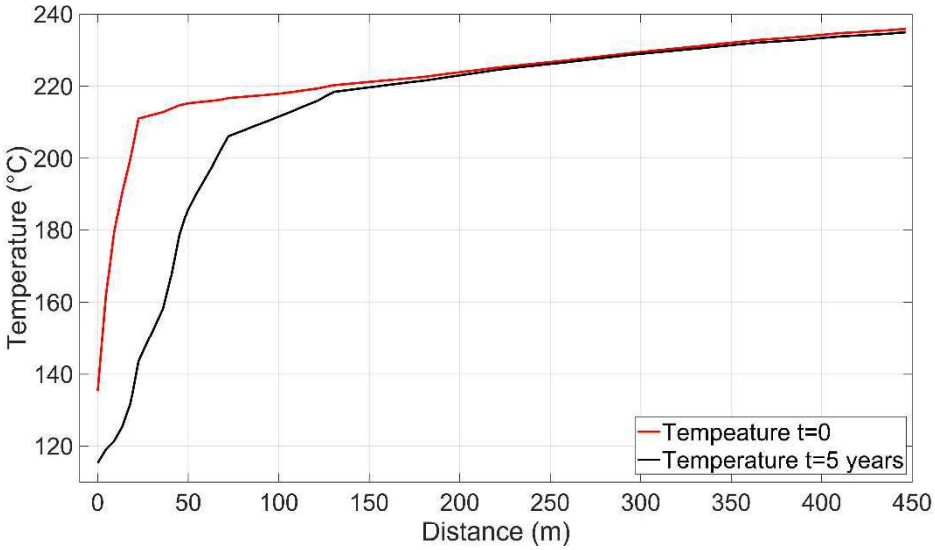

Figure 4.35 Temperature comparison between two wells

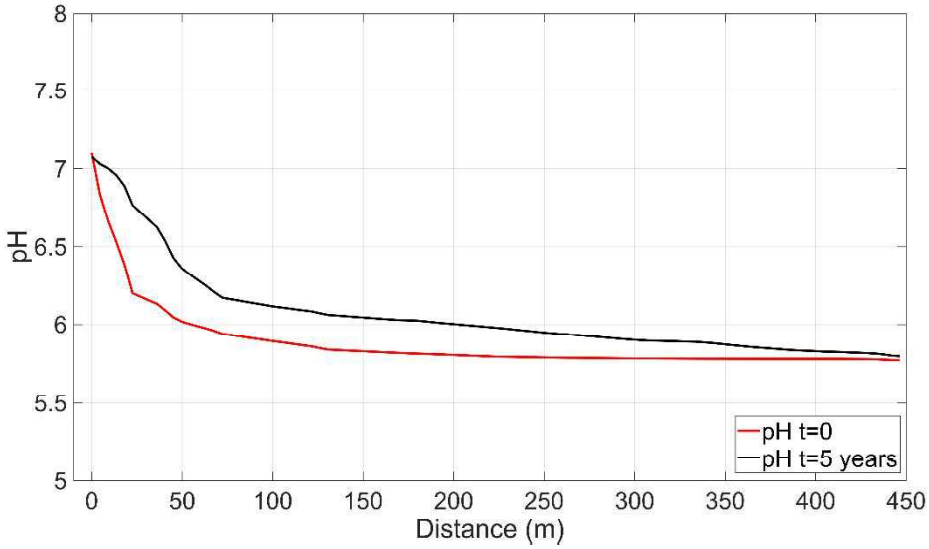

Figure 4.36 pH comparison between two wells

4.5.1.4 Scenario 4

In Scenario 4, injected mixture's temperature is kept at 80 °C. The reason why this temperature is selected is to assess possible amorphous silica precipitation near the injection well. DiPippo [63] explains amorphous silica scaling potential in geothermal plants. After a certain decrease in temperature silica scaling may occur if concentration of dissolved silica is sufficient for precipitation (Figure 4.37). Thus, in TOUGHREACT model (Figure 4.38), water temperature is decreased a little bit more compared to other scenarios and amorphous silica kinetic rates are introduced to the program so that possible amorphous silica precipitation can be demonstrated (Table 4.11).

Table 4.11 Injection and production rates in the model

Well	Rate (kg/s)
Injection well (brine)	-41.67
Injection well CO_2(aq)	-1.6
Production well	41.67

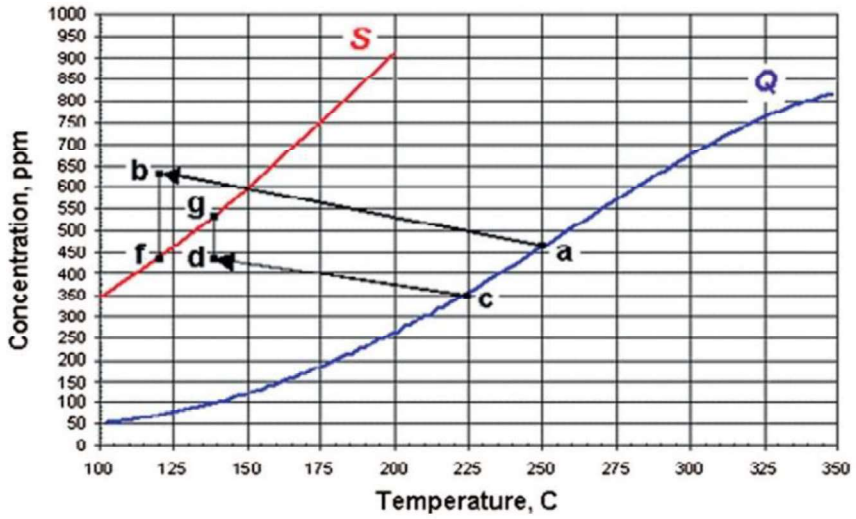

Figure 4.37 Silica concentration graph after flash processes in the geothermal plant [63]

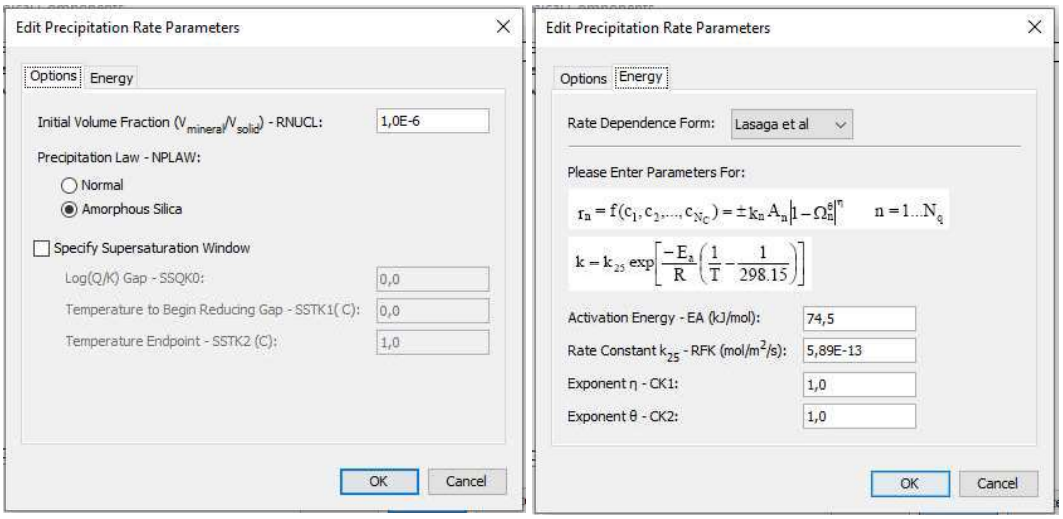

Figure 4.38 Definition of amorphous silica in TOUGHREACT

In order to obtain accurate information about possible amorphous scaling, a comparison between Scenario 3 and scenario 4 has been made. Since Scenario 3 includes brine injection at 100 °C, only quartz can precipitate during reactive transport. The reason why possible amorphous silica precipitation is assessed is that amorphous silica can deposit at pipelines and at bottom of a well and it can cause problems in terms of plant operation and flow assurance. It may also clog possible flow paths in the reservoir impairing flow of geothermal fluid. There are several factors that affect amorphous silica precipitation, however, in this research, temperature and pH effect are considered as main factors and they are examined, accordingly.

4.5.1.4.1 Mineral Assembly 1

Scenario 1 includes schist minerals which are given in Table 4.5. Quartz and silica volume comparison near the injection well are illustrated below. Dissolved SiO_2(aq) decreases more in Scenario 4 compared to Scenario 3 as seen in Figure 4.39. In addition, Amorphous silica precipitation is higher than Quartz precipitation. It shows when temperature decreases to a certain level, amorphous silica may precipitate near

the injection well. As van den Heuvel et al. [64] stated, even though amorphous silica precipitation is observed commonly in geothermal systems, its precipitation conditions are still debated. However, it is for sure that amorphous silica precipitation requisites rapid temperature decrease. DiPippo's [63] work (Figure 4.37) demonstrates that after flash process, amorphous silica precipitation may occur depending on the concentration of silica and temperature. Even though amorphous silica solubility in pure water is higher than that of quartz at any temperature, Kitahara [65] states that silica solubility in hot water is controlled by the amount of quartz. On the other hand, silica solubility in re-injection fluid at lower temperature is controlled by amorphous silica. The re-injection brine used in this study can be classified as a lower temperature brine. Moreover, DiPippo [63] stated that there are five conditions affecting kinetics of amorphous silica precipitation: The initial degree of supersaturation, temperature, salinity of solution, pH of solution, presence of particulate siliceous material. Between, these parameters pH value plays a key role since pH is near-neutral at the injection zone. DiPippo [63] further stated that near-neutral pH values provide maximum precipitation rate for amorphous silica. When these are considered, it can be stated that amorphous silica precipitation can occur at wellbore, pipelines or injection zones where temperature decrease is large and rapid due to flashing brine provided that water chemistry is favorable. In Scenario 2 and 3, similar results are obtained since main parameters triggering amorphous silica precipitation are temperature and chemistry of the water rather than mineral composition.

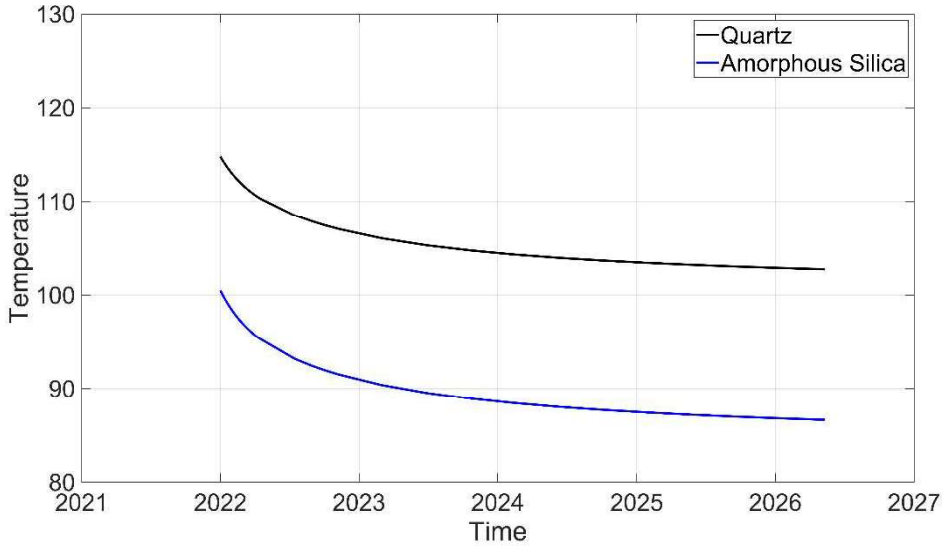

Figure 4.39 Temperature difference between two scenarios at the injection well block (Quartz represents Scenario 3 and amorphous silica represents Scenario 4.)

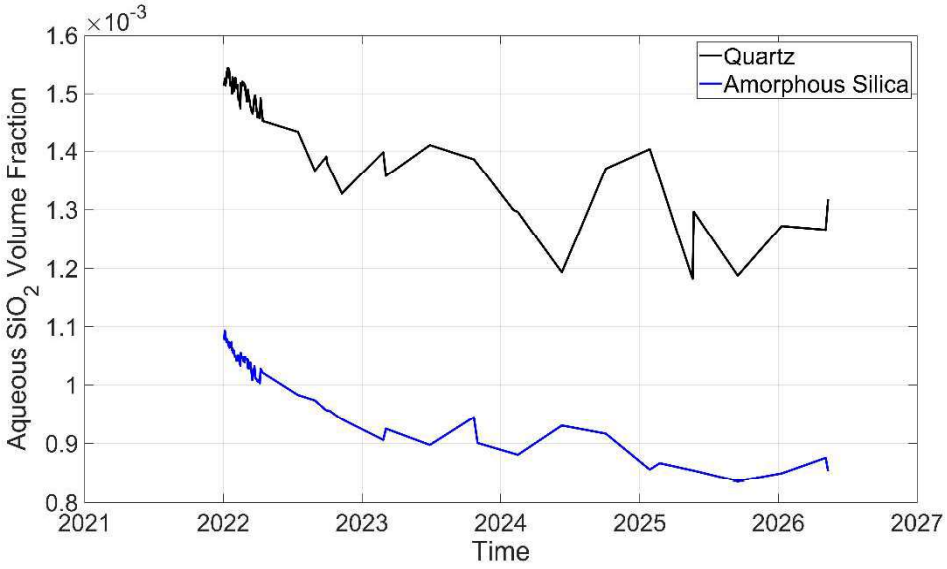

Figure 4.40 Aqueous SiO_2 volume fraction comparison between two scenarios at the injection well block (Quartz represents Scenario 3 and amorphous silica represents Scenario 4.)

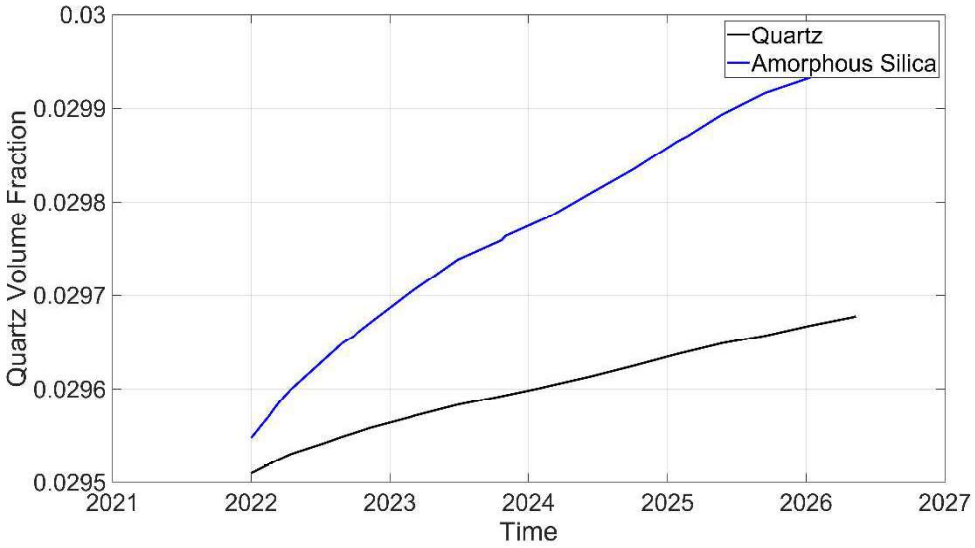

Figure 4.41 Quartz volume fraction comparison between two scenarios at the injection well block (Quartz represents Scenario 3 and amorphous silica represents Scenario 4.)

CHAPTER 5

RESULTS AND DISCUSSION

In this study, four different scenarios with three different mineral assemblies are simulated in TOUGHREACT to observe carbon sequestration during brine and CO_2 injection. It is further aimed to demonstrate possible impacts of CO_2 injection in a metamorphic reservoir rock saturated with brine and CO_2. Apart from Scenario 2 and 4, similar results are obtained.

In order to create a geochemical model, first a static model has been created. The static model that is in accord with the conceptual model of the field, includes geological parameters like faults and their geometry, temperature and pressure changes as a function of depth and finally mineral distribution. In the static model, wells are shut in and only heat source, which is located at the bottom of the model is enabled. The static model study is divided into two parts. The first one is development of a natural state model to get equilibrated pressure, temperature and CO_2 distribution. The second part includes a reactive natural state model to get equilibrated mineral distributions in the model. The results of these natural state models constitute input data for dynamic model. Thus, it is important to achive equilibrium conditions in static models to create realistic representation of an untapped (i.e. virgin) geothermal reservoir, which consist of metamorphic reservoir rocks at a temperature of 220 °C. Both models are run for very long time (e.g. 100'000 natural state and 200 years for reactive natural state) and the simulation results are examined to find out whether natural state has been reached. Note that, size of the model and grid structure may affect the appropriate simulation time. For three different mineral assemblies, three different reactive natural state models were constructed.

After obtaining output data from static models, dynamic models can be constructed. As their names imply dynamic models include dynamic production and injection wells operating at designated values. Important parameters like water chemistry and reservoir properties are also defined in dynamic models. To represent Kızıldere geothermal reservoir, rock and fluid parameters are defined according to fault distribution since wells are drilled at high permeable fault zones which is explained and shown in chapter 4.

In Scenario 1, the aim is to demonstrate how conventional injection affects mineral fractions and the reservoir parameters. In particular, it is observed that Hematite and Albite precipitates around the injection well. Moreover, Muscovite, Quartz, Smectite and, Chlorite precipitates whereas Kaolinite dissolves. Since precipitations occur around the injection well, decrease in porosity and permeability is observed. Due to favorable pH and reservoir temperature, natural CO_2 present in the geothermal brine causes mineral reactions in the reservoir. First two scenarios gave similar results, however, in Scenario 3 ,where Calcite volume fraction is 0.85, very large amount of Hematite and Smectite precipitation have been observed. As Druckenmiller and Maroto-Valer [61] stated that Calcite precipitation can be observed between 60°C and 150°C. When calcite dominates rock composition at reservoir temperature which is approximately 220°C, reactions become slower and there is more time for Hematite and Smectite precipitation.

In Scenario 2, supercritical CO_2 is injected to demonstrate possible impacts of pure CO_2 injection in the geothermal reservoir. As soon as supercritical CO_2 injection is commenced, the CO_2 at the injection well block instantantaneously changes to gasous phase, the reservoir temperature increases to almost 240 °C and pH is reduced to 4.5. Mineral reaction occurs right after the beginning of injection. Since the injected CO_2 changes to gaseous phase and the pressure is not sufficient to push the CO_2 gas plume, compressibility of the geothermal fluid at the injection well block increases causing convergence error and failure of the simulation. It is illustrated that a CO_2 bubble (plume) with a radius of approximately 80 m forms around injection well blocks. It is obvious that CO_2 plume causes injection problems near the injection

well due to two-phase flow effects and increased compressibility. For a healty geothermal power plant operation, decreased injectivity severely limits geothermal electricity production. In this regard, supercritical CO_2 injection is not feasible, as it will create impaired injectivity. It is quite difficult to solve such problems since reservoir temperature is generally high and pressure is not sufficient to prevent the CO_2 plume formation by either keeping it in the liquid phase or to completely mixing it with the reservoir fluid.

In Scenario 3, CO_2 is mixed with brine prior to injection. This scenario is quite easy to implement in Turkish geothermal reservoirs where CO_2 mass fraction is between 0.32 and 0.34 at the injection zone. In this scenario, CO_2 mass fraction is kept equal to 0.38 in the injected brine to create a difference with the reservoir condition. Mineral assemblies, water chemistry, and brine temperature are kept same. Results were similar to those obtained with Scenario 1; however, dissolution rate was somewhat higher for Kaolinite with lower precipitation rates. Compared to Scenario 1, porosity and permeability were decreased but the reservoir pressure was higher. Since injection temperature is lower compared to reservoir temperature, decreasing temperature within 100 m radius of the injection well was observed. However, the model was able to compensate the temperature approaching the production well. Results of Scenario 3 were very similar to scenario 1; however, Calcite formation was observed around the injection well. In contrast Calcite was dissolved in Scenario 1 and 2. Calcite formation amount is higher in the upper part of the reservoir where temperature is less than the injection zone. In accordance with the results, it can be inferred that calcite mineralization can be expected in the geothermal reservoirs where the temperature is lower than 100 °C. However, as a conclusion from this scenario, injecting CO_2 with brine provides pressure support with somewhat decreased porosity and, thus, permeability.

In Scenario 4, the aim is to demonstrate possible amorphous Silica precipitation during mixed CO_2 and brine injection. Obviously, amorphous silica precipitation is unwanted in both pipelines and the wellbore. It is also critical to prevent amorphous Silica scaling near the injection well as the injectivity will be significantly

deecreased. To observe amorphous Silica precipitation near the injection well, temperature of injection mixture is reduced to 85 °C, based on DiPippo's study. It is intended to show how injection temperature can be an important factor controlling mineralization in geothermal reservoirs. In order to model amorphous silica precipitation, reaction kinetics of amorphous silica are introduced in the model (Figure 4.38). For each Mineral Assembly, without changing any other parameter, simulations are run for 5 years. When Scenario 3 and 4 is compared for dissolved SiO_2(aq) fraction in the brine and quartz precipitation, it is observed Quartz precipitation is pronounced and there is less dissolved SiO_2(aq) in the brine in Scenario 4. In this regard supersaturation, salinity of solution and pH of solution are crucial together with temperature for amorphous silica precipitation. Moreover, sensitivity analysis two different temperatures showed that amorphous Silica precipitation is higher than Quartz precipitation at the same temperature even though amorphous Silica solubility is higher than that of Quartz (Figure 5.1 and 5.2).

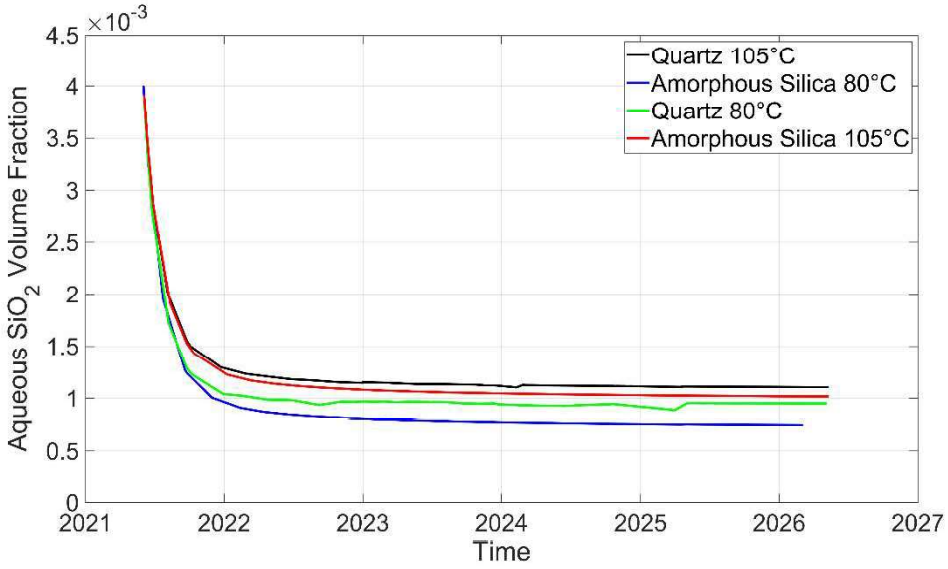

Figure 5.1 Aqueous SiO_2 volume fraction comparison in sensitivity analysis

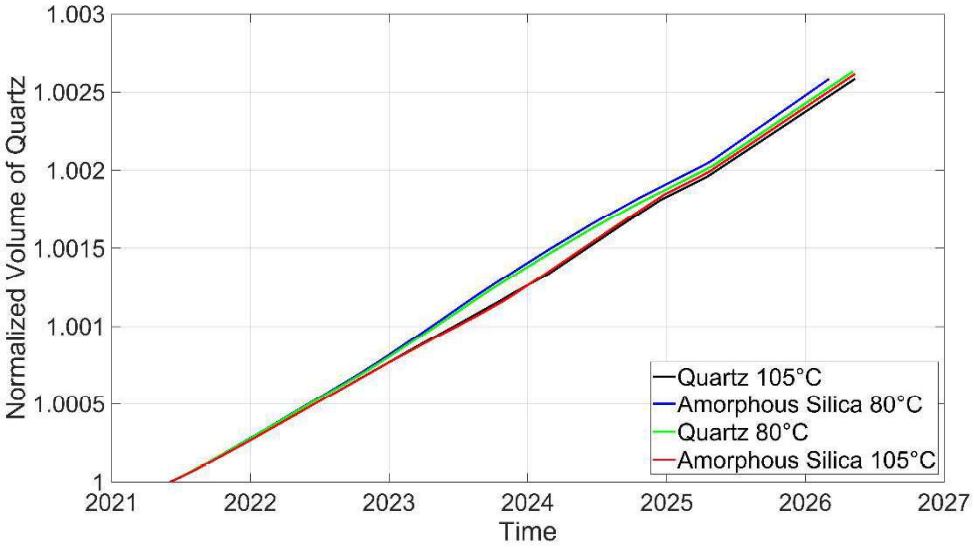

Figure 5.2 Quartz normalized volume comparison in sensitivity analysis

CHAPTER 6

CONCLUSIONS

A numerical model developed with TOUGHREACT was used to demonstrate the applicability of CO_2 sequestration via mineralization in deep metamorphic geothermal reservoirs. The model represented a doublet injection and production well pair located in Kizildere geothermal reservoir. Model calibration during native state and dynamic modeling stages resulted in a representative doublet model. Primary and secondary minerals of the reactive transport model were selected by using PHREEQC. Three different mineral assemblies and four different injection scenarios have been developed to study CO_2 sequestration via mineralization. The following conclusions were obtained.

- It has been concluded that a geothermal reservoir with relatively high temperature and CO_2 in the brine is not an ideal candidate for calcite mineralization. The only added benefit of reinjecting CO_2 in the reservoir is pressure support, which improves reservoir performance and delays pressure decrease.
- It has been observed that mixed CO_2 – brine injection is better than supercritical CO_2 injection. When supercritical CO_2 is injected, a phase change occurs, and a large gas plume develops around the injection well that significantly decreases the injectivity.
- Calcite formation is only observed in mixed CO_2 – brine injection where calcite volume fractions as high as 0.85 are observed with very low precipitation rates. Calcite starts to dissolve with injection due to high reservoir temperature (220 °C).
- It is observed that amorphous Silica precipitation occurs in case of lower temperature brine injection. As the dissolved amount of SiO_2 in aqueous phase decreases, amorphous Silica precipitation occurs. The results showed

that supersaturation, rapid temperature decrease, salinity of solution, pH play a crucial role on amorphous Silica precipitation.

REFERENCES

[1] V. Kakkar, N. K. Agarwal, and N. Kumar, "Geothermal energy: new prospects," *International Journal of Advances in Engineering & Technology,* vol. 4, no. 2, p. 333, 2012.

[2] J. W. Lund, "100 years of geothermal power product," in *Proceedings Thirtieth Workshop on Geothermal Reservoir Engineering Stanford University*, 2005.

[3] BP. (2020). *Statistical Review of World Energy (69th ed.)*. Available: https://www.bp.com/en/global/corporate/energy-economics/statistical-review-of-world-energy/renewable-energy.html#geothermal

[4] MTA. (2020). *GEOTHERMAL ENERGY POTENTIAL OF TURKEY AND RESEARCH STUDIES*. Available: https://www.mta.gov.tr/eng/mta/jeotermal-enerji-arastirmalari

[5] F. C. Kilic, "Geothermal energy in Turkey," *Energy & Environment,* vol. 27, no. 3-4, pp. 360-376, 2016.

[6] I. Dincer, *Comprehensive energy systems*. Elsevier, 2018.

[7] J. Bonafin, C. Pietra, A. Bonzanini, and P. Bombarda, "CO_2 emissions from geothermal power plants: Evaluation of technical solutions for CO_2 reinjection," in *Proceedings of the European Geothermal Congress*, 2019.

[8] R. Bertani and I. Thain, "Geothermal power generating plant CO_2 emission survey," *IGA news,* vol. 49, pp. 1-3, 2002.

[9] D. Berstad and L. O. Nord, "Acid gas removal in geothermal power plant in Iceland," *Energy Procedia,* vol. 86, pp. 32-40, 2016.

[10] D. L. Mamrosh, K. E. McIntush, C. Beitler, S. Markusson, and K. Einarsson, "Screening of H_2S abatement options for geothermal power noncondensable gas at Bjarnarflag," *GRC Transactions,* vol. 36, p. 121725, 2012.

[11] Carbfix. *How it works?* Available: https://www.carbfix.com/how-it-works

[12] H. Kaieda *et al.*, "Field experiments for studying on CO_2 sequestration in solid minerals at the Ogachi HDR geothermal site, Japan," in *Proceedings 34th workshop on geothermal reservoir engineering*, 2009: Stanford University.

[13] GECO. *About*. Available: https://geco-h2020.eu/about/

[14] İ. Yücetaş, N. Ergiçay, and S. Akın, "Carbon dioxide injection field pilot in Umurlu Geothermal Field, Turkey," *GRC Transactions,* vol. 42, 2018.

[15] N. J. Hyne, *Dictionary of Petroleum Exploration, Drilling, and Production*. Tulsa, Oklahoma: PennWell, 1991.

[16] B. Guo, K. Sun, and A. Ghalambor, *Well productivity handbook*. Elsevier, 2014.

[17] S.O.Glossary.*Permeability*. Available: https://www.glossary.oilfield.slb.com/en/Terms/p/permeability.aspx

[18] S. Erol, S. J. Fowler, M. Nehler, E. De Boever, V. Harcouët-Menou, and B. Laenen, "An Analytical Algorithm of Porosity–Permeability for Porous and Fractured Media: Extension to Reactive Transport Conditions and Fitting via Flow-Through Experiments Within Limestone and Dolomite," *Transport in Porous Media,* vol. 129, no. 1, pp. 343-383, 2019.

[19] L. Luquot, O. Rodriguez, and P. Gouze, "Experimental characterization of porosity structure and transport property changes in limestone undergoing different dissolution regimes," *Transport in Porous Media,* vol. 101, no. 3, pp. 507-532, 2014.

[20] L. Luquot and P. Gouze, "Experimental determination of porosity and permeability changes induced by injection of CO_2 into carbonate rocks," *Chemical Geology,* vol. 265, no. 1-2, pp. 148-159, 2009.

[21] C. Noiriel, P. Gouze, and D. Bernard, "Investigation of porosity and permeability effects from microstructure changes during limestone dissolution," *Geophysical research letters,* vol. 31, no. 24, 2004.

[22] A. J. Luhmann, X.-Z. Kong, B. M. Tutolo, K. Ding, M. O. Saar, and W. E. Seyfried Jr, "Permeability reduction produced by grain reorganization and accumulation of exsolved CO_2 during geologic carbon sequestration: A new CO_2 trapping mechanism," *Environmental science & technology,* vol. 47, no. 1, pp. 242-251, 2013.

[23] Y. Hao, M. Smith, Y. Sholokhova, and S. Carroll, "CO_2-induced dissolution of low permeability carbonates. Part II: Numerical modeling of experiments," *Advances in water resources,* vol. 62, pp. 388-408, 2013.

[24] B. R. Munson, D. F. Young, and T. H. Okiishi, "Fundamentals of fluid mechanics," *Oceanographic Literature Review,* vol. 10, no. 42, p. 831, 1995.

[25] J. Kleppe, "Reservoir Simulation: Review Of Basic Steps In Derivation Of Flow Equations," 2018.

[26] H. Darcy, *Les fontaines publiques de la ville de Dijon: exposition et application*. Victor Dalmont, 1856.

[27] D. W. Peaceman, *Fundamentals of numerical reservoir simulation*. Elsevier, 2000.

[28] K. Aziz and A. Settari, *Petroleum Reservoir Simulation*. Applied Science Publishers, 1979.

[29] E. Artun, *An Overview of Numerical Reservoir Simulation*. ASTM International, 2016.

[30] G. D. Smith, G. D. Smith, and G. D. S. Smith, *Numerical solution of partial differential equations: finite difference methods*. Oxford university press, 1985.

[31] R. E. Ewing, *The mathematics of reservoir simulation*. SIAM, 1983.

[32] K. Pruess, *Mathematical modeling of fluid flow and heat transfer in geothermal systems: an introduction in five lectures*. Orkustofnun, 2002.

[33] J. F. Pankow, R. L. Johnson, J. P. Hewetson, and J. A. Cherry, "An evaluation of contaminant migration patterns at two waste disposal sites on fractured porous media in terms of the equivalent porous medium (EPM) model," *Journal of Contaminant Hydrology,* vol. 1, no. 1-2, pp. 65-76, 1986.

[34] S. P. Neuman, "Stochastic continuum representation of fractured rock permeability as an alternative to the REV and fracture network concepts," in *Groundwater Flow and Quality Modelling*: Springer, 1988, pp. 331-362.

[35] J. Bundschuh, *Introduction to the numerical modeling of groundwater and geothermal systems: Fundamentals of mass, energy and solute transport in Poroelastic rocks*. CRC Press, 2010.

[36] J. C. Long, J. Remer, C. Wilson, and P. Witherspoon, "Porous media equivalents for networks of discontinuous fractures," *Water resources research,* vol. 18, no. 3, pp. 645-658, 1982.

[37] P. W. Huntoon, "Is it appropriate to apply porous media groundwater circulation models to karstic aquifers," *Groundwater models for resources analysis and management,* pp. 339-358, 1995.

[38] G. I. Barenblatt, I. P. Zheltov, and I. Kochina, "Basic concepts in the theory of seepage of homogeneous liquids in fissured rocks [strata]," *Journal of applied mathematics and mechanics,* vol. 24, no. 5, pp. 1286-1303, 1960.

[39] J. Warren and P. J. Root, "The behavior of naturally fractured reservoirs," *Society of Petroleum Engineers Journal,* vol. 3, no. 03, pp. 245-255, 1963.

[40] K. Pruess, C. Oldenburg, and G. Moridis, "A general purpose numerical simulator for multiphase fluid and heat flow," *LBNL-29400, Lawrence Berkeley National Laboratory, Berkeley, California,* 1991.

[41] Y. Xiong, P. Fakcharoenphol, P. Winterfeld, R. Zhang, and Y.-S. Wu, "Coupled geomechanical and reactive geochemical model for fluid and heat flow: application for enhanced geothermal reservoir," in *SPE Reservoir Characterization and Simulation Conference and Exhibition*, 2013: Society of Petroleum Engineers.

[42] M. H. Reed, "Calculation of multicomponent chemical equilibria and reaction processes in systems involving minerals, gases and an aqueous phase," *Geochimica et Cosmochimica Acta,* vol. 46, no. 4, pp. 513-528, 1982.

[43] G. T. Yeh and V. S. Tripathi, "A model for simulating transport of reactive multispecies components: model development and demonstration," *Water Resources Research,* vol. 27, no. 12, pp. 3075-3094, 1991.

[44] C. I. Steefel and A. C. Lasaga, "A coupled model for transport of multiple chemical species and kinetic precipitation/dissolution reactions with application to reactive flow in single phase hydrothermal systems," *American Journal of science,* vol. 294, no. 5, pp. 529-592, 1994.

[45] T. Xu, E. Sonnenthal, N. Spycher, and K. Pruess, "TOUGHREACT user's guide: A simulation program for non-isothermal multiphase reactive geochemical transport in variable saturated geologic media," Lawrence Berkeley National Lab.(LBNL), Berkeley, CA (United States)2004.

[46] C. I. Steefel, D. J. DePaolo, and P. C. Lichtner, "Reactive transport modeling: An essential tool and a new research approach for the Earth sciences," *Earth and Planetary Science Letters,* vol. 240, no. 3-4, pp. 539-558, 2005.

[47] J. L. Palandri and Y. K. Kharaka, "A compilation of rate parameters of water-mineral interaction kinetics for application to geochemical modeling," Geological Survey Menlo Park CA2004.

[48] J. I. Drever, *Geochemistry of Natural Waters*, 3rd ed. Prentice Hall, 1997, p. 436.

[49] E. Sonnenthal and P. J. Ortoleva, "Numerical simulations of overpressured compartments in sedimentary basins," 1994.

[50] P. K. Weyl, "Pressure solution and the force of crystallization: a phenomenological theory," *Journal of geophysical research,* vol. 64, no. 11, pp. 2001-2025, 1959.

[51] USGS. (2021). *PHREEQC Version 3*. Available: https://www.usgs.gov/software/phreeqc-version-3

[52] S. R. Charlton and D. L. Parkhurst, "Modules based on the geochemical model PHREEQC for use in scripting and programming languages," *Computers & Geosciences,* vol. 37, no. 10, pp. 1653-1663, 2011.

[53] Ş. Şimşek, M. Parlaktuna, and S. Akın, "Data Gathering and Evaluation of Kızıldere Geothermal Field," *Report prepared for Zorlu Energy,* 2009.

[54] J. R. Haizlip, M. M. Stover, S. K. Garg, F. Haklidir, and N. Prina, "Origin and impacts of high concentrations of carbon dioxide in geothermal fluids of western Turkey," in *Proceedings*, 2016, pp. 22-24.

[55] T. Akın, "Kızıldere jeotermal sahasındaki termal akışkanın üretimden enjeksiyona geçirdiği jeokimyasal evrimin modellenmesi," 2019.

[56] İ. H. Karamanderesi and K. Ölçenoğlu, "Geology of the Denizli Sarayköy (Gerali) Geothermal Field, Western Anatolia, Turkey," in *Proceedings*, 2005.

[57] O. Imasuen, K. Tazaki, W. Fyfe, and N. Kohyama, "Experimental transformations of kaolinite to smectite," *Applied clay science,* vol. 4, no. 1, pp. 27-41, 1989.

[58] L. Zhang, Y. Soong, R. Dilmore, and C. Lopano, "Numerical simulation of porosity and permeability evolution of Mount Simon sandstone under geological carbon sequestration conditions," *Chemical Geology,* vol. 403, pp. 1-12, 2015.

[59] K. F. Evans, A. Zappone, T. Kraft, N. Deichmann, and F. Moia, "A survey of the induced seismic responses to fluid injection in geothermal and CO_2 reservoirs in Europe," *Geothermics,* vol. 41, pp. 30-54, 2012.

[60] T. Ratouis, S. O. Snæbjörnsdóttir, G. Gunnarsson, I. Gunnarsson, B. R. Kristjánsson, and E. S. Aradóttir, "Modelling the Complex Structural Features Controlling Fluid Flow at the CarbFix2 Reinjection Site, Hellisheiði Geothermal Power Plant, SW-Iceland," in *44th Workshop on Geothermal Reservoir Engineering Stanford University*, 2019, pp. 11-13.

[61] M. L. Druckenmiller and M. M. Maroto-Valer, "Carbon sequestration using brine of adjusted pH to form mineral carbonates," *Fuel Processing Technology,* vol. 86, no. 14-15, pp. 1599-1614, 2005.

[62] S. R. Gislason *et al.*, "Mineral sequestration of carbon dioxide in basalt: A pre-injection overview of the CarbFix project," *International Journal of Greenhouse Gas Control,* vol. 4, no. 3, pp. 537-545, 2010.

[63] R. DiPippo, *Geothermal power plants: principles, applications, case studies and environmental impact*. Butterworth-Heinemann, 2012.

[64] D. B. van den Heuvel, E. Gunnlaugsson, I. Gunnarsson, T. M. Stawski, C. L. Peacock, and L. G. Benning, "Understanding amorphous silica scaling under well-constrained conditions inside geothermal pipelines," *Geothermics,* vol. 76, pp. 231-241, 2018.

[65] S. Kitahara, "The polymerization of silicic acid obtained by the hydrothermal treatment of quartz and the solubility of amorphous silica," *The Review of Physical Chemistry of Japan,* vol. 30, no. 2, pp. 131-137, 1960.

APPENDICES

A. Appendix A

A.1 Scenario1

A.1.1 Mineral Assembly 2

Mineral Assembly 2 includes schist and marble minerals, which are given in Table 4.6. Mineral volume, aqueous species' volume, porosity, permeability, pH, temperature, and pressure change at the injection well block have been illustrated in Figures A.1 through A.6.

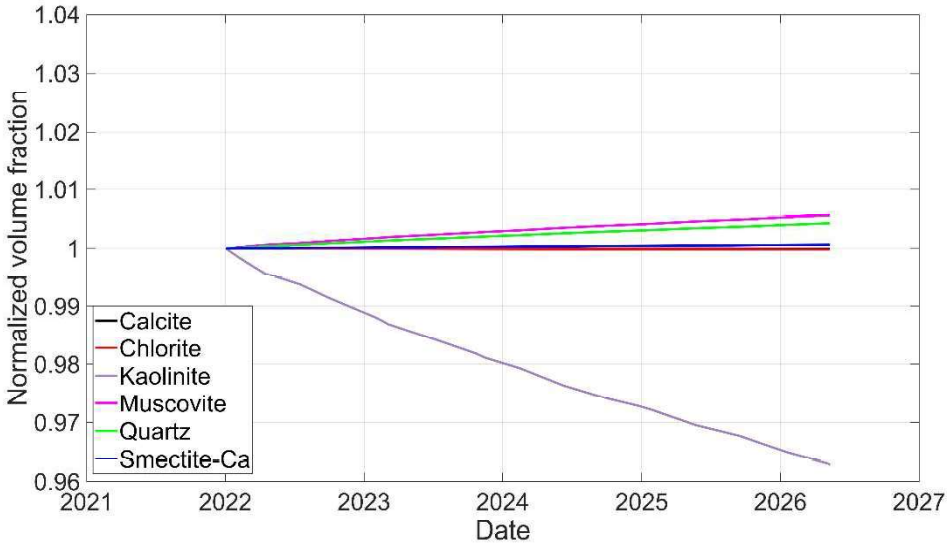

Figure A.1 Change in mineral volumes around injection well

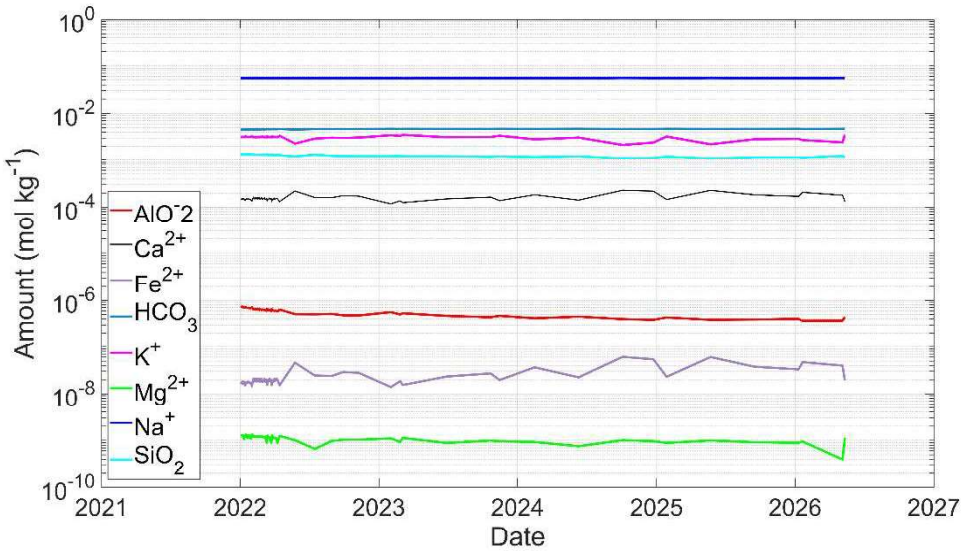

Figure A.2 Change in aqueous species volume around injection well

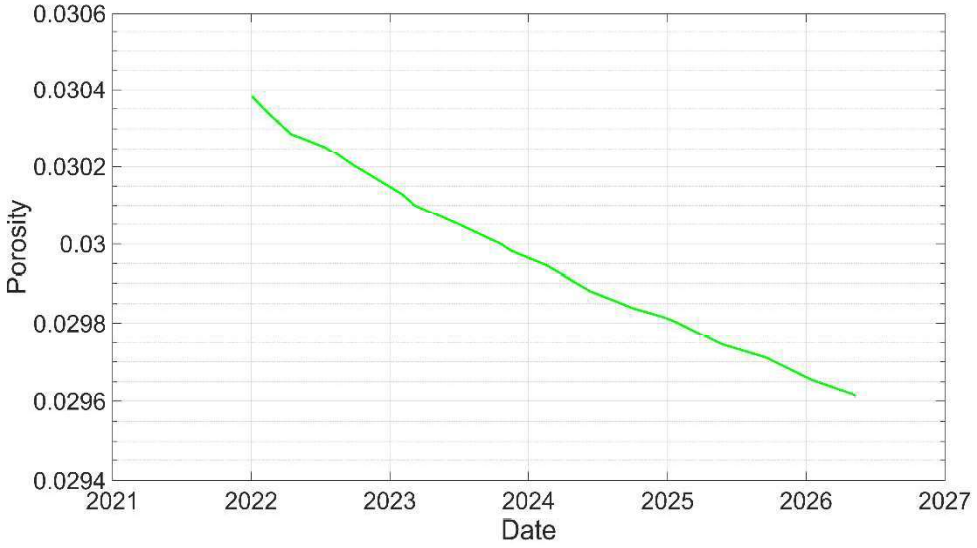

Figure A.3 Change in porosity around injection well

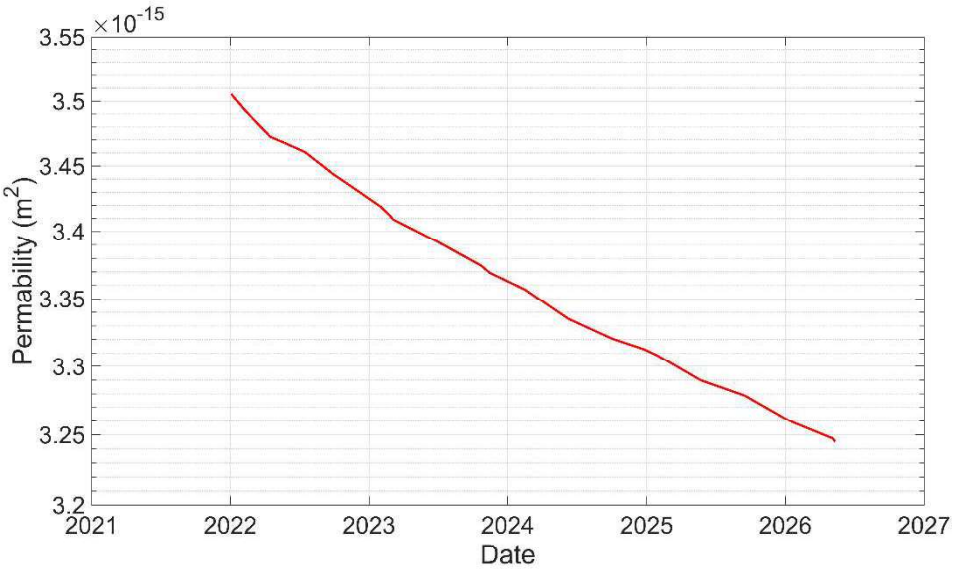

Figure A.4 Change in permeability around injection well

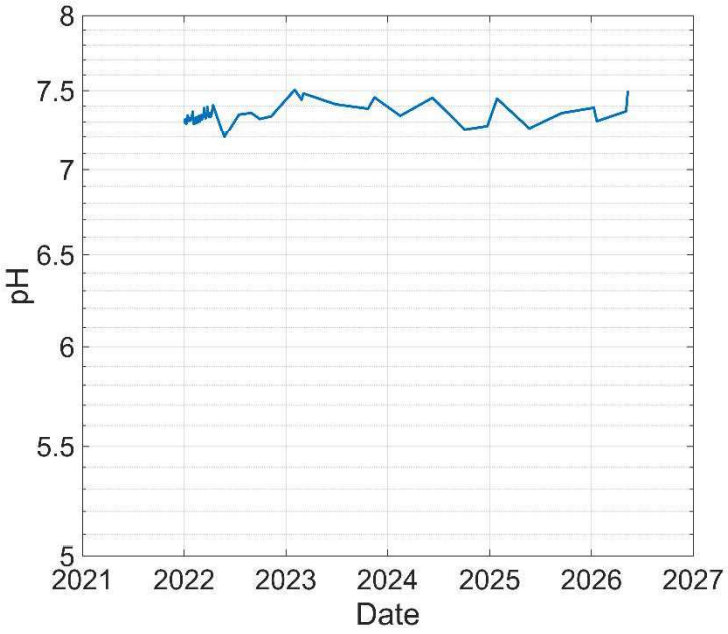

Figure A.5 Change in pH around injection well

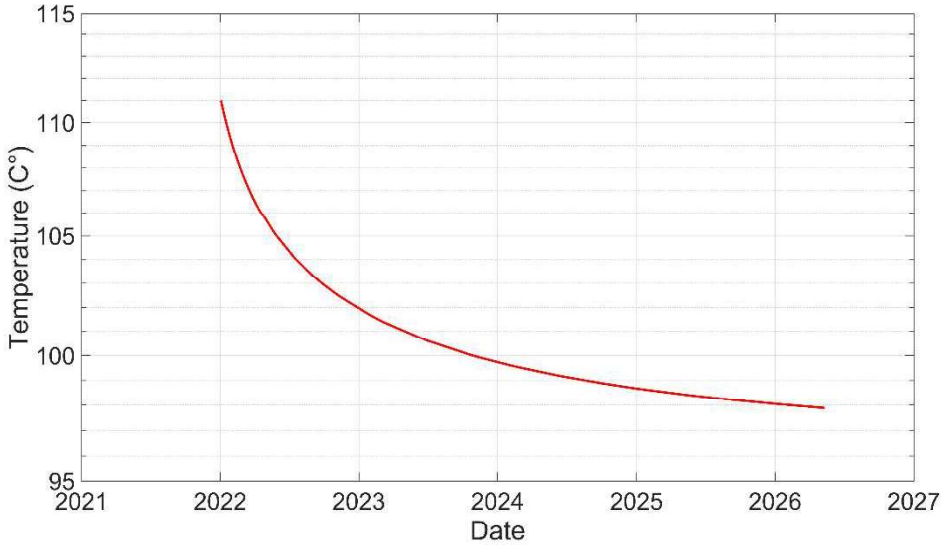

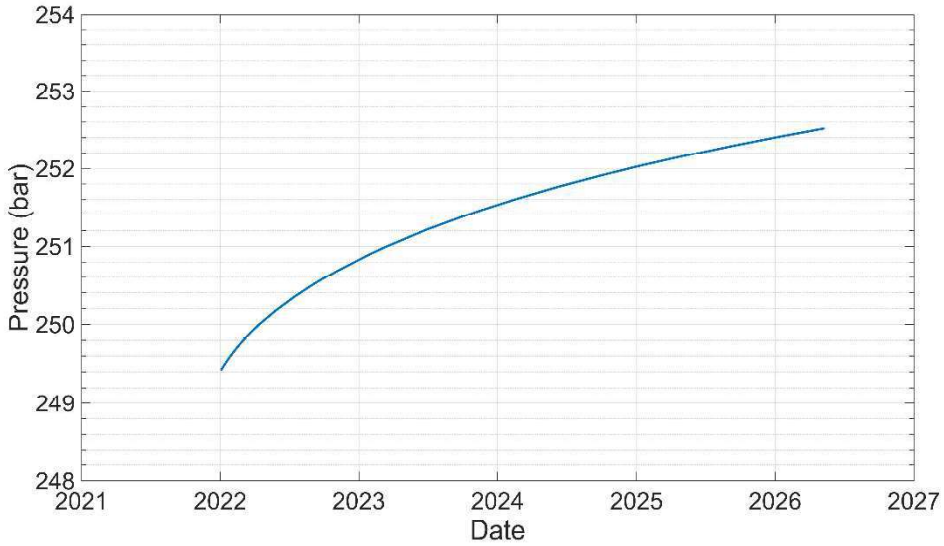

Figure A.6 Change in temperature and pressure around injection well

A.1.2 Mineral Assembly 3

Mineral Assembly 3 includes marble minerals, which are given in Table 4.7. Mineral volume, aqueous species' volume, porosity, permeability, pH, temperature, and pressure change at the injection well block have been illustrated in Figures A.7 through A.13.

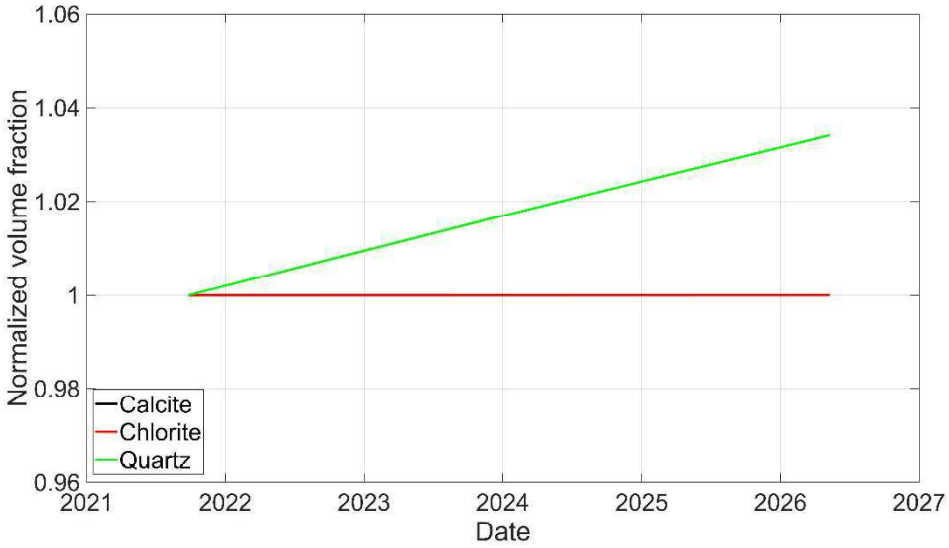

Figure A.7 Change in mineral volumes around injection well

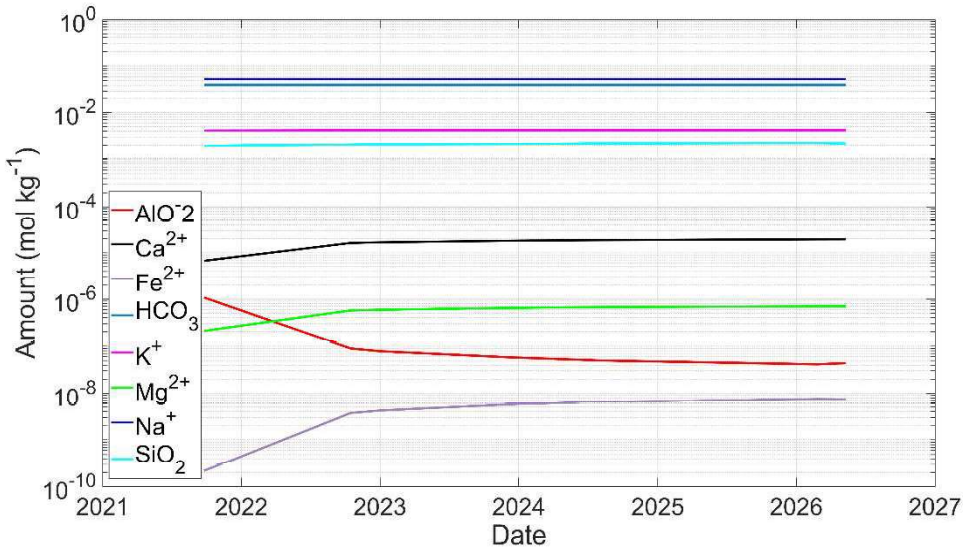

Figure A.8 Change in aqueous species volumes around wellbore

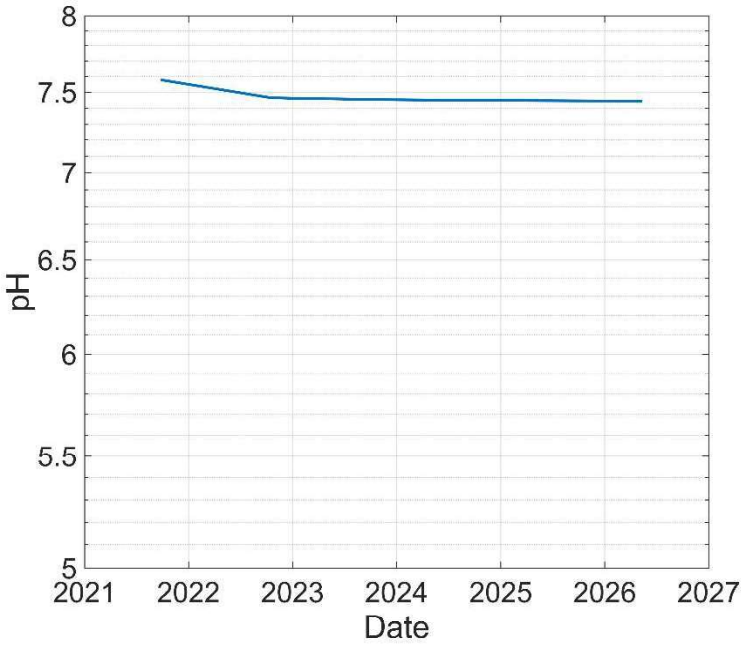

Figure A.9 Change in pH around injection well

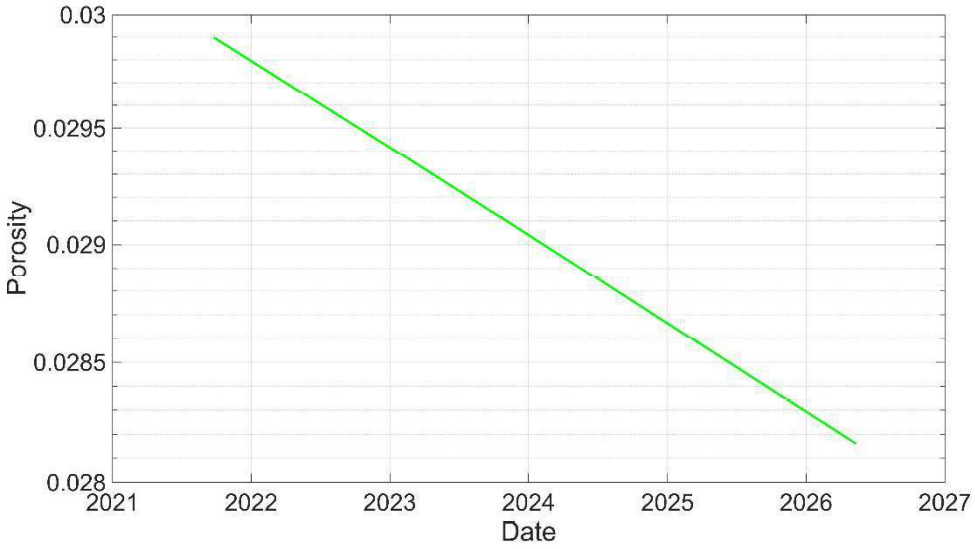

Figure A.10 Change in porosity around injection well

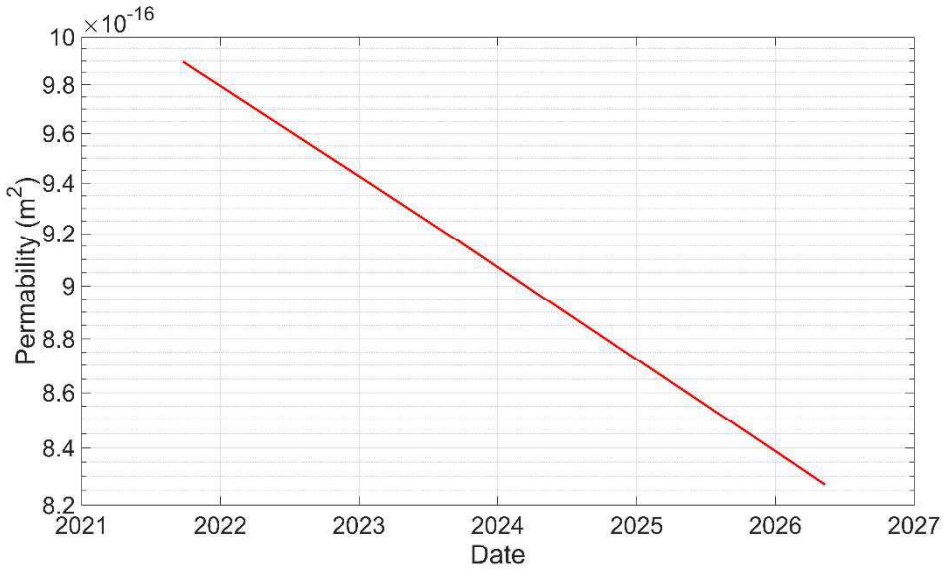

Figure A.11 Change in permeability around injection well

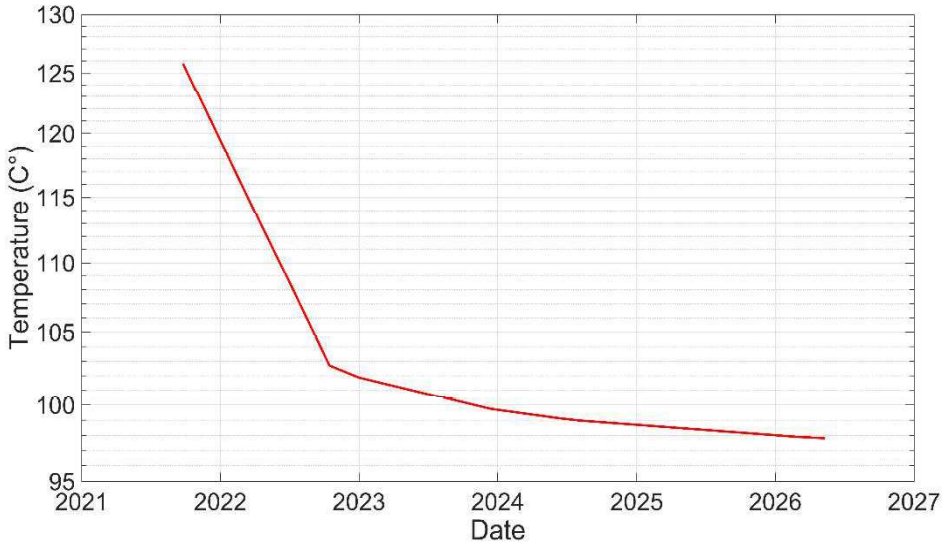

Figure A.12 Change in temperature around injection well

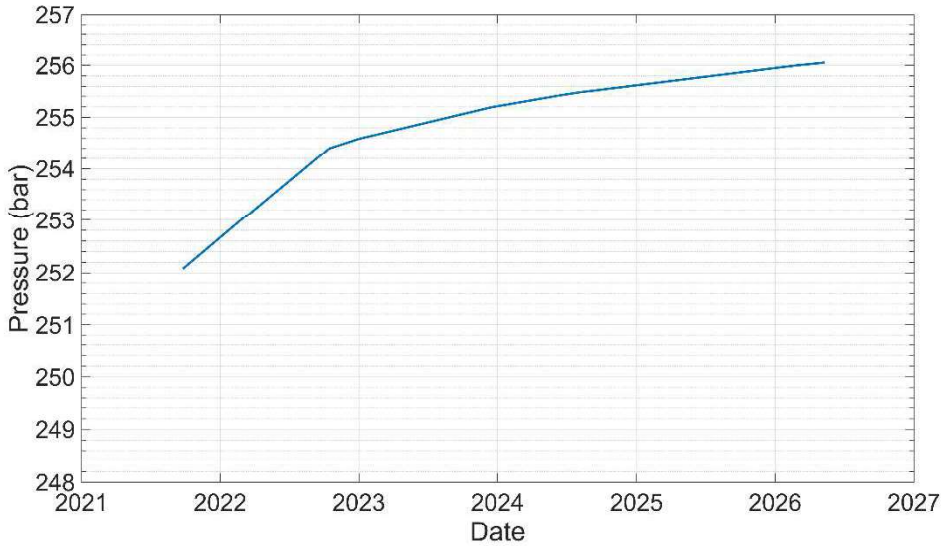

Figure A.13 Change in pressure around injection well

A.2 Scenario 2

A.2.1 Mineral Assembly 2

Mineral Assembly 2 includes schist and marble minerals, which are given in Table 4.6. CO_2 plum and pH after 5 years have been illustrated in Figure A.14 and Figure A.15., respectively.

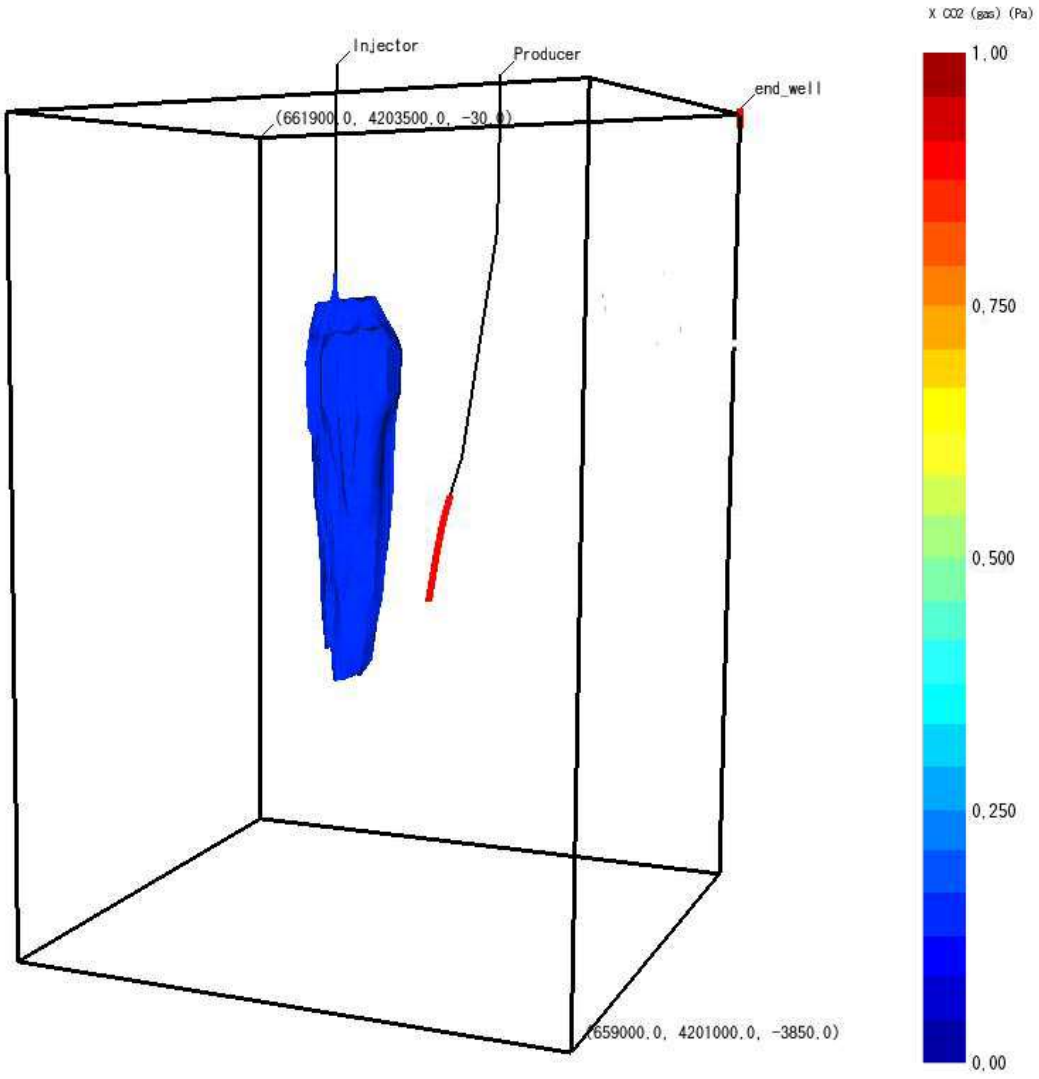

Figure A.14 CO_2 bubble around injection well

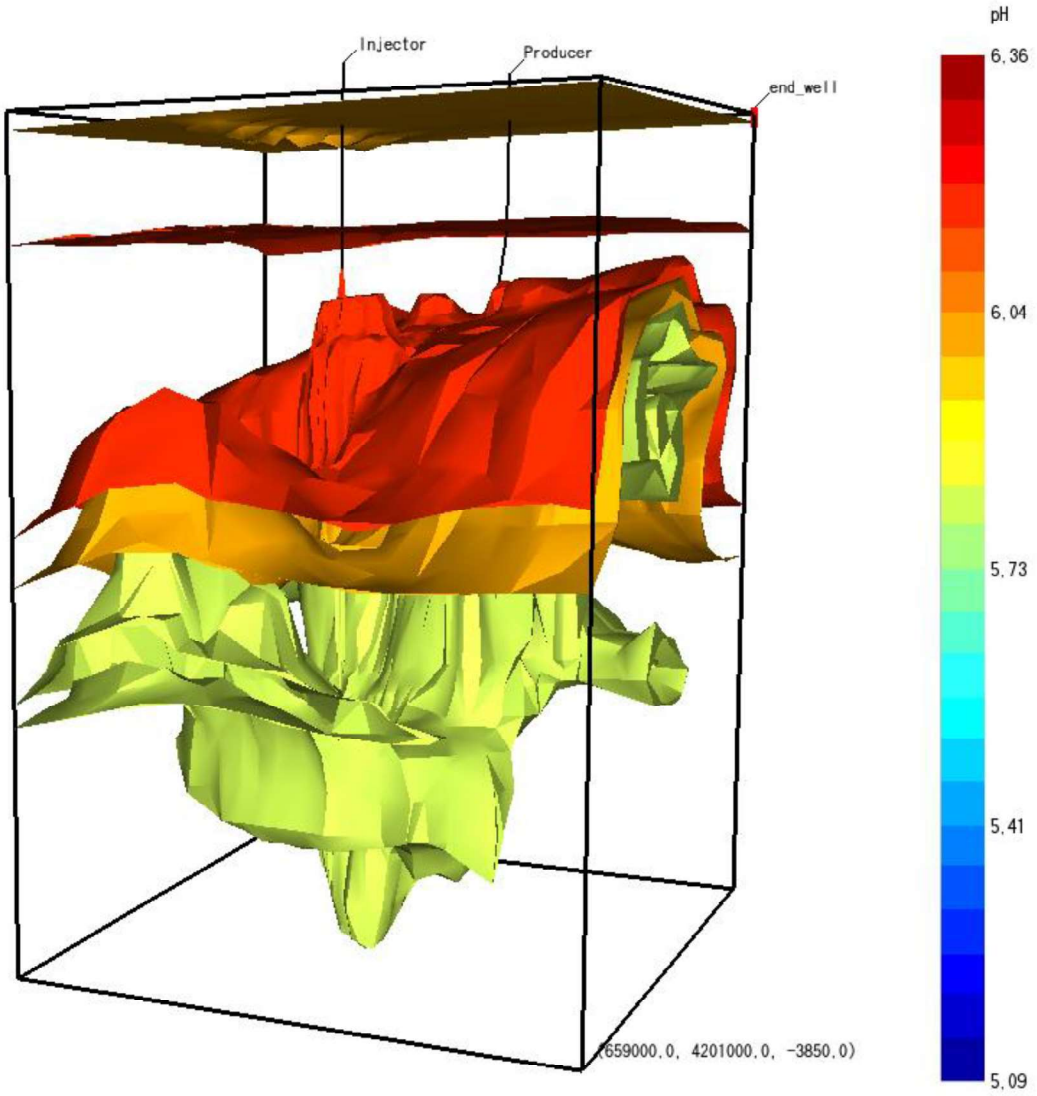

Figure A.15 pH of the model after CO_2 injection in supercritical state

A.2.2 Mineral Assembly 3

Mineral Assembly 3 includes marble minerals, which are given in Table 4.7. CO_2 plum and pH after 5 years have been illustrated in Figure A.16 and Figure A.17., respectively.

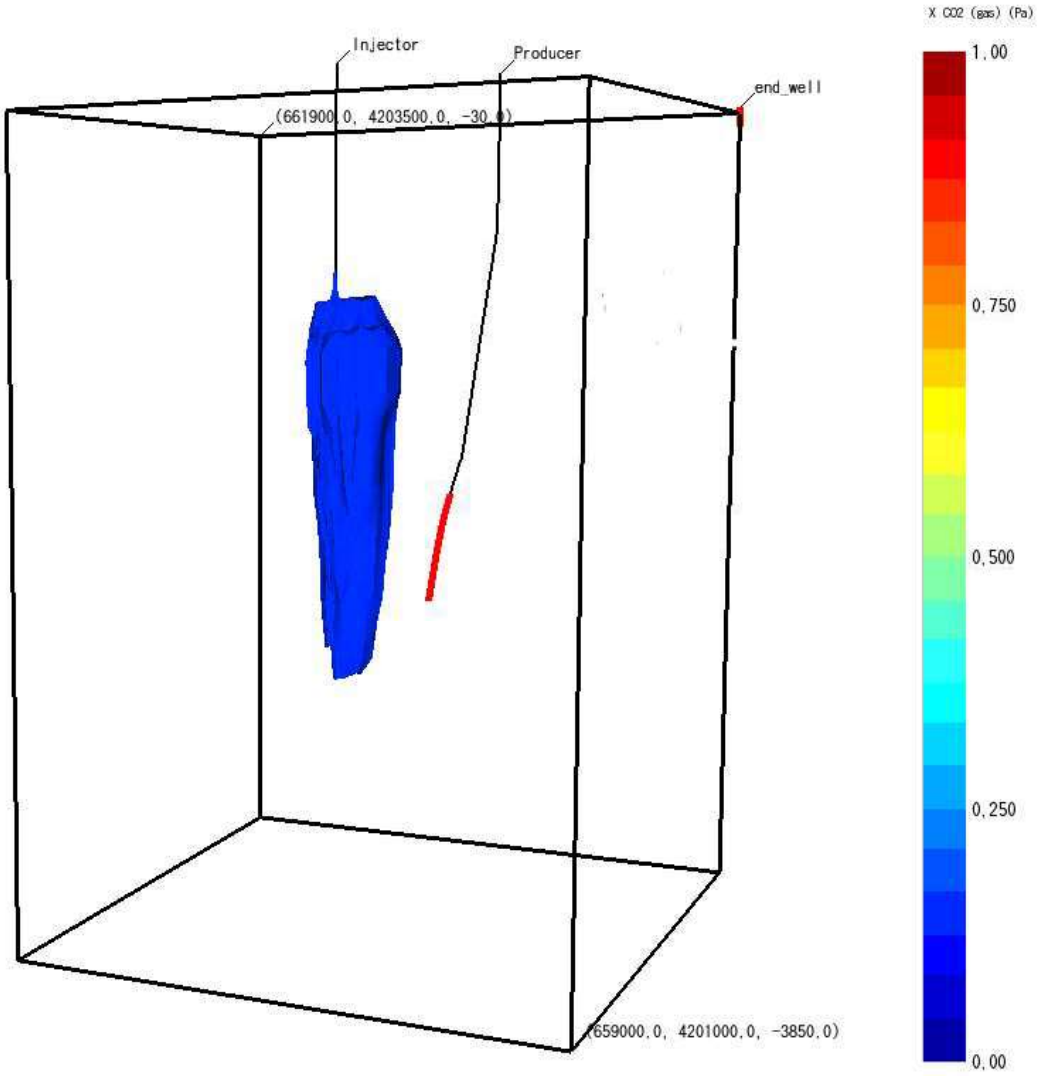

Figure A.16 CO_2 around injection well

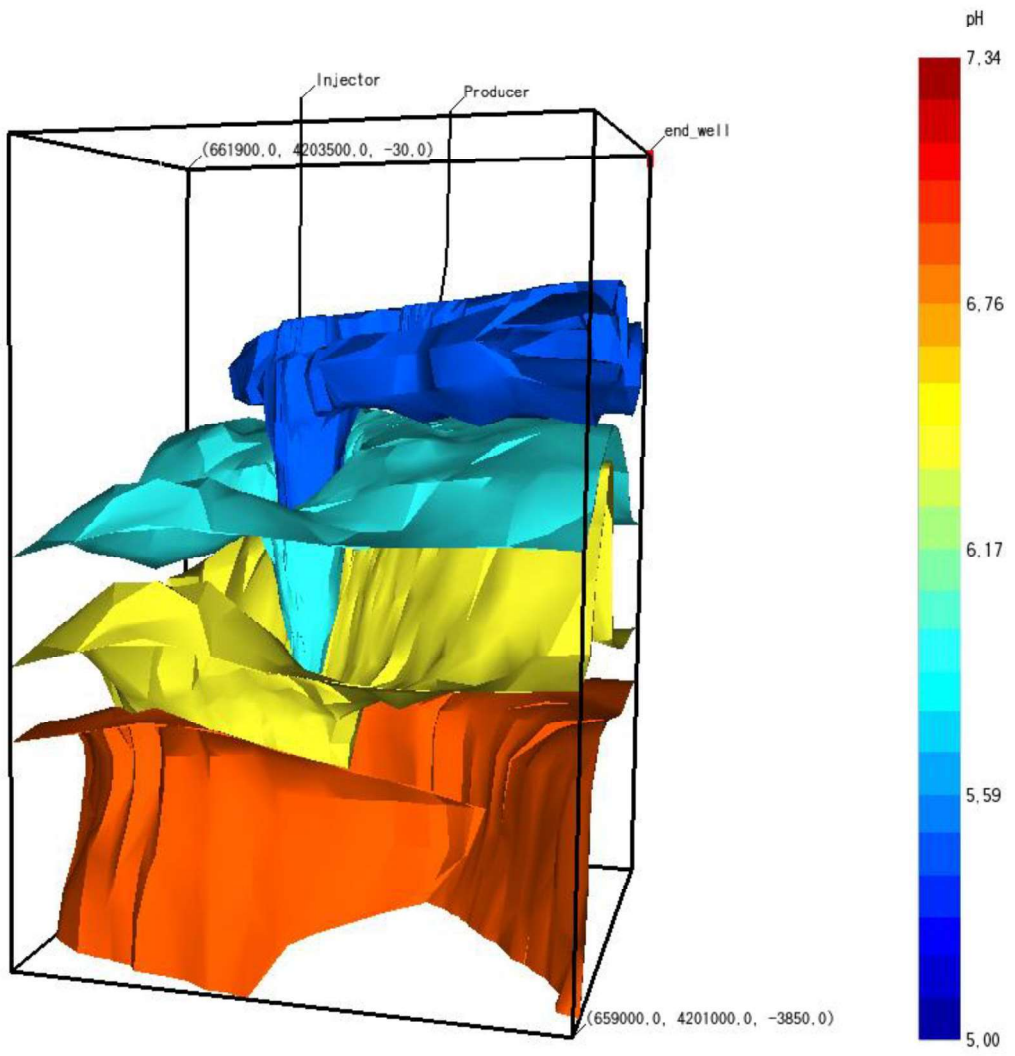

Figure A.17 pH of the model after CO_2 injection in supercritical state

A.3 Scenario 3

A.3.1 Mineral Assembly 2

Mineral Assembly 2 includes schist and marble minerals, which are given in Table 4.5. Mineral volume, aqueous species' volume, porosity, permeability, pH, temperature, and pressure change at the injection well block have been illustrated in Figures A.18 through A.24.

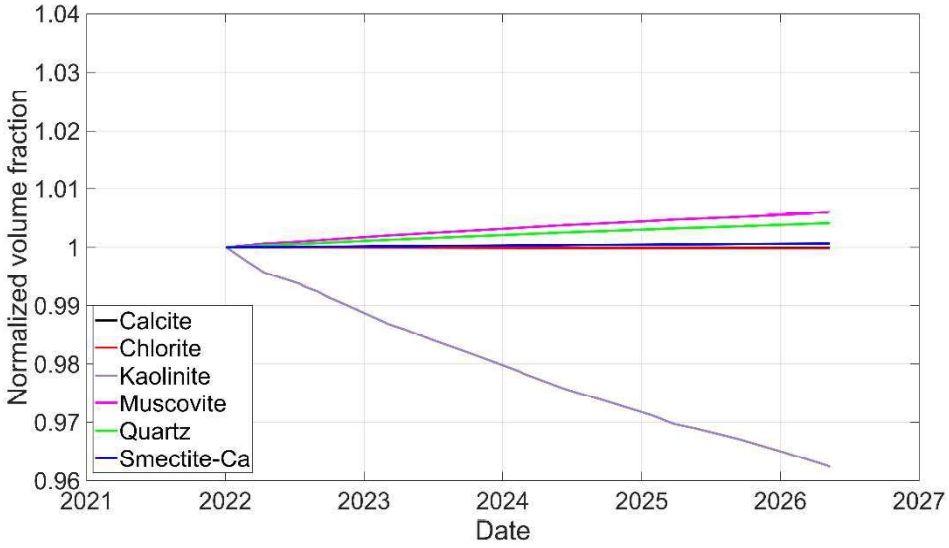

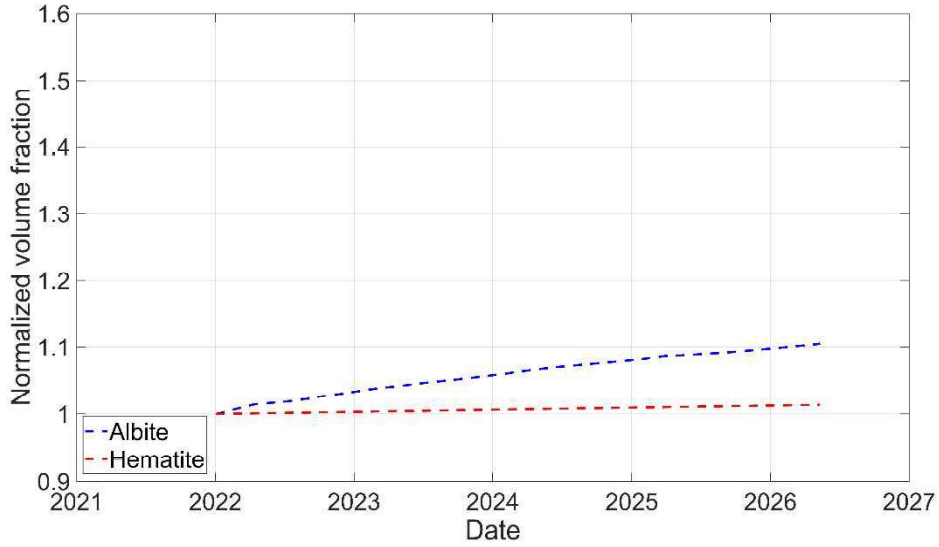

Figure A.18 Change in mineral volumes around injection well

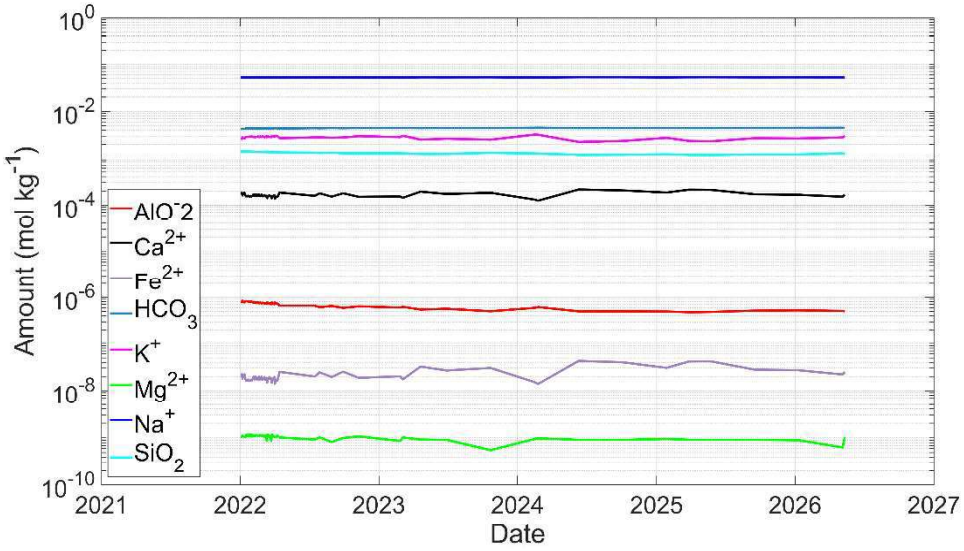

Figure A.19 Change in aqueous species volumes around injection well

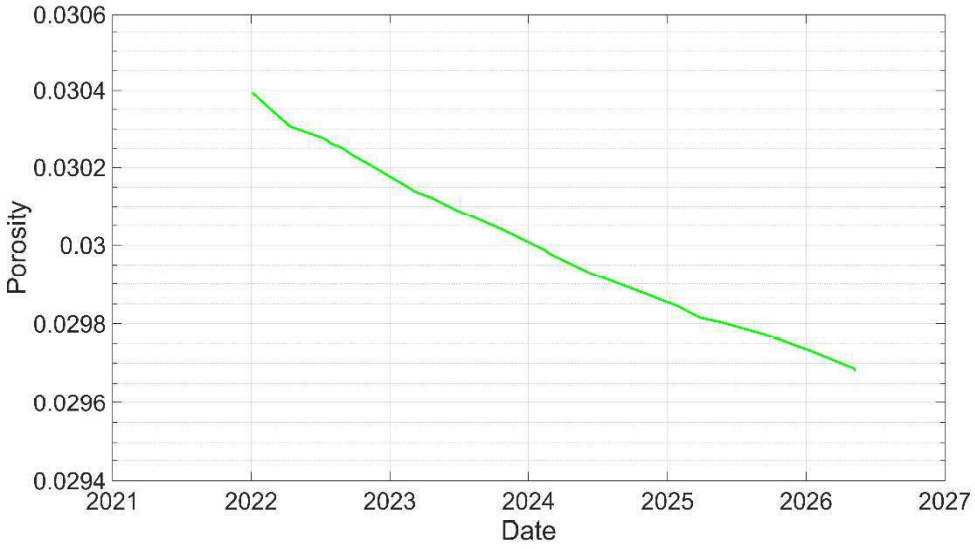

Figure A.20 Change in porosity around injection well

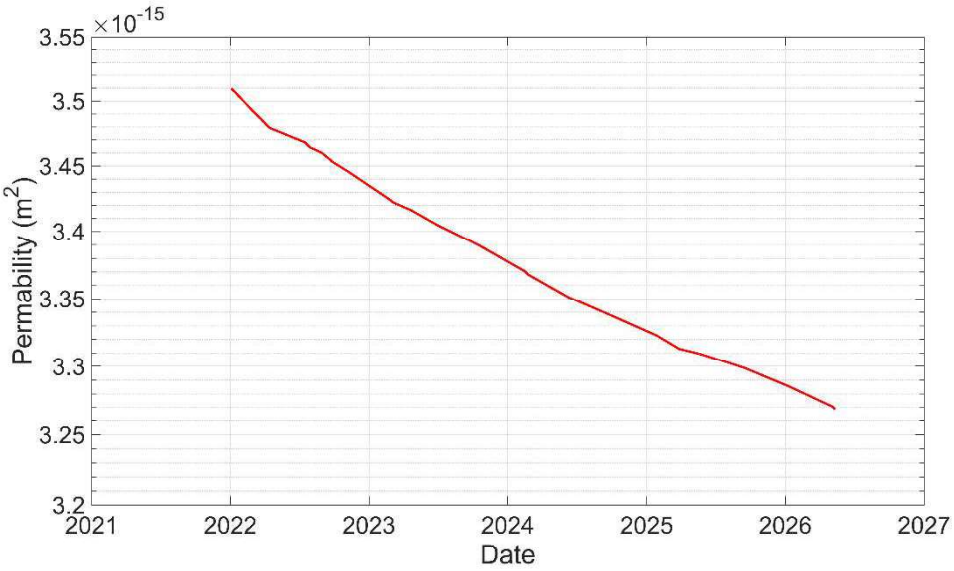

Figure A.21Change in permeability around injection well

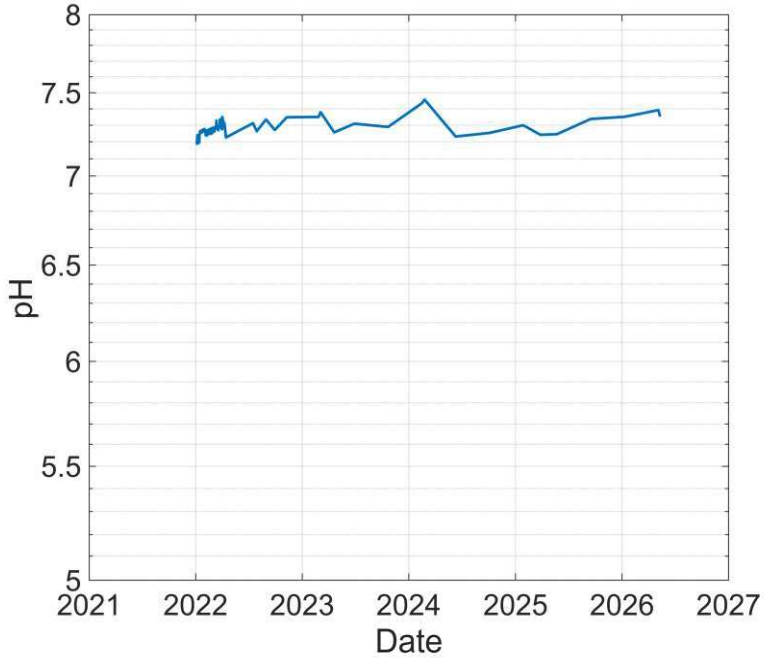

Figure A.22 Change in pH around injection well

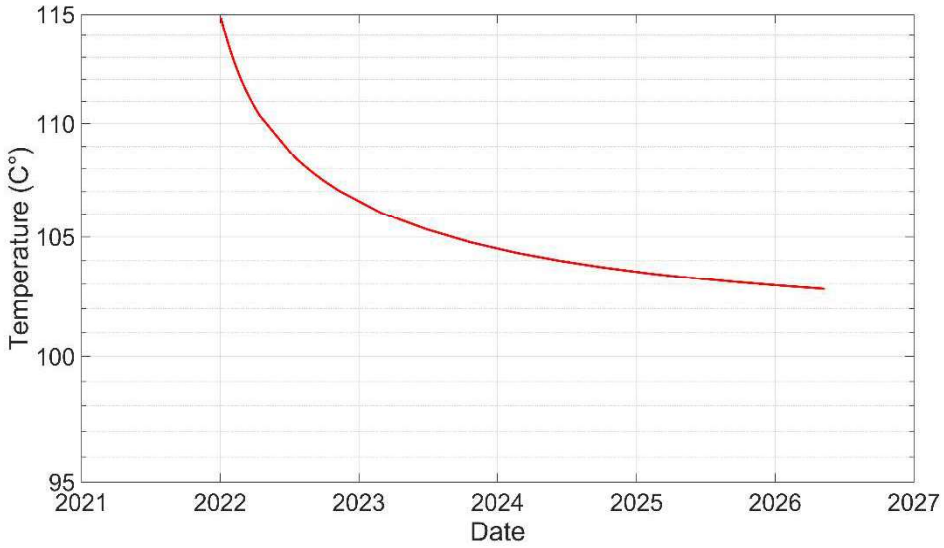

Figure A.23 Change in temperature around injection well

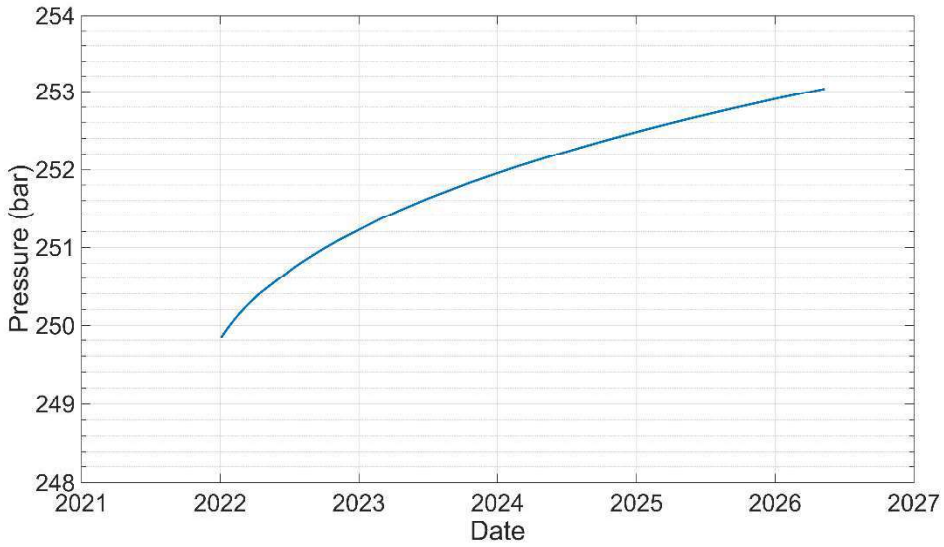

Figure A.24 Change in pressure around injection well

A distance-based comparison between injection and production well for Scenario 1 and 3 has been conducted (Figure A.25 – A.28). In these figures "0" represents

injection well location whereas 446m represents the production well at an approximate depth of 2350m.

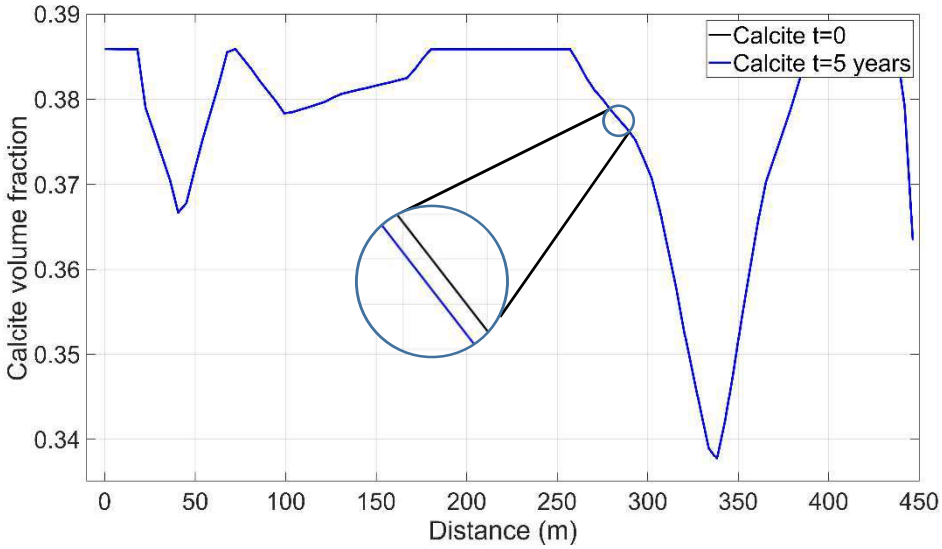

Figure A.25 Calcite volume fraction comparison between two wells

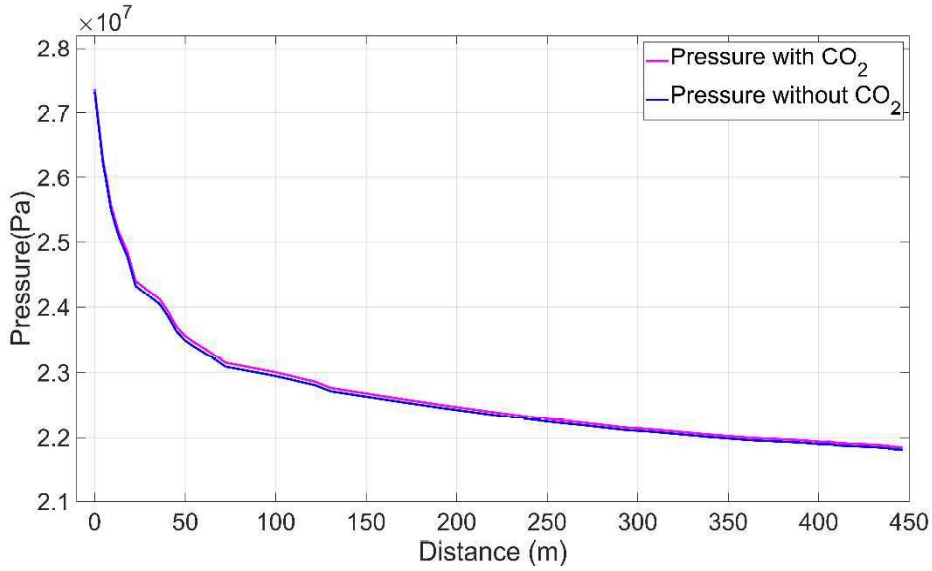

Figure A.26 Pressure comparison between scenario 1 and 3 between two wells after 5 years

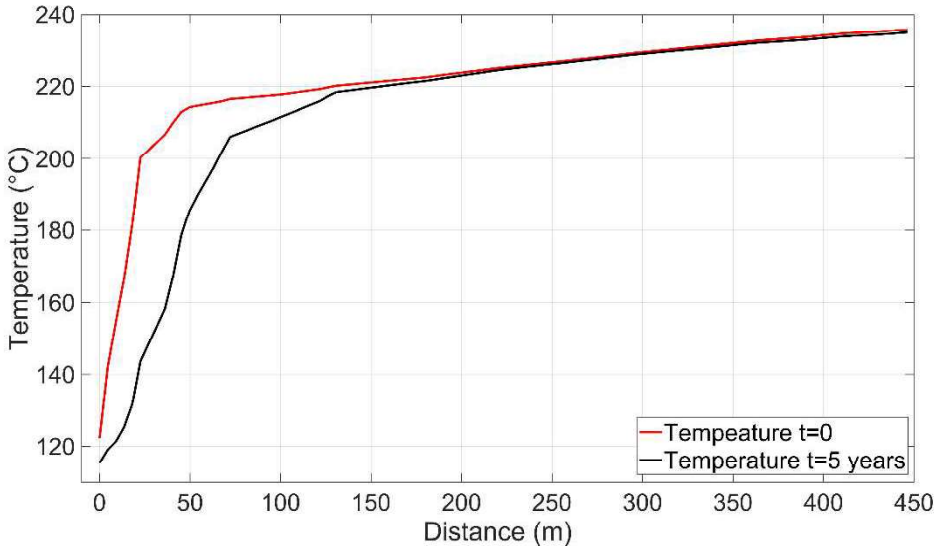

Figure A.27 Temperature comparison between two wells

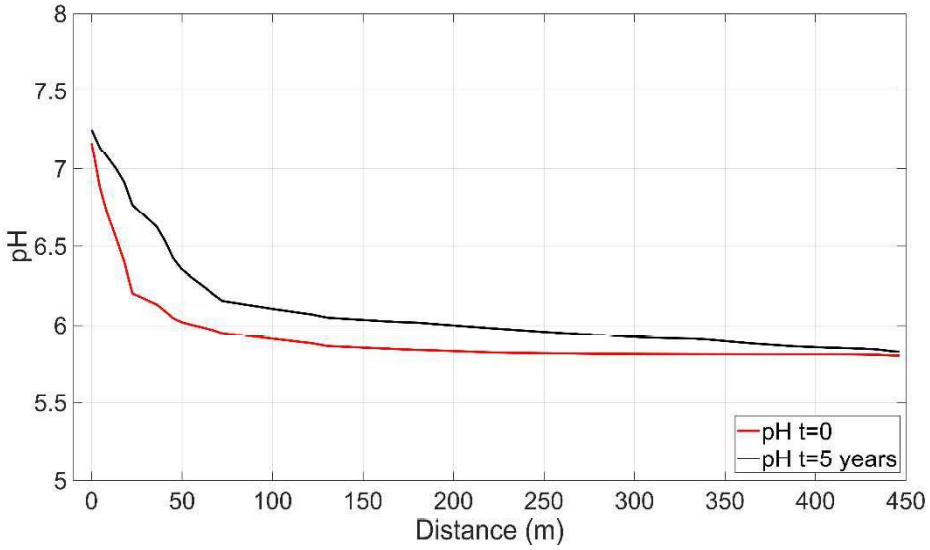

Figure A.28 pH comparison between two wells

A.3.2 Mineral Assembly 3

Mineral Assembly 3 includes marble minerals, which are given in Table 4.5. Mineral volume, aqueous species' volume, porosity, permeability, pH, temperature, and pressure change at the injection well block have been illustrated in Figures A.29 through A.35.

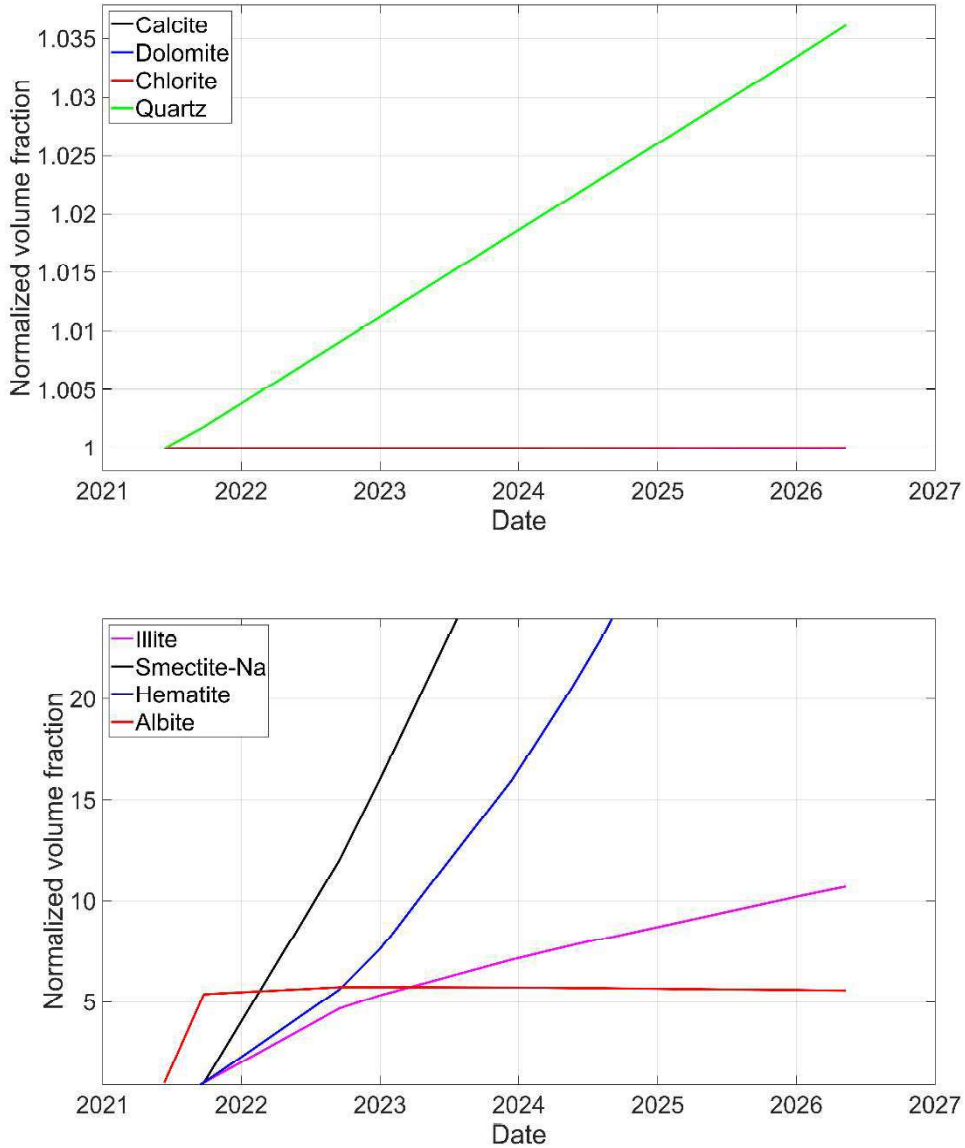

Figure A.29 Change in mineral volumes around injection well

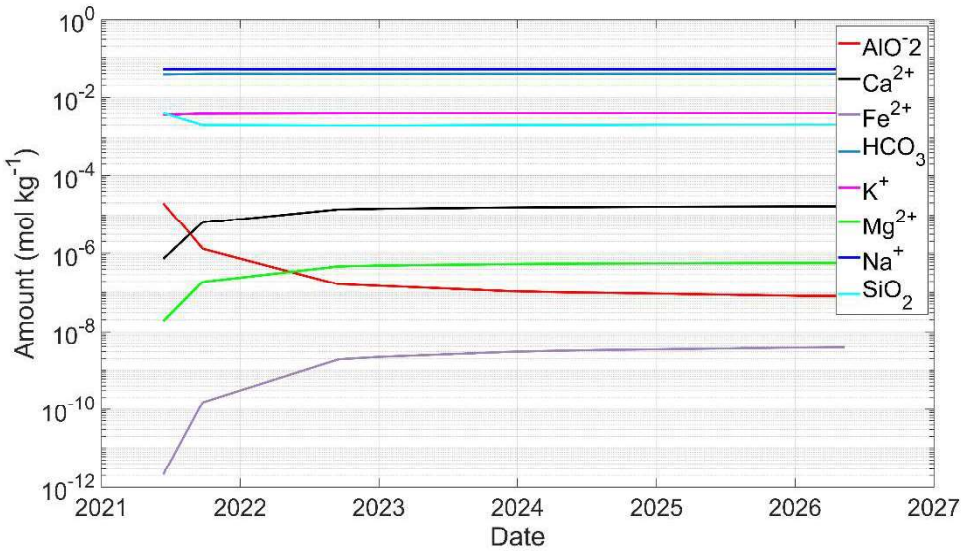

Figure A.30 Change in aqueous species volume around injection well

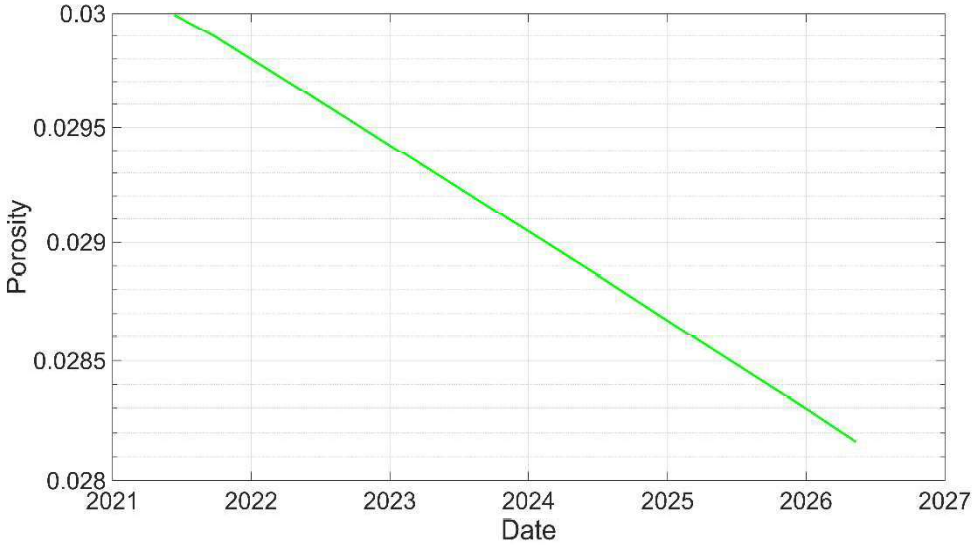

Figure A.31 Change in porosity around injection well

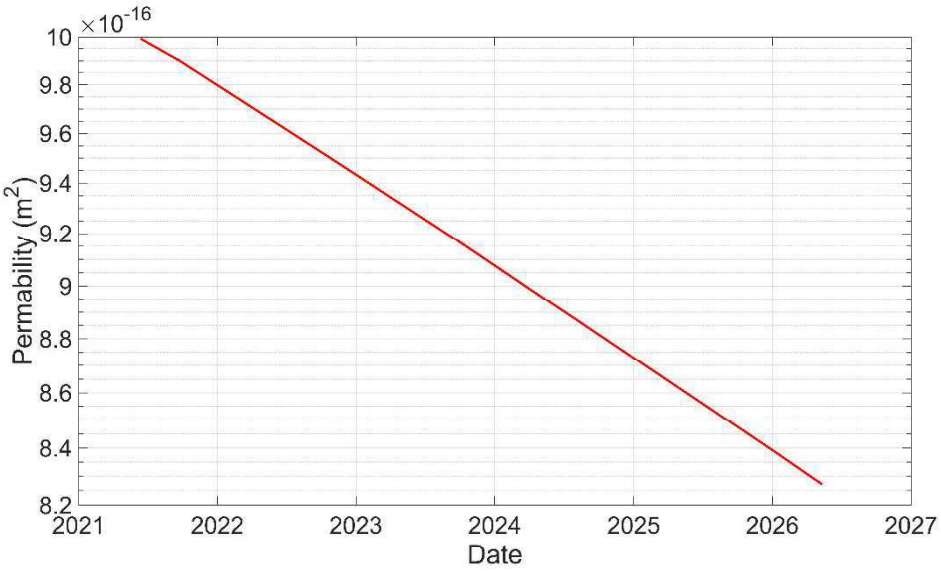

Figure A.32 Change in permeability around injection well

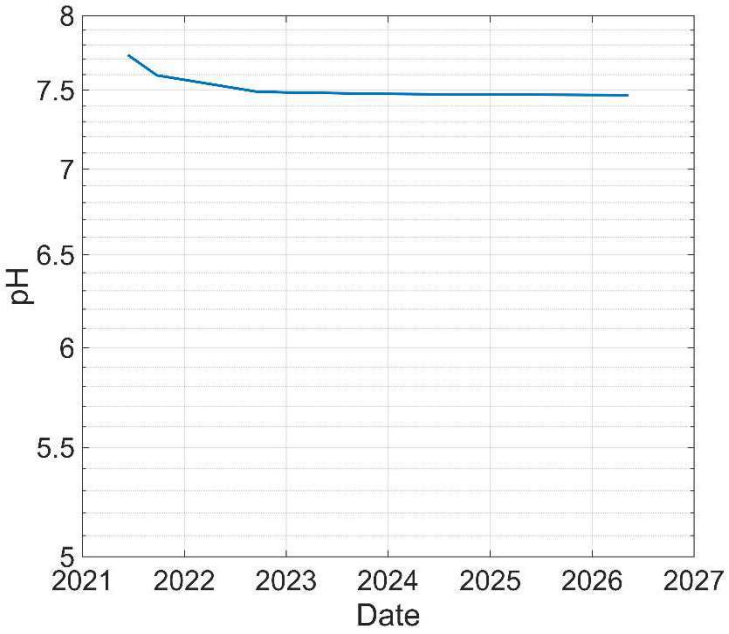

Figure A.33 Change in pH around injection well

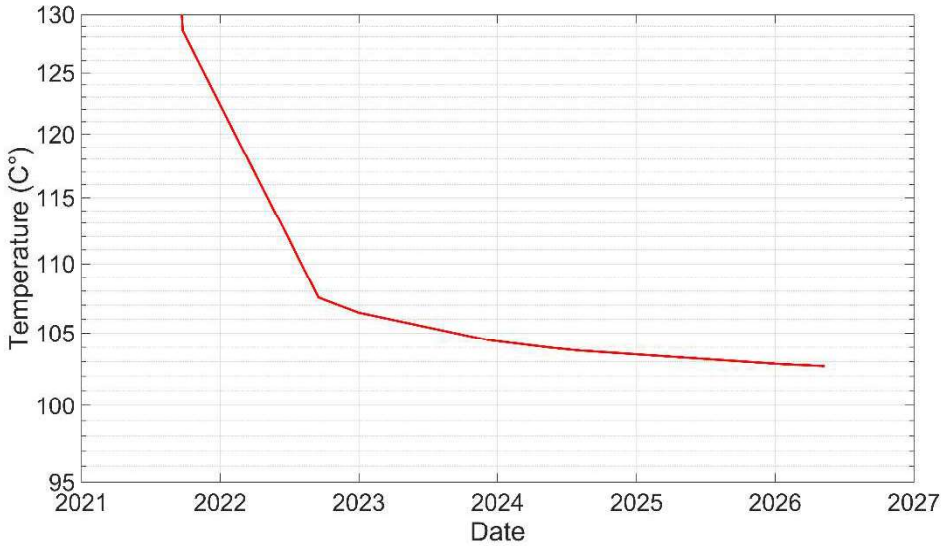

Figure A.34 Change in temperature around injection well

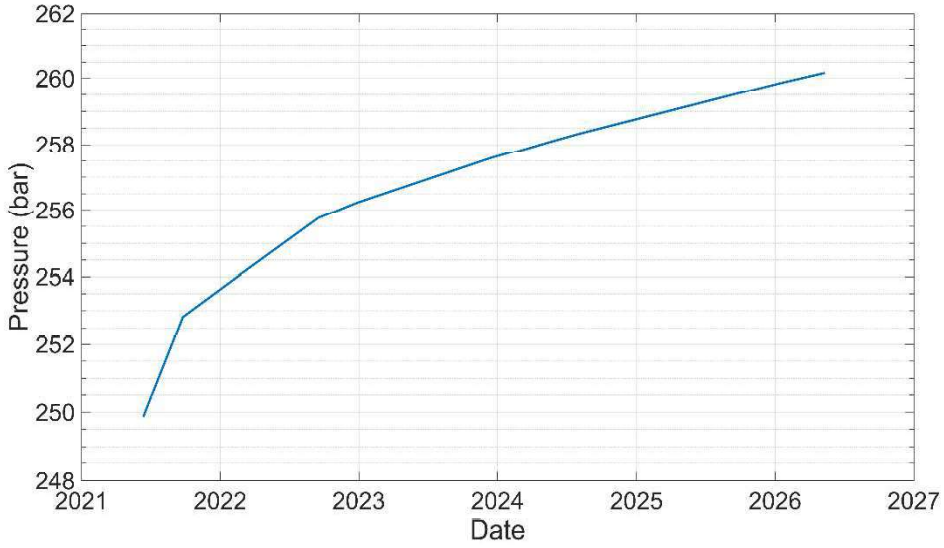

Figure A.35 Change in pressure around injection well

A distance-based comparison between injection and production well for Scenario 1 and 3 has been conducted (Figure A.36 – A.39). In these figures "0" represents injection well location whereas 446m represents the production well at an approximate depth of 2350m.

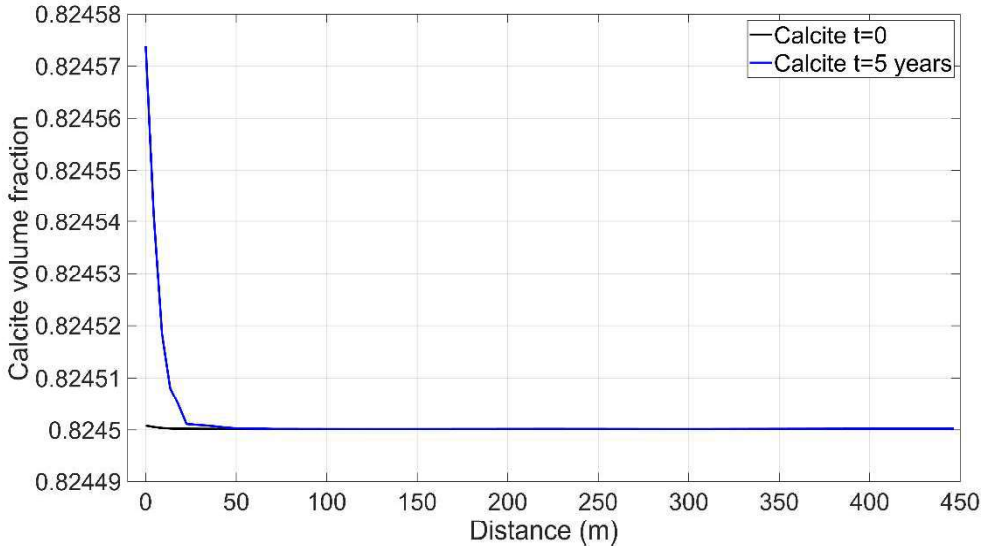

Figure A.36 Calcite volume fraction comparison between two wells

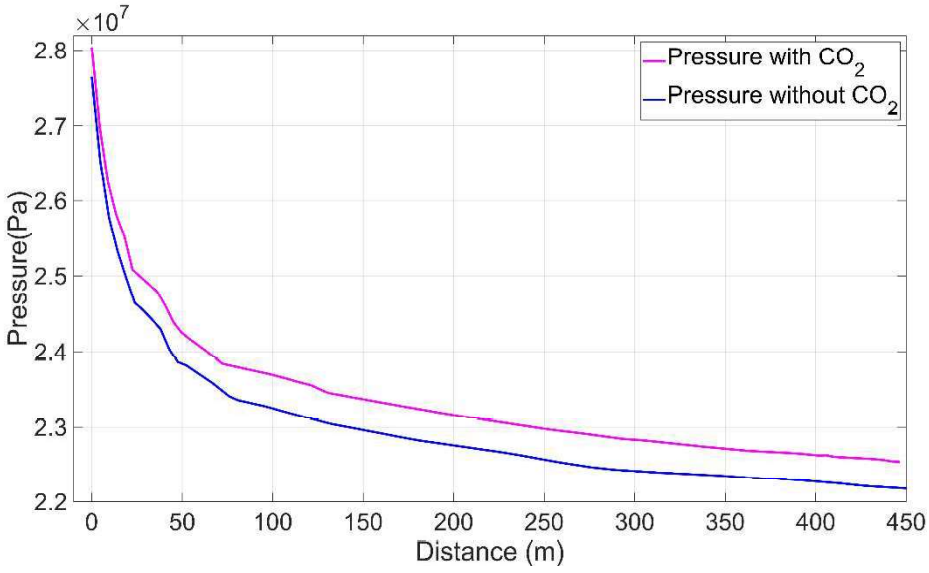

Figure A.37 Pressure comparison between scenario 1 and 3 between two wells after 5 years

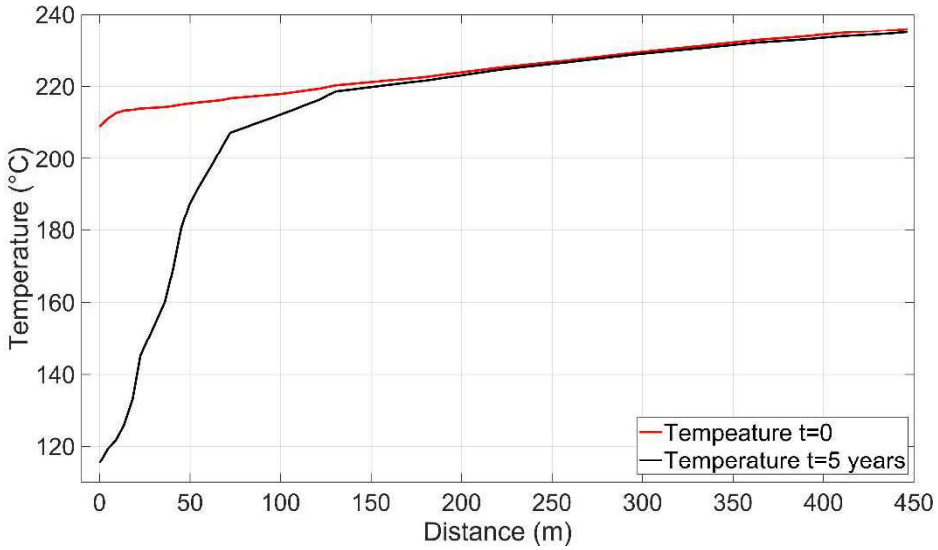

Figure A.38 Temperature comparison between two wells

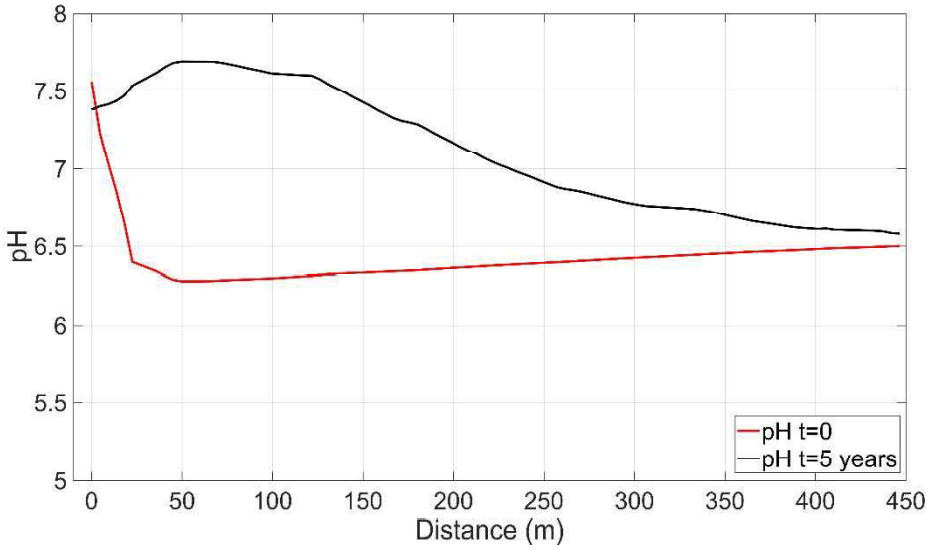

Figure A.39 pH comparison between two wells

A.4 Scenario 4

A.4.1 Mineral Assembly 2

Mineral Assembly 2 includes schist and marble minerals, which are given in Table 4.6. Quartz and silica volume comparison at the injection well block have been illustrated in Figures A.40 through A.42..

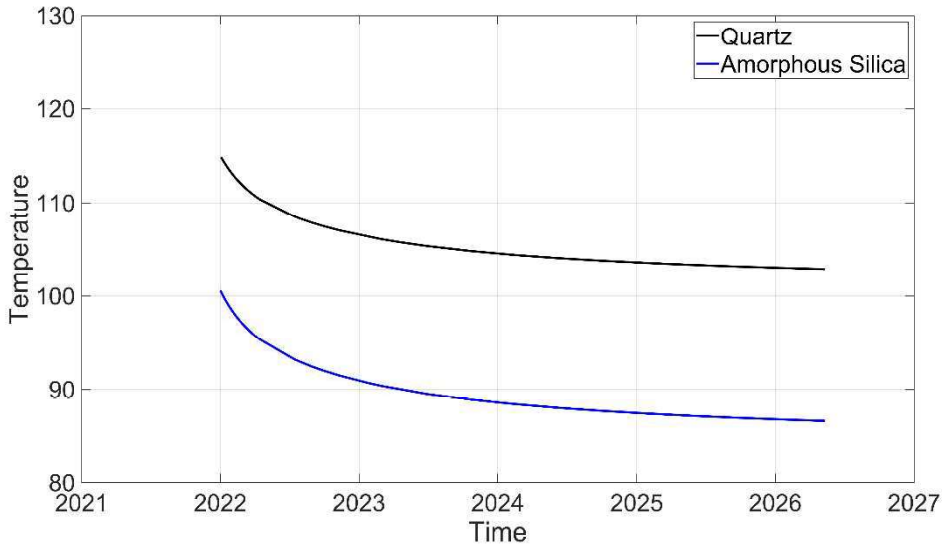

Figure A.40 Temperature difference between two strategies at the injection well block (Quartz represents scenario 3 and amorphous silica represents scenario 4.)

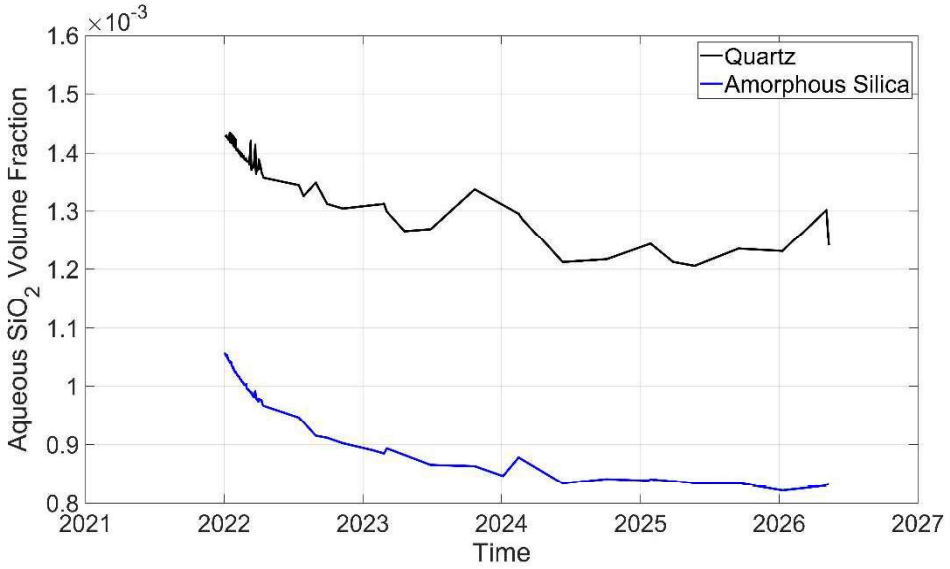

Figure A.41 Aqueous SiO_2 volume fraction comparison between two strategies at the injection well block (Quartz represents scenario 3 and amorphous silica represents scenario 4.)

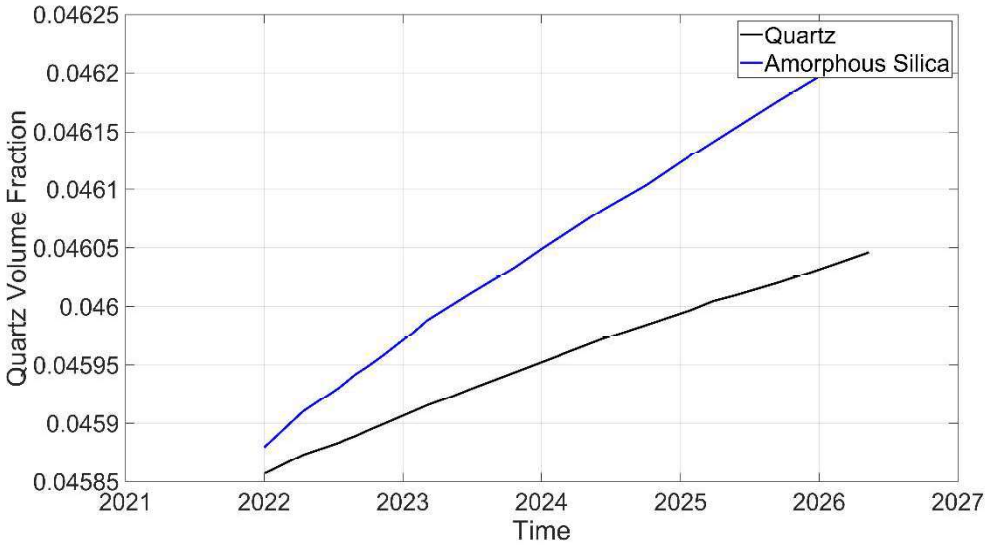

Figure A.42 Quartz volume fraction comparison between two strategies at the injection well block (Quartz represents scenario 3 and amorphous silica represents scenario 4.)

A.4.2 Mineral Assembly 3

Mineral Assembly 3 includes marble minerals, which are given in Table 4.7. Quartz and silica volume comparison at injection well block have been illustrated in Figures A.43 through A.45.

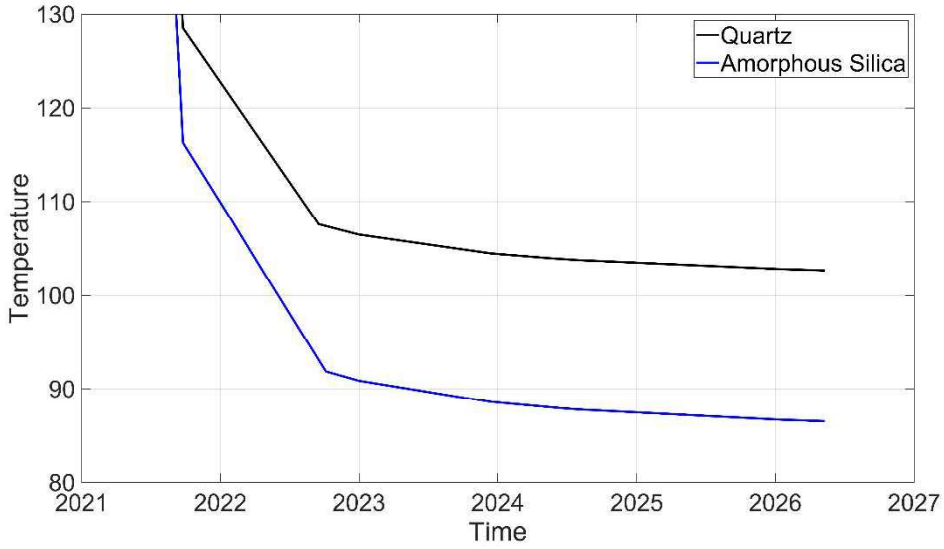

Figure A.43 Temperature difference between two strategies at the injection well block (Quartz represents scenario 3 and amorphous silica represents scenario 4.)

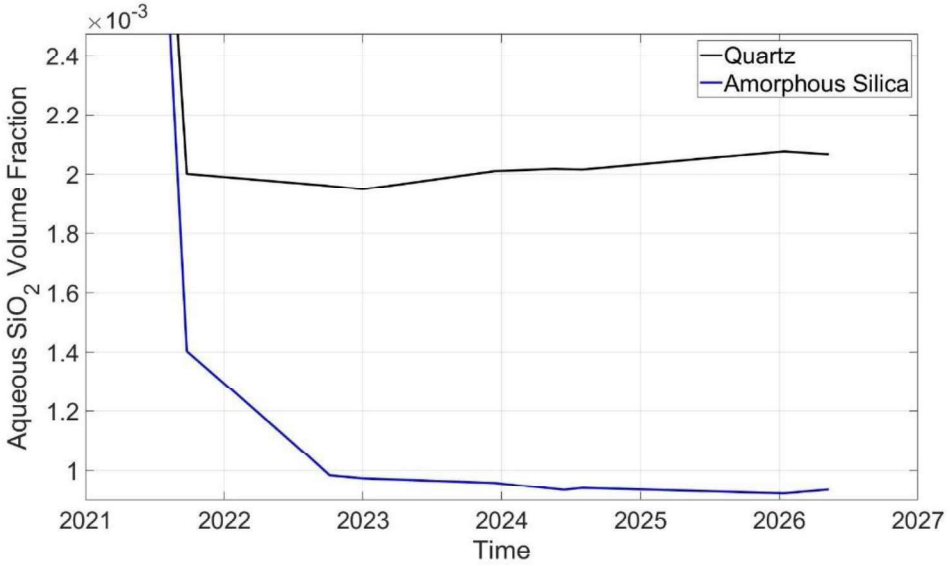

Figure A.44 Aqueous SiO_2 volume fraction comparison between two strategies at the injection well block (Quartz represents scenario 3 and amorphous silica represents scenario 4.)

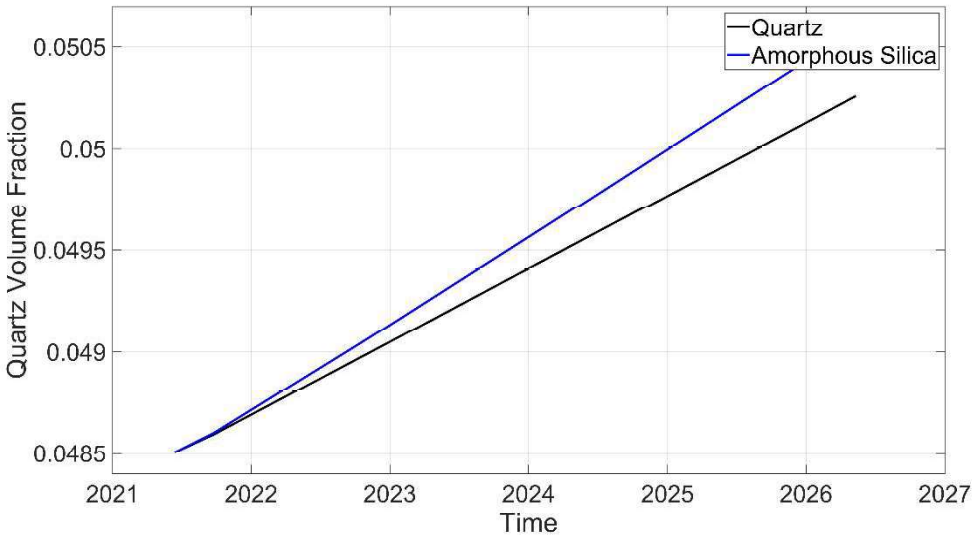

Figure A.45 Quartz volume fraction comparison between two strategies at the injection well block (Quartz represents scenario 3 and amorphous silica represents scenario 4.)

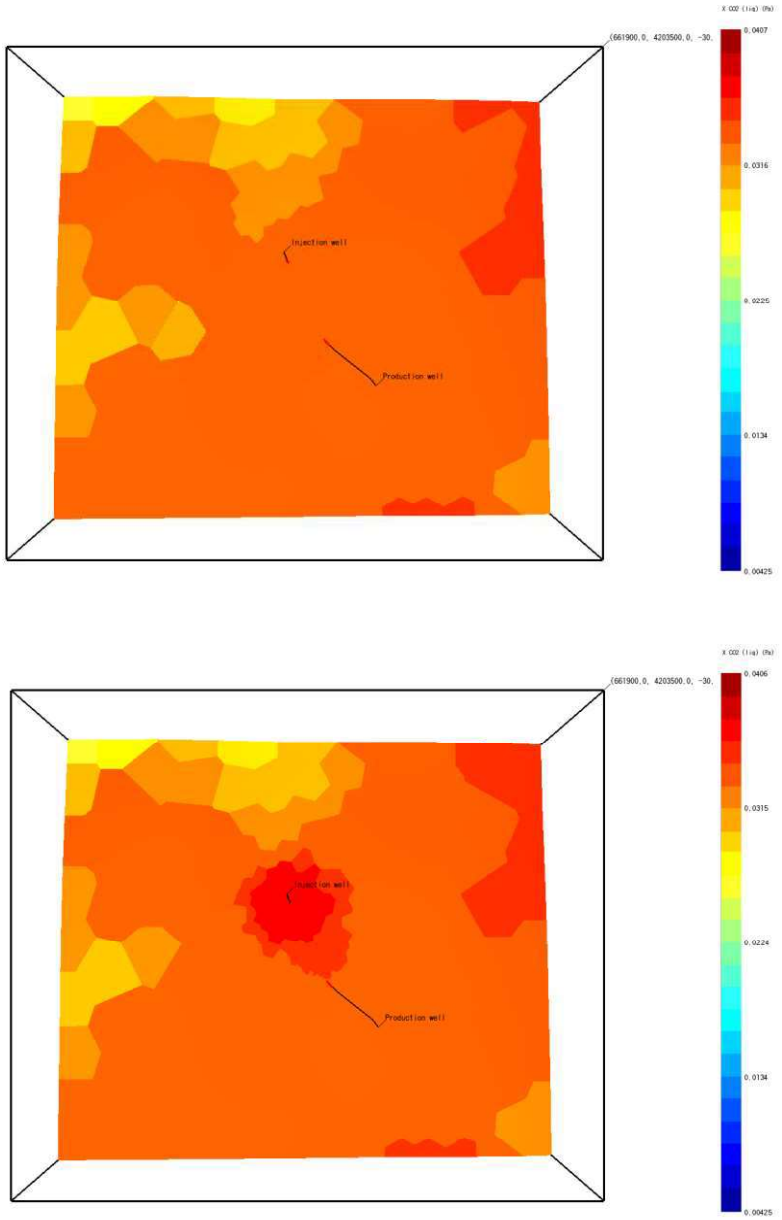

Figure A.46 Propagation of CO_2 due to injection in Scenario 3 and 4 (top view)